

Interacting Anyons in One and Two Dimensions: Strong Zero Modes in Anyon Chains and Non-Abelian Anyons on a Torus

Darragh Millar



Thesis presented for the degree of

Doctor of Philosophy

to the

National University of Ireland Maynooth

Department of Theoretical Physics

24/02/2021

Department Head

Prof. Peter Coles

Research advisor

Dr. Joost Slingerland

To my family

Declaration

This thesis has not been submitted in whole, or in part, to this or any other university for any other degree and is, except where otherwise stated, the original work of the author.

Darragh Millar, 24 February 2021

Acknowledgements

I'll begin by thanking my supervisor, Joost Slingerland. His advice, knowledge and support throughout the past five years have led me to where I am now. I am grateful for the direction and calm he provided when I could find none of my own.

I thank the members of our research group, past and present; Mikael, Niall, Domenico, Aaron, Babatunde, Gert and Nathan. They couldn't have been a more welcoming group and were always willing to give help, physics related or otherwise, when it was needed. Our group meetings have given some welcome human interaction this year in particular. I also thank Graham Kells for many insightful conversations.

I thank John, Aoife, Stephen, Aonghus and Goran for making our office feel like home. I will never forget the hours upon hours spent talking about anything and everything except our work. I also thank Una, Phil, Shane, Adam, Aoibhinn and Dale for all the shared lunches and for making the department a nice place to be.

I give special thanks to Peter Coles and Suzie Duffy for their hard work in running the department and for the many early(ish) morning chats.

I am grateful for my friends, especially Keith, Nathan, Conor and Ciaran for offering fun and distraction when it was needed most.

I'd like to thank my family; my parents, my brother, Keith, and my sister, Emma, for their love and encouragement over the years. They made me feel ten feet tall, even at my worst.

I cannot finish without thanking my girlfriend, Becky. She has given love, support and companionship for the last eight years. She means the world to

me.

I acknowledge financial support from the Irish Research Council Government of Ireland Postgraduate Scholarship GOIPG/2015/2828 and from the Science Foundation Ireland through the Principal Investigator Award 16/IA/4524.

Abstract

The work in this thesis is split into two distinct parts. The first focuses on the identification and construction of strong zero modes in non-abelian anyon chains. We show a Tambara-Yamagami chain is equivalent to a \mathbb{Z}_n chiral clock model. We then present numerical evidence for a strong zero mode in an $SU(2)_4$ anyon chain. By rewriting the chain as an XXZ spin chain, we construct the zero mode explicitly in terms of spin operators. Finally, we write the zero mode in the diagrammatic formalism of anyons.

In the second part, we construct a hopping model of non-abelian anyons on a torus. We demonstrate that the model possesses a translational symmetry around each non-trivial torus loop. By calculating the level spacing statistics of the model, we show that the model is non-integrable for Fibonacci anyons, Ising anyons and abelian anyons. Lastly, we carry out the groundwork for a future project. We add local interactions between the anyons to the Hamiltonian. We then calculate the entanglement spectrum of a ground state of the system after cutting the torus into two cylindrical pieces. The low lying states of this spectrum have a linear dispersion relation for several systems we examined, suggesting the entanglement spectrum is described by a conformal field theory spectrum.

Contents

1	Introduction	1
1.1	Topological Order and Strong Zero Modes	3
1.2	Tight Binding	4
1.3	Overview	5
2	Anyon Theory	7
2.1	Fusion Models	7
2.2	Fusion Vector Space	8
2.3	Diagrammatic Formalism	10
2.4	Braiding	14
3	Construction of Strong Zero Modes	19
3.1	Strong Zero Modes	19
3.2	Quantum Ising Chain	20
3.3	\mathbb{Z}_n Chiral Clock Model	24
4	Strong Zero Modes and Anyon Chains	27
4.1	The Models	27
4.2	Tambara-Yamagami Fusion Model	29
4.3	Fibonacci Anyon Chain	34
4.4	$SU(2)_4$ Anyon Chain	41
4.5	Constructing the Zero Mode	47
4.6	Strong Zero Mode in Modified XXZ Chain	62
4.7	Conclusion	67

5	Anyonic Tight Binding	68
5.1	Tight Binding Model of Spinless Fermions	68
5.2	Anyons on a Torus	70
5.2.1	Abelian Anyons	70
5.2.2	Non-Abelian Anyons	74
5.3	The Model	80
5.4	Translation Symmetry	86
5.4.1	$[T_x, T_y] = 0$	86
5.4.2	$[H, T_x] = [H, T_y] = 0$	88
5.4.3	Eigenvalues of T_x and T_y	90
5.5	Single Particle Solution and Level Statistics	92
5.6	Interactions and Entanglement	97
5.7	Conclusion	103
6	Conclusions and Outlook	104
A	\mathbb{Z}_N Anyon Torus Construction	108
B	Gauge Choice for Hopping Model of Non-Abelian Anyons	111
	Bibliography	114

Chapter 1

Introduction

In our three (spatial) dimensional world, we are familiar with two types of particles, bosons and fermions. One way of distinguishing these particles is by their exchange statistics. Exchanging the positions of two bosons leaves their wavefunction unchanged whereas exchanging two fermions multiplies their wavefunction by -1 . These are the only exchange statistics permitted in three dimensions. Things become a bit more interesting in two dimensions. In 1977, Leinaas and Myrheim [1] showed that two dimensional systems may harbour quasiparticles with arbitrary exchange statistics i.e. their wavefunction may pick up any phase, $e^{i\theta}$, under exchange. These quasiparticles were later dubbed "anyons" by Frank Wilczek [2] due to this fact.

The exchanges of N particles in two dimensions may be described mathematically by the N -strand braid group [3]. This is the infinite group whose elements are all possible exchanges of N strings where the bottom ends of the strings remain fixed. The generators of the group are local counter-clockwise and clockwise exchanges of pairs of strings.

$$\sigma_i = \begin{array}{c} \diagup \quad \diagdown \\ i \quad i+1 \end{array} \quad \sigma_i^{-1} = \begin{array}{c} \diagdown \quad \diagup \\ i \quad i+1 \end{array} \quad (1.1)$$

These generators satisfy the relations

$$\begin{aligned} \sigma_i \sigma_j &= \sigma_j \sigma_i & |i - j| \geq 2 \\ \sigma_i \sigma_{i+1} \sigma_i &= \sigma_{i+1} \sigma_i \sigma_{i+1} \end{aligned} \tag{1.2}$$

This group can be represented diagrammatically by representing group multiplication by the stacking of braids. For example, for a 5-strand group

$$\begin{aligned} \sigma_1^{-1} \sigma_1 &= \begin{array}{c} \diagup \quad \diagdown \\ \diagdown \quad \diagup \\ \hline 1 \quad 2 \end{array} \quad \begin{array}{c} | \\ | \\ | \\ \hline 3 \quad 4 \quad 5 \end{array} = \mathbb{1} \\ \sigma_3 \sigma_1 &= \begin{array}{c} | \quad | \\ \diagdown \quad \diagup \\ \hline \end{array} \quad \begin{array}{c} \diagup \quad \diagdown \\ \diagdown \quad \diagup \\ \hline \end{array} \quad \begin{array}{c} | \\ | \\ | \\ \hline \end{array} = \begin{array}{c} \diagup \quad \diagdown \\ \diagdown \quad \diagup \\ \hline \end{array} \quad \begin{array}{c} | \quad | \\ \diagdown \quad \diagup \\ \hline \end{array} \quad \begin{array}{c} | \\ | \\ | \\ \hline \end{array} = \sigma_1 \sigma_3 \\ \sigma_1 \sigma_2 \sigma_1 &= \begin{array}{c} \diagup \quad \diagdown \\ \diagdown \quad \diagup \\ \hline \end{array} \quad \begin{array}{c} | \quad | \\ \diagdown \quad \diagup \\ \hline \end{array} \quad \begin{array}{c} | \\ | \\ | \\ \hline \end{array} = \begin{array}{c} \diagdown \quad \diagup \\ \diagup \quad \diagdown \\ \hline \end{array} \quad \begin{array}{c} | \quad | \\ \diagdown \quad \diagup \\ \hline \end{array} \quad \begin{array}{c} | \\ | \\ | \\ \hline \end{array} = \sigma_2 \sigma_1 \sigma_2 \end{aligned} \tag{1.3}$$

Two elements of the group are equivalent if they can be continuously deformed into one another without moving the endpoints of the strings.

We can think of the strings as the worldlines of particles which lie on a two dimensional surface and so the unitary representations of the group describe the counter-clockwise and clockwise exchanges of particles on the surface. The one dimensional unitary representations of the braid group are given by

$$\sigma_j \rightarrow e^{i\theta} \quad \theta \in [0, 2\pi) \tag{1.4}$$

where $\theta = 0$ describes a bosonic system while $\theta = \pi$ describes a fermionic one. Particles with $\theta \notin \{0, \pi\}$ are referred to as abelian anyons, since $\sigma_i \sigma_j = \sigma_j \sigma_i$ for all i and j when the system is described by a one dimensional representation

of the braid group. The deployment of the phrase, "abelian anyons", alludes to the fact that there are also non-abelian anyons. This refers to anyons whose exchanges are described by higher (>1) dimensional unitary representations of the braid group [4,5]. When braids are represented by unitary matrices instead of phases then they do not commute in general, making them non-abelian. It is these non-abelian anyons that will be the focus of this thesis.

In the short time since the discovery of particles with exotic exchange statistics, anyon models have been described rigorously in terms of braided tensor categories [6–10]. The topic graduated from a mathematical curiosity to a widely pursued topic of research upon the discovery that certain fractional quantum Hall (FQH) [11–14] states may harbour anyons. This popularity was further bolstered by the potential applications of anyons to fault-tolerant quantum computation [15–17]. While non-abelian anyons have not yet been observed experimentally, there exists some recently published work which experimentally observes particles with fractional exchange statistics [18,19].

In this thesis we will attempt to translate some well known physics concepts to the language of anyons and gain some insight into systems of interacting anyons in one and two dimensions. In particular, we will look at strong zero modes (SZM) and tight binding in the diagrammatic formalism of anyon models written in [20].

1.1 Topological Order and Strong Zero Modes

Anyon theory is strongly linked to the idea of topological order [21–23]. For instance, FQH states which are known to support anyonic excitations exhibit topological order. Kitaev's toric code [16], whose quasiparticle excitations are anyons, is another system which has topological order. But what is topological order? A system is said to have topological order if gapped ground states of the system which lie in different phases may not be adiabatically transformed into one another without closing the energy gap [24–26]. Oftentimes systems with topological order possess a symmetry which protects the topological invariants

of the system. These systems are known as symmetry protected topological (SPT) phases. An indicator that a system is in an SPT phase is the existence of gapless, zero energy edge modes, also known as zero modes. The Ising chain possesses two such modes, one at each end of the chain [27]. The ground states of the Ising chain in the topological phase may be used to form a qubit. The presence of a symmetry in the system means this qubit is robust against local perturbations which do not break the symmetry, making this type of system ideal for use in a quantum computer if the symmetry is preserved in realistic systems. The zero modes present in the Ising chain are known as strong zero modes as they induce a two-fold degeneracy in the entire spectrum [28–30]. A weak zero mode is one which only causes approximate degeneracy of low energy states of the system. Due to their applications to quantum computing, much work has been done to describe the SZMs of different 1D chains [28, 29, 31–35]. We will attempt to do the same for select 1D anyon chains as well as write a SZM in diagrammatic notation.

1.2 Tight Binding

A rather older idea which we will turn our attention to is the concept of tight binding [36–39]. A procedure for formulating a tight binding model was first written in Slater and Koster’s 1954 paper [40]. Originally used to describe electronic structure in molecules and solids, the tight binding model provides the foundation for more complicated models. For example, the Hubbard model [41], which is used to model interacting particles on a lattice, has a tight binding or hopping component in its Hamiltonian. A tight binding or hopping Hamiltonian can be written in the second quantisation formalism as

$$H = \epsilon \sum_j c_j^\dagger c_j - t \sum_{\langle i,j \rangle} (c_j^\dagger c_i + c_i^\dagger c_j) \quad (1.5)$$

where i and j label sites on a lattice, c_j^\dagger and c_j create and annihilate a particle at site j respectively, $\langle i, j \rangle$ is the set of all nearest neighbour pairs of lattice

sites and $\epsilon, t \in \mathbb{R}$. The second term, the hopping term, causes particles to hop from one site to another and is the term we will initially focus on in this thesis i.e. we focus on models with $\epsilon = 0$ leaving

$$H = -t \sum_{\langle i,j \rangle} (c_j^\dagger c_i + c_i^\dagger c_j) \quad (1.6)$$

Later, we will study an anyon hopping model with interactions between the anyons. In this thesis we will construct a tight binding Hamiltonian for a 2D system of non-abelian anyons. We will assume any particles in the systems we study are "hard-core", so that no two particles may occupy the same lattice site. This hard-core constraint is a key difference between the work presented here and early work on an anyon Hubbard model [42, 43] and anyonic tight binding [44]. We note that a hard-core constraint is possible in the anyon Hubbard model as presented in [45] but so far, any work on this model has focused on 1D systems only.

1.3 Overview

The structure of this thesis is as follows:

In Chapters 2 and 3 we introduce some concepts which are important for understanding the work in this thesis. Chapter 2 focuses entirely on introducing basic anyon theory and the diagrammatic notation used throughout the thesis. Chapter 3 provides an introduction to strong zero modes. A sample construction of the SZMs in the Ising chain is presented here along with a brief description of \mathbb{Z}_n chiral clock models.

Chapter 4 is based on a paper in preparation. We construct Hamiltonians for anyon chain models and show numerical evidence for the presence of a SZM in a chain of $SU(2)_4$ anyons. We construct this zero mode in the diagrammatic notation by comparing the $SU(2)_4$ anyon chain to an XXZ spin chain.

In Chapter 5 we introduce anyon models on a torus. We then construct a tight binding model on the surface of a torus and present the level spacing

statistics for several anyon models on the torus. We then add local interactions between anyons to the model and calculate the entanglement spectrum of a ground state of the system. The structure of the entanglement spectrum suggests that it may be described by a conformal field theory spectrum of a state at the edge of the system.

Chapter 2

Anyon Theory

In this chapter we introduce the basic anyon theory that serves as the backbone for the work in this thesis.

We begin by defining fusion models, the basic operations we can perform on the objects in our fusion models and we introduce the powerful diagrammatic notation for anyon models as presented in [20, 46, 47]. We close out the chapter with a useful example of how to resolve a diagram that we will use later in the thesis.

Before we begin in earnest, let us clarify the difference between fusion and anyon models, as we will mention both over the course of this thesis. In mathematical parlance fusion models are called unitary tensor categories while anyon models are known as unitary braided tensor categories. For our purposes it will suffice to say that an anyon model is a fusion model which also permits braiding.

2.1 Fusion Models

A fusion model consists of a finite set, \mathcal{C} , along with fusion rules, which for $a, b \in \mathcal{C}$, are given by

$$a \times b = \sum_{c \in \mathcal{C}} N_{ab}^c c \tag{2.1}$$

\mathcal{C} is the set of all possible labels or charges for the quasi-particles in our model. N_{ab}^c are called the fusion multiplicities and are non-negative integers. They in-

indicate the number of unique ways in which a and b may fuse to give c . Fusion is associative and, for all models we will encounter, commutative. We require that \mathcal{C} contains an identity particle, \mathbb{I} , such that

$$\mathbb{I} \times a = a \quad \forall a \in \mathcal{C} \quad (2.2)$$

We also require that for each $a \in \mathcal{C}$, there exists a conjugate particle $\bar{a} \in \mathcal{C}$ such that

$$N_{a\bar{a}}^{\mathbb{I}} = 1 \quad (2.3)$$

\bar{a} is often referred to as the antiparticle of a .

2.2 Fusion Vector Space

For each fusion product we may define a vector space V_{ab}^c whose dimension is given by N_{ab}^c and whose states describe the ways in which charges, a and b , can fuse to c . The dual vector space, V_c^{ab} , corresponds to the process whereby a charge c splits into two charges, a and b . We label the orthonormal basis vectors of V_c^{ab} as $|a, b; c, \mu\rangle$ (and $\langle a, b; c, \mu|$ for V_{ab}^c) where $\mu \in \{1, 2, 3, \dots, N_{ab}^c\}$. All of the models encountered in this thesis have $N_{ab}^c \in \{0, 1\}$ for any possible values of a , b and c so we will drop the label μ in all future definitions. These models are called multiplicity-free. The vector spaces associated with the fusion or splitting of more than two charges may be written as tensor products of two charge fusion/splitting spaces. For example the vector space, V_d^{abc} may be written

$$V_d^{abc} \cong \bigoplus_e V_e^{ab} \otimes V_d^{ec} \quad (2.4)$$

We could have also written

$$V_d^{abc} \cong \bigoplus_f V_d^{af} \otimes V_f^{bc} \quad (2.5)$$

The different decompositions correspond to splitting charges in a different order. In the first case d splits to e and c before e splits to a and b . In the second example d splits to a and f which further splits to b and c . In order to enforce that fusion is associative we require isomorphisms between different decompositions of the same fusion vector space. These isomorphisms are called F-moves. They are written as

$$|a, b; e\rangle \otimes |e, c; d\rangle = \sum_f [F_d^{abc}]_{e,f} |a, f; d\rangle \otimes |b, c; f\rangle \quad (2.6)$$

For anyon models these F-moves are unitary. We may write the fusion/splitting space of n charges by decomposing the fusion/splitting space into the tensor product of many 2 charge fusion/splitting spaces:

$$V_c^{a_1, a_2, \dots, a_n} \cong \bigoplus_{b_1, b_2, \dots, b_{n-2}} V_{b_1}^{a_1 a_2} \otimes V_{b_2}^{b_1 a_3} \otimes \dots \otimes V_c^{b_{n-2} a_n} \quad (2.7)$$

We now define an important quantity. The quantum dimension, d_a , of a charge a is defined as

$$d_a = d_{\bar{a}} = |[F_a^{a\bar{a}a}]_{1,1}|^{-1} \quad (2.8)$$

It is worth noting here that many of the quantities defined in this thesis may be defined in a broader mathematical context. For instance, the definition given above for the quantum dimension is only applicable to unitary categories, which are the only categories we deal with in the thesis. Some properties of the quantum dimension are

$$d_a d_b = \sum_c N_{ab}^c d_c \quad (2.9)$$

$$d_a \geq 1$$

with equality if and only if a is abelian. A particle, a , is said to be abelian if the fusion of a with any other particle in \mathcal{C} has a unique result. A fusion model is abelian if all charges in \mathcal{C} are abelian.

2.3 Diagrammatic Formalism

While perfectly usable, the bra/ket notation can be a bit unwieldy when applied to anyon models. Fortunately a more elegant solution exists in the form of diagrammatic notation. To begin writing our models in this notation we simply associate each anyon label with an oriented line. Reversing the orientation of the line is equivalent to conjugating the charge.

$$\begin{array}{c} | \\ \hline \uparrow \\ \hline \\ \hline \end{array} a = \begin{array}{c} | \\ \hline \downarrow \\ \hline \\ \hline \end{array} \bar{a} \tag{2.10}$$

We write fusion and splitting states as trivalent vertices

$$(d_c/d_a d_b)^{1/4} \begin{array}{c} c \\ | \\ \wedge \\ \swarrow \quad \searrow \\ a \quad b \end{array} = \langle a, b; c | \qquad (d_c/d_a d_b)^{1/4} \begin{array}{c} a \quad b \\ \wedge \\ | \\ c \end{array} = | a, b; c \rangle \tag{2.11}$$

$(d_c/d_a d_b)^{1/4}$ is a normalisation factor which ensures that diagrams are in the isotopy invariant convention. A diagram is isotopy invariant if the state is not changed by smooth deformations which leave open endpoints fixed and don't pass lines through each other or around open endpoints. To properly define isotopy invariance we also need to be able to introduce and remove bends in a line which we will do later. An open endpoint corresponds to some topological obstruction through which we cannot pass a line such as the edge of the system.

In diagrammatic notation F-moves are written

$$\begin{array}{c} a \quad b \quad c \\ \wedge \quad \wedge \\ \swarrow \quad \searrow \\ e \quad d \end{array} = \sum_f [F_d^{abc}]_{e,f} \begin{array}{c} a \quad b \quad c \\ \wedge \quad \wedge \\ \swarrow \quad \searrow \\ f \quad d \end{array} \tag{2.12}$$

The F-matrices for a model are determined by a set of consistency equations

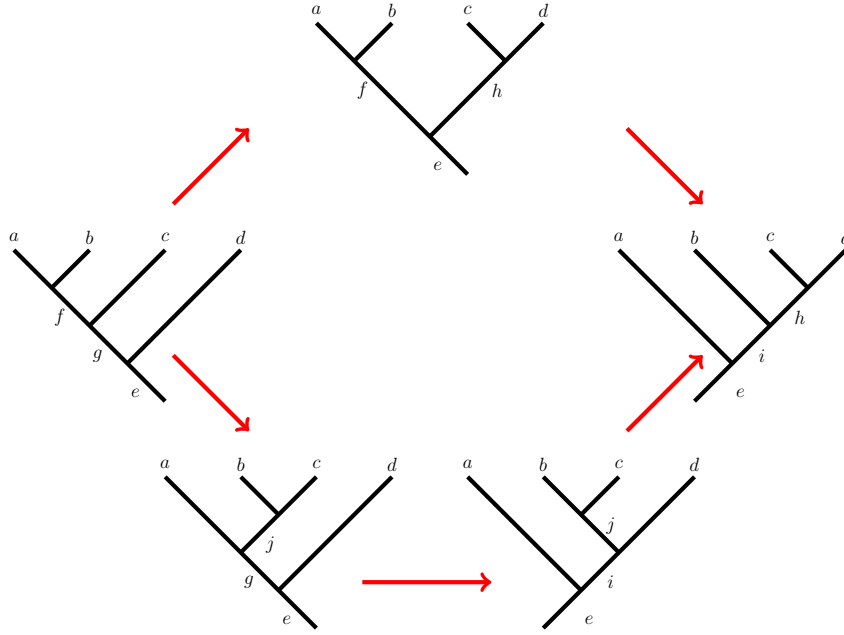


Figure 2.1: The Pentagon equations say that the upper path and the lower path in the figure must give the same result.

called the Pentagon equations. These enforce the condition that any two sequences of F-moves which have the same initial and final states must be equal. Ocneanu rigidity [48] guarantees finitely many gauge equivalence classes of solutions to the Pentagon equations for a given set of fusion rules. This gauge freedom is determined by a basis change, $[u_c^{ab}]$, for the fusion spaces V_c^{ab} . In multiplicity-free models the fusion and splitting spaces are one dimensional so the basis change amounts to multiplication by a complex number. Under a gauge transformation, the F-symbols and R-symbols, which we will define very soon, transform as

$$\begin{aligned}
 [F_d^{abc}]'_{ef} &= \frac{u_d^{ab} u_f^{bc}}{u_e^{ab} u_d^{bc}} [F_d^{abc}]_{ef} \\
 [R_c^{ab}]' &= \frac{u_c^{ba}}{u_c^{ab}} [R_c^{ab}]
 \end{aligned}
 \tag{2.13}$$

The Pentagon equations are written

$$[F_e^{abh}]_{fi} [F_e^{fcd}]_{gh} = \sum_j [F_i^{bcd}]_{jh} [F_e^{ajd}]_{gi} [F_g^{abc}]_{fj}
 \tag{2.14}$$

We can perform inner products on our states by stacking diagrams so that

fusion/splitting lines connect

$$\begin{array}{c} c \\ \uparrow \\ \text{diamond} \\ \downarrow \\ c' \end{array}
 \begin{array}{c} a \quad b \end{array}
 = \delta_{c,c'} \sqrt{\frac{d_a d_b}{d_c}}
 \begin{array}{c} c \\ \uparrow \\ \text{vertical line} \end{array}
 \quad (2.15)$$

This diagrammatically encodes charge conservation and forbids tadpole diagrams such as

$$\begin{array}{c} c \\ \uparrow \\ \text{diamond} \\ \downarrow \\ a \quad b \end{array}
 , c \neq \mathbb{I}
 \quad (2.16)$$

An unknotted loop carrying a charge a evaluates to d_a

$$\begin{array}{c} a \\ \text{loop} \end{array}
 = d_a
 \quad (2.17)$$

The identity operator on a pair of anyons with charges a and b is written

$$\mathbb{I}_{ab} = \sum_c |a, b; c\rangle \langle a, b; c|
 \quad (2.18)$$

which in diagrammatic notation is

$$\begin{array}{c} a \quad b \\ \text{vertical lines} \end{array}
 = \sum_c \sqrt{\frac{d_c}{d_a d_b}}
 \begin{array}{c} a \quad b \\ \text{square diagram} \\ c \end{array}
 \quad (2.19)$$

For isotopy invariance we need to be able to remove bends in a line. Horizontal bends, which maintain the upward flow of a line, are trivial. However we need to perform an F-move when bending a line vertically. This F-move is

$$\begin{array}{c}
\begin{array}{c} a \\ \uparrow \\ \text{---} \\ \uparrow \\ c \end{array} \begin{array}{c} e \\ \text{---} \\ \downarrow \\ \text{---} \\ \downarrow \\ d \end{array} \begin{array}{c} b \\ \uparrow \\ \text{---} \\ \uparrow \\ d \end{array} \\
\downarrow \\
f \\
\uparrow \\
\begin{array}{c} c \\ \uparrow \\ \text{---} \\ \downarrow \\ d \end{array}
\end{array}
= \sum_g [F_f^{ceb}]_{d,g}^{-1}
\begin{array}{c}
\begin{array}{c} a \\ \uparrow \\ \text{---} \\ \uparrow \\ c \end{array} \begin{array}{c} e \\ \text{---} \\ \downarrow \\ \text{---} \\ \downarrow \\ g \end{array} \begin{array}{c} b \\ \uparrow \\ \text{---} \\ \uparrow \\ e \end{array} \\
\downarrow \\
f \\
\uparrow \\
\begin{array}{c} c \\ \uparrow \\ \text{---} \\ \downarrow \\ d \end{array}
\end{array}
\end{array}
\quad (2.24)$$

We can now use 2.15 to remove the bubble so our final result is

$$[F_{cd}^{ab}]_{e,f} = \sqrt{\frac{d_e d_f}{d_a d_d}} [F_f^{ceb}]_{d,a}^{-1} \quad (2.25)$$

Similarly if we write

$$\begin{array}{c}
\begin{array}{c} a \\ \uparrow \\ \text{---} \\ \uparrow \\ c \end{array} \begin{array}{c} e \\ \text{---} \\ \downarrow \\ \text{---} \\ \downarrow \\ d \end{array} \begin{array}{c} b \\ \uparrow \\ \text{---} \\ \uparrow \\ d \end{array} \\
\downarrow \\
f \\
\uparrow \\
\begin{array}{c} c \\ \uparrow \\ \text{---} \\ \downarrow \\ d \end{array}
\end{array}
= \sum_f [\tilde{F}_{cd}^{ab}]_{e,f}
\begin{array}{c}
\begin{array}{c} a \\ \downarrow \\ \text{---} \\ \downarrow \\ c \end{array} \begin{array}{c} b \\ \downarrow \\ \text{---} \\ \downarrow \\ d \end{array} \\
\uparrow \\
f \\
\downarrow \\
\begin{array}{c} c \\ \uparrow \\ \text{---} \\ \downarrow \\ d \end{array}
\end{array}
\end{array}
\quad (2.26)$$

Then

$$[\tilde{F}_{cd}^{ab}]_{e,f} = \sqrt{\frac{d_e d_f}{d_b d_c}} [F_f^{aed}]_{c,b}^{-1} \quad (2.27)$$

This F-move allows us to write the effect of bending a line vertically around a fusion/splitting vertex. For example

$$\begin{array}{c}
\begin{array}{c} a \\ \uparrow \\ \text{---} \\ \uparrow \\ c \end{array} \begin{array}{c} b \\ \text{---} \\ \downarrow \\ \text{---} \\ \downarrow \\ \bar{b} \end{array} \\
\downarrow \\
f \\
\uparrow \\
\begin{array}{c} c \\ \uparrow \\ \text{---} \\ \downarrow \\ \bar{b} \end{array}
\end{array}
= \sqrt{\frac{d_a d_b}{d_c}} [\tilde{F}_a^{ab\bar{b}}]_{c,1}
\begin{array}{c}
\begin{array}{c} a \\ \uparrow \\ \text{---} \\ \uparrow \\ c \end{array} \begin{array}{c} b \\ \text{---} \\ \downarrow \\ \text{---} \\ \downarrow \\ \bar{b} \end{array} \\
\downarrow \\
f \\
\uparrow \\
\begin{array}{c} c \\ \uparrow \\ \text{---} \\ \downarrow \\ \bar{b} \end{array}
\end{array}
\quad (2.28)$$

2.4 Braiding

In addition to what we have already shown, we may also exchange the positions of two charges in our model. Here we are talking specifically about anyon models, because fusion models which are not anyon models do not permit

braiding. The operations to braid two anyons, called R-moves, are given by

$$R_{ab} = \begin{array}{c} \swarrow a \quad \searrow b \\ \nearrow \quad \nwarrow \\ \quad \quad \quad \end{array} \quad R_{ab}^\dagger = R_{ab}^{-1} = \begin{array}{c} \swarrow b \quad \searrow a \\ \nearrow \quad \nwarrow \\ \quad \quad \quad \end{array} \quad (2.29)$$

If we apply this to basis vectors of the splitting space we get

$$R_{ab}|a, b; c\rangle = R_c^{ab}|a, b; c\rangle \quad (2.30)$$

$$\begin{array}{c} a \quad b \\ \swarrow \quad \searrow \\ \quad \quad \quad \nearrow \\ \quad \quad \quad \downarrow c \end{array} = R_c^{ab} \begin{array}{c} a \quad b \\ \swarrow \quad \searrow \\ \quad \quad \quad \downarrow c \end{array} \quad (2.31)$$

In diagrammatic notation the braid operator is

$$R_{ab} = \sum_c \sqrt{\frac{d_c}{d_a d_b}} [R_c^{ab}] \begin{array}{c} a \quad b \\ \swarrow \quad \searrow \\ \quad \quad \quad \downarrow c \\ \quad \quad \quad \uparrow c \\ b \quad a \\ \swarrow \quad \searrow \end{array} \quad (2.32)$$

The R-matrices are determined by a set of consistency equations similar to the Pentagon equations. The Hexagon equations enforce that different sequences of F and R moves with the same initial and final states must be equal as in figure 2.2. The Hexagon and Pentagon equations together imply that the braid operators form a representation of the braid group. The Hexagon equations are written

$$\begin{aligned} [R_e^{ca}][F_d^{abc}]_{e,g}[R_g^{cb}] &= \sum_f [F_d^{cab}]_{e,f}[R_d^{cf}][F_d^{abc}]_{f,g} \\ [(R_e^{ac})^{-1}][F_d^{abc}]_{e,g}[(R_g^{bc})^{-1}] &= \sum_f [F_d^{cab}]_{e,f}[(R_d^{fc})^{-1}][F_d^{abc}]_{f,g} \end{aligned} \quad (2.33)$$

The R-matrices satisfy the ribbon property

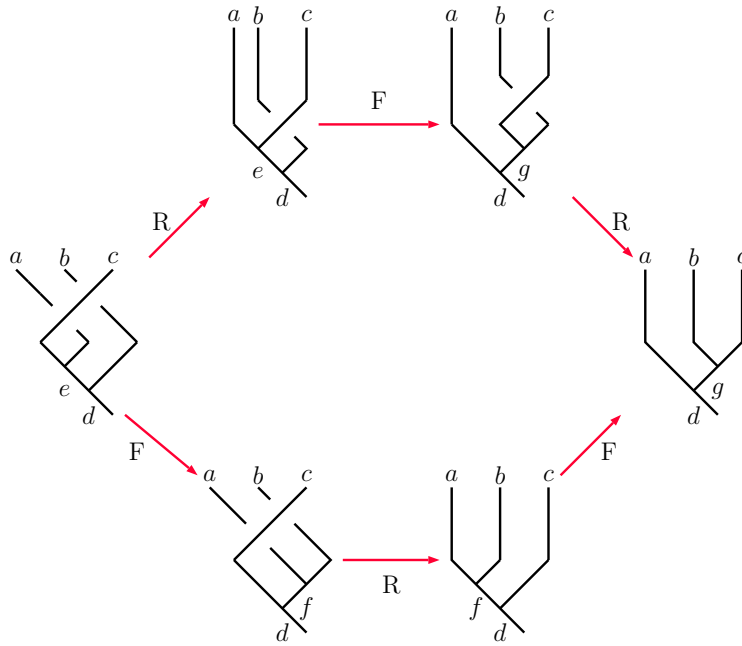


Figure 2.2: The Hexagon equations say that the upper paths and the lower paths in the figures must give the same result. We get another set of equations by reversing all of the braids shown in the figure. A fusion model which is not an anyon model has solutions for the Pentagon equations but not for the Hexagon equations.

$$[R_c^{ab}][R_c^{ba}] = \frac{\theta_c}{\theta_a \theta_b} \quad (2.34)$$

where θ_a is a root of unity known as the topological spin of a , defined by

$$\theta_a = \theta_{\bar{a}} = \sum_c \frac{d_c}{d_a} [R_c^{aa}] \quad (2.35)$$

When applicable, this is related to s_a , the spin or CFT conformal scaling dimension of a by

$$\theta_a = e^{2\pi i s_a} \quad (2.36)$$

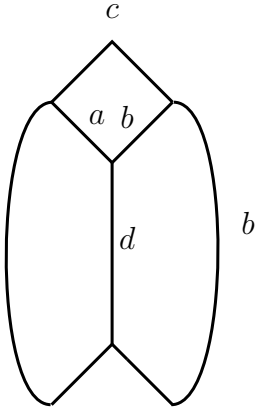
We finish the chapter by defining one more important object [49]

$$(S_c)_{ab} = \frac{1}{\mathcal{D}\sqrt{d_c}} \begin{array}{c} c \\ \triangle \\ a \quad b \end{array} \quad (2.37)$$

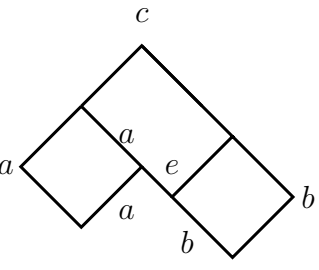
where \mathcal{D} is what is known as the total quantum dimension and is given by

$$\mathcal{D} = \sqrt{\sum_a d_a^2} \quad (2.38)$$

If $c = 1$ then $(S_c)_{ab}$ is just written S_{ab} and is called the topological S-matrix. When we define a system of anyons living on the surface of a torus the S-matrix will define an isomorphism between two bases corresponding to the two non-trivial loops of the torus as described in [9, 47, 50]. It is useful to see such a diagram resolved at least once and as this is such an important quantity, we will resolve this diagram now. We use 2.19 and two braid operators to write the above diagram as

$$\sum_d \sqrt{\frac{d_d}{d_a d_b}} R_d^{ab} R_d^{ba} a$$

(2.39)

We now perform the F-move defined in 2.25 to get

$$\sum_{d,e} \sqrt{\frac{d_d}{d_a d_b}} R_d^{ab} R_d^{ba} [F_{ab}]_{d,e}^{-1} a$$

(2.40)

Another pair of F-moves will allow us to form loops labelled by a and b and enforces that $e = c$.

$$\sum_d \sqrt{\frac{d_d}{d_a d_b}} R_d^{ab} R_d^{ba} [F_{ab}]_{d,c}^{-1} [F_1^{cbb}]_{b,c} [F_c^{caa}]_{a,1} \cdot \text{Diagram} \quad (2.41)$$

Resolving any closed loops and using 2.25, the final expression is

$$(S_c)_{ab} = \frac{1}{\mathcal{D}\sqrt{d_c}} \sum_d d_d d_c R_d^{ab} R_d^{ba} [F_d^{acb}]_{a,b} [F_1^{cbb}]_{b,c} [F_c^{caa}]_{a,1} \quad (2.42)$$

Which simplifies to

$$S_{ab} = \frac{1}{\mathcal{D}} \sum_d d_d R_d^{ba} R_d^{ab} \quad (2.43)$$

when $c = 1$. This concludes our introduction to basic anyon theory. Having described the tools at our disposal for manipulating anyonic systems we are almost ready to construct some models explicitly. Before we do that though, we present a brief introduction to the idea of strong zero modes and how they might relate to the fusion models we are interested in.

Chapter 3

Construction of Strong Zero Modes

Here we present the definition of a strong zero mode. The quantum Ising chain [51] is a simple example of a model with a pair of strong zero modes. We explicitly construct the zero mode operators following [28]. We conclude the chapter with a description of the \mathbb{Z}_n chiral clock model or \mathbb{Z}_n parafermionic model [28, 29, 31, 32], another model with strong zero modes and one we will meet in the context of fusion models.

3.1 Strong Zero Modes

A strong zero mode is an operator ψ which commutes with the Hamiltonian up to terms which go to zero in the thermodynamic limit.

$$[H, \psi] = \mathcal{O}(e^{-\frac{L}{\xi}}) \quad (3.1)$$

Where L is the length of the system and $\xi > 0$ is some constant length scale. ψ does not commute with some operator Q which implements a discrete symmetry

$$[H, Q] = 0, \quad [\psi, Q] \neq 0 \quad (3.2)$$

Additionally, it is required that

$$\psi^N \propto \mathbb{1} \tag{3.3}$$

for some integer, $N > 0$. These conditions enforce that ψ maps between states in different symmetry sectors with the same energy. To see this, consider

$$\psi Q = -Q\psi \tag{3.4}$$

as we will see is the case in the quantum Ising chain. Eigenstates of Q have eigenvalues ± 1 . Say $|q\rangle$ is an eigenstate of Q with eigenvalue 1 and is also an eigenstate of H with eigenvalue E_q . Then

$$\begin{aligned} \psi Q|q\rangle &= \psi|q\rangle \\ &= -Q(\psi|q\rangle) \end{aligned} \tag{3.5}$$

so $\psi|q\rangle$ is an eigenstate of Q with eigenvalue -1 and is also an eigenstate of H with eigenvalue E_q since H and ψ commute. This tells us that ψ maps between symmetry sectors with identical spectra. We also require that ψ is normalisable in the thermodynamic limit.

$$\psi^\dagger \psi = 1 + \mathcal{O}(e^{-\frac{L}{\xi}}) \tag{3.6}$$

We can now construct this operator explicitly for the quantum Ising chain.

3.2 Quantum Ising Chain

The Hamiltonian for the Ising chain with open boundary conditions is

$$H = -f \sum_{j=1}^L \sigma_j^x - J \sum_{j=1}^{L-1} \sigma_j^z \sigma_{j+1}^z \tag{3.7}$$

It acts on a Hilbert space made up of L sites with a spin- $\frac{1}{2}$ particle at each site. The spin at each site may point up or down so the Hilbert space has dimension

2^L . The σ_i^α are the Pauli operators which act non-trivially at site i while f and J are non-negative and real. The Hamiltonian has a \mathbb{Z}_2 symmetry under flipping all spins. The operator generating this symmetry is

$$(-1)^F = \prod_{j=1}^L \sigma_j^x \quad (3.8)$$

Clearly $[H, (-1)^F] = 0$ and $((-1)^F)^2 = 1$. The quantum Ising chain has two phases separated by the critical point $f = J$. For $f < J$ the system is in the ordered phase while for $f > J$ it is in the disordered phase. In the ordered phase the system has a two-fold degenerate ground state. In the disordered phase the system has a unique ground state. These properties are easily seen in the limits $f = 0$ and $J = 0$. When $f = 0$ then clearly the energy is minimised when all spins point in the same direction giving two ground states, one where all spins point up and another where all spins point down. When $J = 0$ the energy is minimised when all spins are in the eigenstate of σ^x with eigenvalue 1 and this ground state is unique.

By performing a Jordan-Wigner transformation the Ising chain may be mapped onto a model of free fermions. At each site we introduce two Majorana fermion operators

$$\begin{aligned} a_j &= \left(\prod_{k=1}^{j-1} \sigma_k^x \right) \sigma_j^z \\ b_j &= i a_j \sigma_j^x = i \left(\prod_{k=1}^{j-1} \sigma_k^x \right) \sigma_j^z \sigma_j^x \end{aligned} \quad (3.9)$$

with Majorana referring to the fact that these operators are Hermitian. These operators satisfy the anti-commutation relations

$$\{a_j, a_k\} = \{b_j, b_k\} = 2\delta_{jk}, \quad \{a_j, b_k\} = 0 \quad (3.10)$$

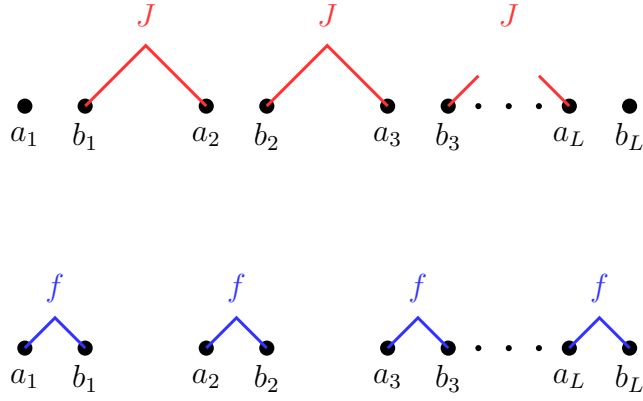


Figure 3.1: The $f = 0$ and $J = 0$ limits of the Ising chain. Note that $f = 0$ leaves isolated Majorana operators a_1 and b_L at either end of the chain. These operators drop out of the Hamiltonian and become exact edge zero modes.

The Hamiltonian may be rewritten in terms of a_j and b_j giving

$$H = if \sum_{j=1}^L a_j b_j + iJ \sum_{j=1}^{L-1} b_j a_{j+1} \quad (3.11)$$

It is also possible to define complex fermions

$$\begin{aligned} c_j^\dagger &= a_j + ib_j \\ c_j &= a_j - ib_j \end{aligned} \quad (3.12)$$

which have the canonical fermion anti-commutation relations. The Hamiltonian written in terms of these variables includes so called "Cooper pairing" terms, $c_j c_{j+1}$ and $c_j^\dagger c_{j+1}^\dagger$. These terms do not preserve fermion number but rather "fermion parity" i.e. they preserve fermion number modulo 2. The symmetry operator now measures fermion number modulo 2.

$$(-1)^F = \sum_{j=1}^L (-ia_j b_j) \quad (3.13)$$

with F being the fermion number. This operator commutes with the product of an even number of fermion operators and anti-commutes with the product of an odd number of fermion operators, leading to $(-1)^F$ often being referred to as the fermion parity operator. The Hamiltonian consists solely of fermion bilinears which clearly commute with the parity operator so the spectrum will be divided into even and odd sectors of the fermion parity operator.

Visualizing the chain as in 3.1, we can see that when $f = 0$, a_1 and b_L drop out of the Hamiltonian completely. Therefore 3.10 shows that they commute with the fermion bilinears remaining in the Hamiltonian when $f = 0$. Since a_1 and b_L are single fermion operators they anti-commute with $(-1)^F$. The operators, a_1 and b_L , satisfy our definition of a strong zero mode but commute exactly with the Hamiltonian so are exact strong zero modes. On top of this they are what are known as edge zero modes. As the name implies, an edge zero mode is a zero mode which is localized to the edge of a system. In particular, if ψ is an edge zero mode its dependence on operators away from the edge of the system is exponentially small in their distance away from the edge.

We will now perform an iterative construction [28] to show that these zero modes persist throughout the entire ordered phase. Operators, a_1 and b_L , are used as a first guess for what the zero modes might be when $f \neq 0$ and we find

$$[H, a_1] = -2ifb_1 \quad (3.14)$$

We notice that

$$2b_1 = [b_1a_2, a_2] \quad (3.15)$$

and so we can write an operator which commutes with the first two terms of the Hamiltonian.

$$[ifa_1b_1 + iJb_1a_2, a_1 + \frac{f}{J}a_2] = 0 \quad (3.16)$$

Notice that $\frac{f}{J}a_2$ will not commute with ifa_2b_2 but it is easy to show

$$\begin{aligned} [H, a_j] &= -2ifb_j + 2iJb_{j-1} \\ [H, b_j] &= 2ifa_j - 2iJa_{j+1} \end{aligned} \quad (3.17)$$

where a_{L+1} and b_0 are taken to be zero. Using these commutation relations we iterate the process above to write our new zero mode operators

$$\psi_{left} = a_1 + \frac{f}{J}a_2 + \left(\frac{f}{J}\right)^2 a_3 + \dots \quad \psi_{right} = b_L + \frac{f}{J}b_{L-1} + \left(\frac{f}{J}\right)^2 b_{L-2} + \dots \quad (3.18)$$

Taking the commutators of these operators with H we get

$$[H, \psi_{left}] = f \left(\frac{f}{J} \right)^{L-1} b_L \quad [H, \psi_{right}] = f \left(\frac{f}{J} \right)^{L-1} a_1 \quad (3.19)$$

and clearly these values go to zero as $L \rightarrow \infty$ as long as $f < J$. These operators are normalisable when $f < J$ and have exponentially small dependence on terms away from the edge of the chain. Both are sums of single fermion operators so anti-commute with the fermion parity operator and so ψ_{left} and ψ_{right} are edge zero modes in the ordered phase of the Ising chain.

3.3 \mathbb{Z}_n Chiral Clock Model

In this section we introduce a generalised form of the quantum Ising chain. Like the Ising chain, the \mathbb{Z}_n chiral clock models or chiral Potts models [52–54] possess ordered and disordered phases with the ordered phase allowing for the existence of strong zero modes while also exhibiting richer physics than the Ising model [55–57]. Similar to how the Ising model could be rewritten in terms of non-local fermionic operators via a Jordan-Wigner transformation, these models can be written in terms of non-local parafermionic operators [58] via an analogous transformation. Much work has been done to find the zero modes for these chains and determine when they exist [28, 29, 31–35]. In particular, it has been shown that when they exist, one may perform an iterative construction of the strong zero modes similar to the example of the quantum Ising chain [28, 33]. Here we will only give a brief description of the model. Later we will present a fusion model which is equivalent to the chiral clock models.

The \mathbb{Z}_n chiral clock model on L sites has Hilbert space consisting of L n -state "spins". The Hamiltonian is written

$$H_n = -f \sum_{j=1}^L \sum_{m=1}^{n-1} \alpha_m (\tau_j)^m - J \sum_{j=1}^{L-1} \sum_{m=1}^{n-1} \hat{\alpha}_m (\sigma_j^\dagger \sigma_{j+1})^m \quad (3.20)$$

where $f, J \geq 0$ and

$$\alpha_m^* = \alpha_{n-m}, \quad \hat{\alpha}_m^* = \hat{\alpha}_{n-m} \quad (3.21)$$

τ_j and σ_j act non-trivially on site j and satisfy

$$\sigma^n = \tau^n = 1, \quad \sigma^\dagger = \sigma^{n-1}, \quad \tau^\dagger = \tau^{n-1}, \quad \sigma\tau = \omega\tau\sigma \quad (3.22)$$

with $\omega = e^{\frac{2\pi i}{n}}$ an n^{th} root of unity. σ and τ are generalisations of the Pauli operators and in particular, if we choose a representation where σ is diagonal we can write

$$\sigma = \begin{pmatrix} 1 & 0 & 0 & \dots & 0 \\ 0 & \omega & 0 & \dots & 0 \\ 0 & 0 & \omega^2 & \dots & 0 \\ \dots & \dots & \dots & \dots & \dots \\ 0 & 0 & 0 & \dots & \omega^{n-1} \end{pmatrix}, \quad \tau = \begin{pmatrix} 0 & 0 & 0 & \dots & 1 \\ 1 & 0 & 0 & \dots & 0 \\ 0 & 1 & 0 & \dots & 0 \\ \dots & \dots & \dots & \dots & \dots \\ 0 & 0 & \dots & 1 & 0 \end{pmatrix} \quad (3.23)$$

Notice that when $n = 2$ these matrices are the Pauli operators σ^z and σ^x . If we think of each site of the chain as a "clock" with n distinct values then σ_j reads the value of the clock at site j while τ_j shifts the value by one "tick". As one may have guessed the symmetry operator, $(-1)^F$, generalises to

$$Q_n = \prod_{j=1}^L \tau_j^\dagger \quad (3.24)$$

which turns each clock back one tick. This generates a \mathbb{Z}_n symmetry in the system as

$$\begin{aligned} [H, Q_n] &= 0 \\ (Q_n)^n &= 1 \end{aligned} \quad (3.25)$$

In the same way we wrote the Ising chain in terms of fermionic operators, we

may also write the \mathbb{Z}_n chiral clock model in terms of parafermionic operators.

$$\begin{aligned}\chi_j &= \left(\prod_{k=1}^{j-1} \tau_k \right) \sigma_j \\ \psi_j &= \omega^{\frac{n-1}{2}} \chi_j \tau_j\end{aligned}\tag{3.26}$$

with commutation relations

$$\begin{aligned}\chi_j \chi_k &= \omega \chi_k \chi_j \\ \psi_j \psi_k &= \omega \psi_k \psi_j \\ \chi_j \psi_k &= \omega \psi_k \chi_j \quad \text{for } j < k\end{aligned}\tag{3.27}$$

It is for this reason that these models are also referred to as \mathbb{Z}_n parafermionic models. The Hamiltonian is rewritten in terms of these parafermionic operators in the references given at the start of this section but our description to this point should be sufficient for the purpose of this thesis. We now move on to investigating how we may find and write down zero modes in anyonic systems.

Chapter 4

Strong Zero Modes and Anyon Chains

In this chapter we introduce the anyon/fusion chain models we have studied. The Hamiltonians we write for these chains assign energy values based on nearest neighbour interactions as in [59, 60]. We then investigate these chains for the existence of strong zero modes.

4.1 The Models

We consider chains of L anyons of type j as in 4.1. We primarily consider two bases for our models: the standard fusion basis and a dimerized basis.

Basis states are labelled $|x_1, x_2, x_3, \dots, Q\rangle$ where $x_i, Q \in \mathcal{C}$. We will explicitly state which basis we are working in throughout this thesis. A basis for the Hilbert space is labelled by the elements of the set of all possible combinations

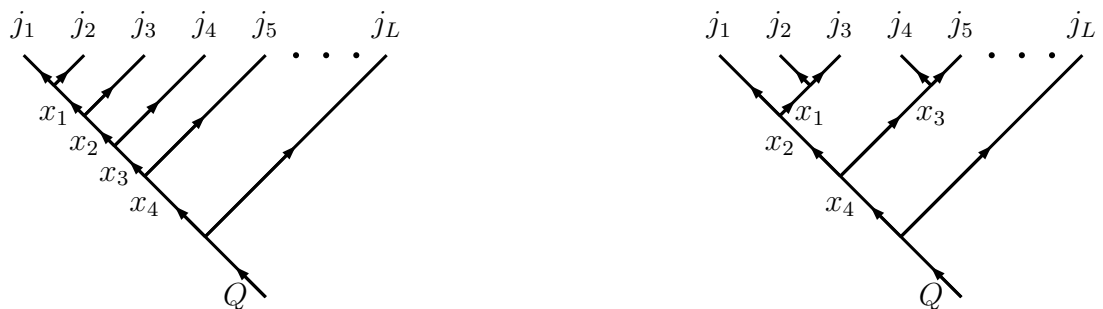


Figure 4.1: Fusion trees in the standard basis (left) and a dimerized basis (right)

$$\begin{aligned}
& h_i \text{ (diagram with } x_{i-2}, x_{i-1}, x_i, j_i, j_{i+1} \text{)} \\
&= \sum_{x'_{i-1}} E_{x'_{i-1}} [F_{x_i}^{x_{i-2}j_i j_{i+1}}]_{x_{i-1}, x'_{i-1}} \text{ (diagram with } x_{i-2}, x_{i-1}, x_i, j_i, j_{i+1}, x'_{i-1} \text{)} \\
&= \sum_{x'_{i-1}, x''_{i-1}} E_{x'_{i-1}} [F_{x_i}^{x_{i-2}j_i j_{i+1}}]_{x_{i-1}, x'_{i-1}} [F_{x_i}^{x_{i-2}j_i j_{i+1}}]^\dagger_{x'_{i-1}, x''_{i-1}} \text{ (diagram with } x_{i-2}, x_{i-1}, x_i, j_i, j_{i+1}, x''_{i-1} \text{)}
\end{aligned}$$

Figure 4.2: The action of h_i

of labels allowed by the fusion rules. For example, in the standard basis, the fusion rules enforce that

$$x_i \times j_{i+2} = x_{i+1} + \dots \quad \forall i \quad (4.1)$$

For chains like this the Hamiltonian is a sum of local Hamiltonians;

$$H = \sum_{i=1}^{L-1} h_i \quad (4.2)$$

where h_i depends on the nearest neighbour interaction between j_i and j_{i+1} . Each h_i acting on a state $|x_1, x_2, \dots, Q\rangle$ applies a basis change to a basis where j_i and j_{i+1} fuse directly, assigns an energy depending on the fusion outcome and applies a basis change back to the original basis. From this we can see that in the dimerized basis h_{2i} will be diagonal. In the standard basis h_i acts as in 4.2.

With the process of constructing a Hamiltonian defined, let us now sink our teeth into some concrete models.

4.2 Tambara-Yamagami Fusion Model

The first model we consider is the Tambara-Yamagami (TY) fusion model [61]. This model has a choice of finite abelian group, G , associated with it. For example, with $G = \mathbb{Z}_2$, we get the well known Ising anyon model [15]. This model only allows for braiding when G is a 2-group [62], i.e. G contains only elements of order 2, and so is not an anyon model in general. However it has solutions for the Pentagon equations for any finite abelian G so we may construct a Hamiltonian for this model for any such G .

\mathcal{C} consists of a label for each group element $g_i \in G$ and one extra label σ . The fusion rules for this model are

$$\begin{aligned} \sigma \times \sigma &= \sum_{g_i \in G} g_i, \\ \sigma \times g_i &= \sigma, \\ g_i \times g_j &= g_i g_j \quad g_i, g_j \in G \end{aligned} \tag{4.3}$$

where $g_i g_j$ is the label corresponding to the element of G which is the result of performing the group operation on g_i and g_j . The F-matrices for this model are

$$\begin{aligned} F^{g_1, g_2, g_3} &= F^{g_1, g_2, \sigma} = F^{\sigma, g_1, g_2} = 1 \\ F^{g_1, \sigma, g_2} &= F_{g_2}^{\sigma, g_1, \sigma} = \chi(g_1, g_2) \\ F_{g_2}^{\sigma, \sigma, g_1} &= F_{g_2}^{g_1, \sigma, \sigma} = 1 \\ [F^{\sigma, \sigma, \sigma}]_{g_1, g_2} &= t^{-1} \chi(g_1, g_2) \\ t &= \pm \sqrt{|G|} \end{aligned} \tag{4.4}$$

The lower label of F has been omitted where the three incoming labels have a unique fusion outcome. The map, χ , is a symmetric, non-degenerate bichar-

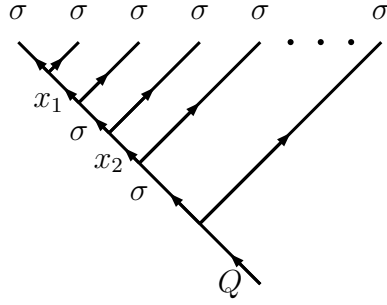


Figure 4.3: Generic basis state of the TY chain in the standard basis

acter which means for $g_1, g_2, g_3 \in G$

$$\begin{aligned}
 \chi(g_1 g_2, g_3) &= \chi(g_1, g_3) \chi(g_2, g_3) \\
 \chi(g_1, g_2 g_3) &= \chi(g_1, g_2) \chi(g_1, g_3) \\
 \chi(g_1, g_2) &= \chi(g_2, g_1)
 \end{aligned} \tag{4.5}$$

where the last condition makes the bicharacter symmetric. For $G = \mathbb{Z}_n$

$$\begin{aligned}
 \chi(1, 1) &= e^{\frac{2\pi i k}{n}} \quad k \in \{a \in \{0, 1, \dots, n-1\} | \gcd(a, n) = 1\} \\
 \chi(a, b) &= \chi(1, 1)^{ab} = e^{\frac{2\pi i k a b}{n}}
 \end{aligned} \tag{4.6}$$

with $\gcd(a, n) = 1$ making the bicharacter non-degenerate. Here we will let $k = 1$. We consider chains of L σ 's in the standard basis as in 4.3. We have included coupling constants $f, J \geq 0$ so the Hamiltonian will read

$$H = J \sum_{i=1}^{\frac{L}{2}} h_{2i-1} + f \sum_{i=1}^{\frac{L-2}{2}} h_{2i} \tag{4.7}$$

Due to fusion constraints, every second intermediate label is σ . In this thesis we will only consider chains of even length. This gives a model with similar couplings to the example of the quantum Ising chain earlier. Setting one of the coupling constants to 0 causes the Hamiltonian to be independent of the final label, creating a degeneracy between states which differ only by the final labels.

We will now construct the local Hamiltonians for this chain. The local Hamiltonians will take a different form depending on whether they act on an

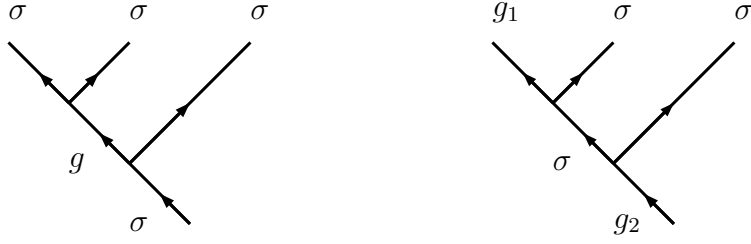


Figure 4.4: Even and odd sites of the TY chain

even or odd site.

First we show h_i for i even. This will act on a state labelled by $|x_1\sigma x_2\dots\sigma g\sigma\dots\sigma Q\rangle$ which we shorten to $|\sigma g\sigma\rangle$.

$$\begin{aligned}
h_i|\sigma g\sigma\rangle &= \sum_{x'_i x''_i} (F^{\sigma\sigma\sigma})^\dagger_{x'_i, x''_i} E_{x'_i} (F^{\sigma\sigma\sigma})_{g, x'_i} |\sigma x''_i \sigma\rangle \\
&= t^{-2} \sum_{x'_i x''_i} E_{x'_i} \chi_{g, x'_i} \chi_{x'_i, x''_i}^\dagger |\sigma x''_i \sigma\rangle \\
&= \frac{1}{n} \sum_{x'_i x''_i} E_{x'_i} \chi_{g, x'_i} \chi_{x'_i, x''_i}^\dagger |\sigma x''_i \sigma\rangle
\end{aligned} \tag{4.8}$$

where $E_{x'_i} \in \mathbb{R}$ is the energy assigned to the fusion of j_i and j_{i+1} , the incoming σ 's in positions i and $i+1$. We can now write the Hamiltonian which acts on the even sites of the chain as

$$H_E = f \sum_{i=1}^{\frac{L-1}{2}} \alpha_{2i} \tag{4.9}$$

where

$$\begin{aligned}
\alpha_{kj} &= \frac{1}{n} \sum_{x'_k} E_{x'_k} \chi_{k, x'_k} \chi_{x'_k, j}^\dagger \\
&= \frac{1}{n} \sum_{x'_k} E_{x'_k} \omega^{x'_k(k-j)}
\end{aligned} \tag{4.10}$$

where $\omega = e^{\frac{2\pi i}{n}}$. Note that k here is merely an index and not the k we previously set to 1. We see each α has the property that if $(i-j) \bmod n = (k-l) \bmod n$, then $\alpha_{ij} = \alpha_{kl}$. Matrices with this property are generated by the matrix τ defined by

$$\tau_{ij} = \delta_{(i-j) \bmod n, 1} \tag{4.11}$$

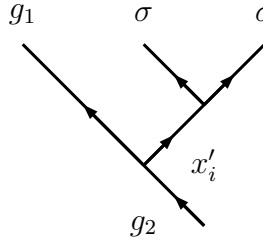
In our case

$$\begin{aligned}\alpha &= \sum_{i=0}^{n-1} \tau^i \left(\sum_{j=0}^{n-1} \omega^{ij} E_j \right) \\ &= \sum_{i=0}^{n-1} \nu_i \tau^i\end{aligned}\tag{4.12}$$

We now shift our focus to the odd sites of the chain. h_i acts on a site labelled by $|x_1 \sigma x_2 \dots g_1 \sigma g_2 \dots \sigma Q\rangle$ which again we shorten to $|g_1 \sigma g_2\rangle$.

$$h_i |g_1 \sigma g_2\rangle = \sum_{x'_i, x''_i} (F_{g_2}^{g_1 \sigma \sigma})^\dagger_{x'_i, x''_i} E_{x'_i} (F_{g_2}^{g_1 \sigma \sigma})_{\sigma, x'_i} |g_1 x''_i g_2\rangle\tag{4.13}$$

Clearly $x''_i = \sigma$ and if we look at the basis where j_i and j_{i+1} fuse



$$\tag{4.14}$$

then it is clear that $x'_i = g_2 - g_1$. By this we mean that

$$g_1 x'_i = g_2\tag{4.15}$$

under the group operation. This gives a unique result for x'_i since G is abelian.

We are left with

$$h_i |g_1 \sigma g_2\rangle = E_{g_2 - g_1} |g_1 \sigma g_2\rangle\tag{4.16}$$

We write the Hamiltonian acting on odd sites of the chain as

$$H_O = J \sum_{i=1}^{\frac{L}{2}} \beta_{2i-1}\tag{4.17}$$

where

$$\beta = \sum_{m=0}^{n-1} \frac{1}{n} \nu_m (\sigma \otimes \sigma^\dagger)^m \quad (4.18)$$

$$\sigma_{ij} = \delta_{ij} \omega^{i-1}$$

Note that $\nu_m^* = \nu_{n-m}$. The full Hamiltonian is now written

$$H = f \sum_{i=2,4,6,\dots}^{L-2} \sum_{m=0}^{n-1} \nu_m (\tau_i)^m + J \sum_{i=1,3,5,\dots}^{L-1} \sum_{m=0}^{n-1} \nu_m (\sigma_i \sigma_{i+1}^\dagger) \quad (4.19)$$

which is the Hamiltonian for a \mathbb{Z}_n chiral clock model! Calculating α and β explicitly for $G = \mathbb{Z}_3$ we get

$$\alpha_i = \frac{1}{3} [(E_0 + E_1 + E_2)\mathbb{I} + (E_0 + \omega E_1 + \omega^2 E_2)\tau + (E_0 + \omega^2 E_1 + \omega E_2)\tau^2]$$

$$\beta_i = \frac{1}{3} [(E_0 + E_1 + E_2)\mathbb{I} + (E_0 + \omega^2 E_1 + \omega E_2)(\sigma^\dagger \otimes \sigma) + (E_0 + \omega E_1 + \omega^2 E_2)(\sigma \otimes \sigma^\dagger)] \quad (4.20)$$

We can rescale and shift E_0 , E_1 and E_2 such that $E_0 + \omega E_1 + \omega^2 E_2 = 3e^{i\phi}$ for $\phi \in [0, 2\pi)$ and so the Hamiltonian can be written in the form

$$H = \sum_i [f(\frac{1}{3}(E_0 + E_1 + E_2)I + e^{-i\phi}\tau_i + e^{i\phi}\tau_i^\dagger) + J(\frac{1}{3}(E_0 + E_1 + E_2)I \otimes I + \sigma_i^\dagger \sigma_{i+1} e^{-i\phi} + \sigma_i \sigma_{i+1}^\dagger e^{i\phi})] \quad (4.21)$$

The Hamiltonian for the \mathbb{Z}_3 chiral clock model is usually written

$$H = -f \sum_{j=1}^L (\tau_j^\dagger e^{-i\phi} + \tau_j e^{i\phi}) - J \sum_{j=1}^{L-1} (\sigma_j^\dagger \sigma_{j+1} e^{-i\psi} + \sigma_j \sigma_{j+1}^\dagger e^{i\psi}) \quad (4.22)$$

which is the same as our result up to a constant term if $\psi = \phi$. So this fusion model really is a chiral clock model in disguise. We note that we can remove the condition that $\psi = \phi$ if we allow our choices of E_i to vary across odd and even sites.

$$E_0^{O/E} + \omega E_1^{O/E} + \omega^2 E_2^{O/E} = 3e^{i\phi/\psi} \quad (4.23)$$

Being equivalent to the \mathbb{Z}_n chiral clock model means this fusion model also has all the same zero modes. While a bit underwhelming in terms of finding new zero modes, this is a good starting point in our investigation into the types of zero modes found in anyonic systems. The existence of strong zero modes in non-abelian fusion models is an indicator that the search for strong zero modes in non-abelian anyon models will bear fruit. In the following sections,

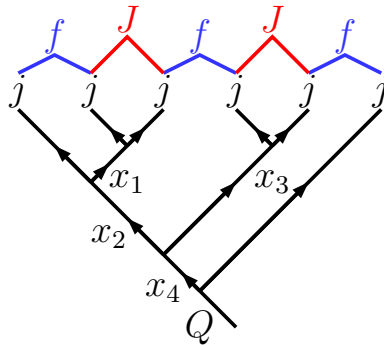


Figure 4.5: Anyon chain of 6 anyons of type j including coupling constants f and J at odd and even sites respectively.

the anyon chains we study will take the form shown in Figure 4.5. The chains will be of even length with

$$H = f \sum_{i \text{ odd}} h_i + J \sum_{i \text{ even}} h_i \quad (4.24)$$

This gives a construction similar to that of the quantum Ising chain. With $f = 0$, it is clear that the Hamiltonian will not depend on the final label, Q . In this case, were a zero mode to be present, we might expect it to change Q while leaving the labels, x_i , unchanged for odd i . Such a zero mode would clearly be exact for $f = 0$. A potential symmetry would then involve a measurement of the final label.

4.3 Fibonacci Anyon Chain

A natural starting point for our study of non abelian anyon chains is the Fibonacci anyon model. This is one of the simplest models which exhibits non abelian statistics [46, 63, 64]. Despite the simplicity of the model, Fibonacci

anyons have been shown to be universal for quantum computation under braiding [63–65]. Due to this, there is great interest in realising Fibonacci models experimentally. In recent years research has suggested that a phase supporting Fibonacci anyons emerges from \mathbb{Z}_3 parafermion systems [66–70]. Projective Hamiltonians as we have described here have already been constructed for chains of interacting Fibonacci anyons, or the "golden chain", as it is often referred to as [59, 60].

The model consists of just two labels, $\mathcal{C} = \{1, \tau\}$, with fusion rules

$$\begin{aligned} 1 \times \tau &= \tau \\ \tau \times \tau &= 1 + \tau \end{aligned} \tag{4.25}$$

and the only non trivial F-matrix, acting on the local Hilbert space $\{|\tau 1 \tau\rangle, |\tau \tau \tau\rangle\}$, is given by

$$(F_{\tau}^{\tau\tau\tau}) = \begin{pmatrix} \phi^{-1} & \phi^{-\frac{1}{2}} \\ \phi^{-\frac{1}{2}} & -\phi^{-1} \end{pmatrix} \tag{4.26}$$

where $\phi = \frac{1+\sqrt{5}}{2}$ is the golden ratio. The dimension of the Hilbert space for a chain of L Fibonacci anyons grows like the Fibonacci sequence. The dimension for this chain is given by the sum of the dimensions of the chains of length $L - 1$ and $L - 2$.

$$\dim(L) = \dim(L - 1) + \dim(L - 2) \tag{4.27}$$

A model with only two types of anyons is appealing as it circumvents a known issue with the zero modes in the chiral clock models. This is the issue of resonance [32]. In extremely brief terms, resonance points occur at the crossings of different energy bands in the unperturbed system. The unperturbed system is the system with $f = 0$. In the chiral clock models the energy of a state in the unperturbed system depends only on the number of each type of so called domain wall in the state. We mentioned previously that a state of the chiral clock model was labelled by L sites with n possible states. If a state is labelled

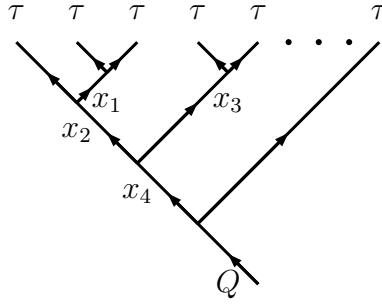


Figure 4.6: Fibonacci chain in the dimerized basis. We write this state as $|x_1 x_2 x_3 \dots x_{L-3} x_{L-2} Q\rangle$ where L is the number of incoming anyons.

by

$$|c_1, c_2, \dots, c_L\rangle \quad c_i \in \mathbb{Z}_n \quad (4.28)$$

then there are $L - 1$ domain walls which are the differences between the values at successive sites modulo n and so are written.

$$(c_1 - c_2, c_2 - c_3, \dots, c_{L-1} - c_L) \bmod n \quad (4.29)$$

Two states are in the same energy band if they have the same number of domain walls of each type. At the points in parameter space where these energy bands cross in the unperturbed system we have different sets of domain walls with the same energy. These can be locally changed into each other by a perturbation, hybridising the bands. This destroys the zero mode at these resonance points.

We will consider chains of L incoming τ anyons in the dimerized basis as in figure 4.6. Setting $f = 0$ then the total energy of this system is $\sum_{i \text{ odd}} E_{x_i}$. In other words the energy bands in this case are given by the number of τ and 1 anyons among the x_i for i odd. For energy bands to cross in the unperturbed system we need

$$\sum_i n_i E_i = \sum_i m_i E_i \quad (4.30)$$

where $i \in \{1, \tau\}$ and n_i and m_i are the numbers of anyons of type i which contribute to the energy. Clearly this does not hold when we only have two anyon types unless $n_i = m_i$ or $E_1 = E_\tau$. In the dimerized basis, the anyons at x_i for i odd correspond to the domain wall types mentioned above. It would appear the Fibonacci chain does not allow for resonances then and we might

naively hope to see a strong zero mode in this chain. However, these hopes are dashed if we notice that if a potential zero mode operator were to map between states with different values of Q , we may not expect such a strong zero mode operator to exist in this chain. This is due to the fact that $Q = 1$ necessitates that $x_{L-2} = \tau$ but $Q = \tau$ allows x_{L-2} to be 1 or τ .

When looking at this system we notice that when $f = 0$ the Hamiltonian does not depend on the final label Q . This gives a doubly degenerate ground state $|1\tau1\tau1\tau\dots1\tau1\tau Q\rangle$, one for each possible label of Q . To check if these states are topologically degenerate we introduce $f > 0$ as a perturbation and check if the energies of these states split. If the ground states remain degenerate up to corrections which go to zero exponentially with increasing system size then we say the ground states are topologically degenerate and we have at least a weak zero mode.

We examine the perturbed Hamiltonian analytically up to second order. The only term in the Hamiltonian which depends on Q is h_{L-1} so the terms which split the degeneracy of the ground states will contain h_{L-1} . Figure 4.7 shows how h_{L-1} acts on a state $|\dots cbaQ\rangle$

$$h_{L-1}|\dots cbaQ\rangle = \sum_{a',b',a'',b''} E_{b'} [F_Q^{cb\tau}]_{a,a'} [F_{a'}^{\tau\tau\tau}]_{b,b'} [F_{a'}^{\tau\tau\tau}]_{b',b''}^\dagger [F_Q^{cb''\tau}]_{a',a''}^\dagger |cb''a''Q\rangle \quad (4.31)$$

The first order correction to H acting on $|\dots cbaQ\rangle$ and containing h_{L-1} is

$$\langle \dots cbaQ | h_{L-1} | \dots cbaQ \rangle = \sum_{a',b'} E_{b'} [F_Q^{cbj}]_{a,a'}^2 [F_{a'}^{jjj}]_{b,b'}^2 \quad (4.32)$$

for a model with incoming anyons of type j . Of course here we have $j = \tau$. Calculating this correction for a ground state ($|GS\rangle$) we see $b = 1$ and so

$$[F_Q^{cb\tau}]_{a,a'}^2 = [F_Q^{c1\tau}]_{a,a'}^2 = 1 \quad \forall Q \quad (4.33)$$

showing the first order correction is independent of Q . The terms in the second

$$\begin{aligned}
& h_{L-1} \text{ (diagram)} = \sum_{a', b', a'', b''} E_{b'} [F_Q^{cb\tau}]_{a,a'} [F_{a'}^{\tau\tau\tau}]_{b,b'} [F_{a''}^{\tau\tau\tau}]_{b',b''}^\dagger [F_Q^{cb'\tau}]_{a',a''}^\dagger \\
& = \sum_{a', b', a'', b''} E_{b'} [F_Q^{cb\tau}]_{a,a'} [F_{a'}^{\tau\tau\tau}]_{b,b'} [F_{a''}^{\tau\tau\tau}]_{b',b''}^\dagger [F_Q^{cb'\tau}]_{a',a''}^\dagger \text{ (diagram)}
\end{aligned}$$

Figure 4.7: h_{L-1} acting at the end of the chain

order correction which may depend on Q are

$$\begin{aligned}
& \sum_i \langle GS | h_{L-1} | m_i \rangle \langle m_i | h_{L-1} | GS \rangle \\
& | m_i \rangle = | 1\tau 1\tau \dots \tau\tau iQ \rangle
\end{aligned} \tag{4.34}$$

Evaluating the sum over i we get

$$([F_Q^{\tau\tau\tau}]_{1,\tau}^2 + [F_Q^{\tau\tau\tau}]_{\tau,\tau}^2) \left[\sum_{b',d'} E_{b'} E_{d'} [F_{\tau}^{\tau\tau\tau}]_{1,b'} [F_{\tau}^{\tau\tau\tau}]_{\tau,d'} [F_{\tau}^{\tau\tau\tau}]_{b',\tau}^\dagger [F_{\tau}^{\tau\tau\tau}]_{d',1}^\dagger \right] \tag{4.35}$$

Any Q dependence of this is contained in the first bracket which we can write simply as

$$\sum_y [F_Q^{\tau\tau\tau}]_{y,\tau}^2 = 1 \tag{4.36}$$

where we sum over all possible labels y . We know this identity holds for any Q since all F-matrices are unitary. So there are no Q dependent terms in the perturbative expansion of H up to second order. Numerical checks show that the splitting of the ground states grows proportionally to f^p where $p \propto L$. This indicates that the order at which terms which split the degeneracy of the ground states appear depends on the length of the chain. We know then that the ground states are degenerate, implying the existence of at least a weak zero mode.

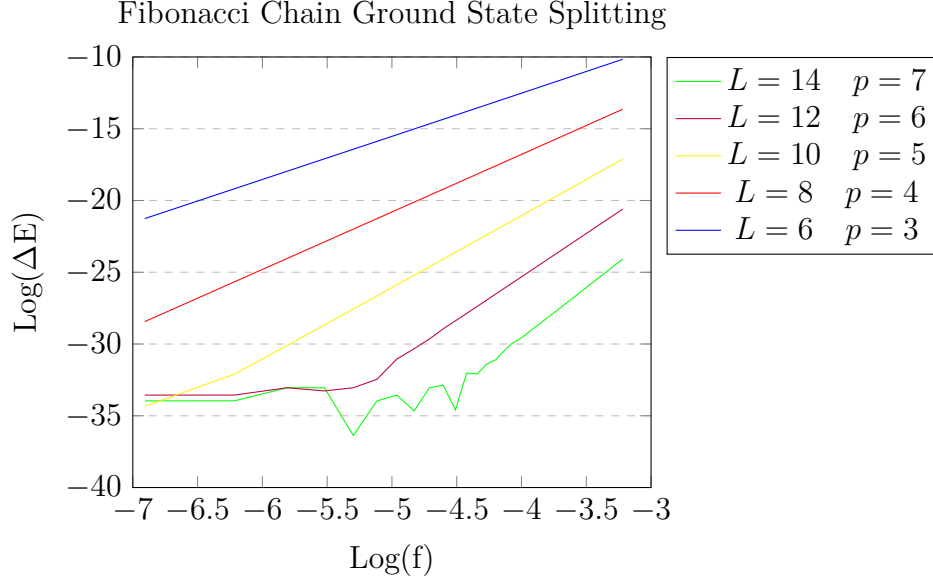


Figure 4.8: Splitting of the two ground states, ΔE , grows proportionally to f^p where $p \propto L$. The plots for $L = 12$ and $L = 14$ are distorted at small f as e^{-35} is close to machine precision.

If this model has a strong zero mode then it should be possible to find a similar result for the excited states. Let us first look at Q dependent terms in the first order correction of H acting on a simple excited state.

$$|\phi_Q\rangle = |1\tau1\tau\dots\tau\tau\tau Q\rangle \quad (4.37)$$

$|\phi_Q\rangle$ is the state which is identical to the ground state except $x_{L-3} = \tau$. The first order correction for H acting on this state is

$$\langle\phi_Q|h_{L-1}|\phi_Q\rangle = \sum_{a,b} E_b [F_Q^{\tau\tau\tau}]_{\tau a}^2 [F_a^{\tau\tau\tau}]_{\tau b}^2 \quad (4.38)$$

We calculate the correction explicitly for $Q = 1$ and $Q = \tau$ and find

$$\begin{aligned} \langle\phi_1|h_{L-1}|\phi_1\rangle &= \phi^{-1}E_1 + \phi^{-2}E_\tau \\ \langle\phi_\tau|h_{L-1}|\phi_\tau\rangle &= \phi^{-3}E_1 + (\phi^{-4} + \phi^{-1})E_\tau \end{aligned} \quad (4.39)$$

The degeneracy is split at first order! This system has no strong zero mode. Before we move on let us take a closer look at the first order correction we just calculated to see why this might be. There is in fact a third state which has a

single τ excitation at x_{L-3} . We see that the state $|m_1\rangle$ from 4.34 is the third state and

$$\langle m_1 | h_{L-1} | m_1 \rangle = \phi^{-2} E_1 + \phi^{-1} E_\tau \quad (4.40)$$

The degeneracy between all three states is broken at first order. The extra degeneracy on the second last label in this case or the labels x_{2i} , which are the labels along the spine of the chain, in general causes the degeneracy of the excited states to split at first order. We did not have this issue for the ground states as in that case the labels x_{2i} were fixed to be τ by the fusion rules.

In circumventing the issue of resonance that exists in the chiral clock model we have bumped up against an 'anyonic resonance'. This is independent of our choices of energy but instead is a consequence of degeneracies created by the fusion rules. We make the comparison to resonance by thinking about the TY chain in the dimerized basis. In this basis, there is a direct correspondence between the domain wall types in the chiral clock model and the differences between the labels, x_i and x_{i+2} for i odd. However, each label on the spine of the tree in this basis is forced to be σ so there are no possible band crossings at $f = 0$ other than those already discussed. This is not the case for general anyon models as seen above for Fibonacci anyons. If we instead choose to label bands by every label of the tree, then we have degenerate bands and thus resonance from trees with the same odd labels but different labels on the spine.

In the Fibonacci chain $Q = 1$ only when $x_{L-2} = \tau$ while Q may be τ regardless of the value of x_{L-2} . The Hilbert space with $Q = 1$ is smaller than that with $Q = \tau$ (although the degeneracy is still split at first order were we to restrict ourselves to states with $x_{L-2} = \tau$). Perhaps this 'resonance' may be avoided if we look at models with anyons that behave identically when fusing with our choice of incoming anyon i.e. models with a set of labels

$$a_i \quad i \in \{1, 2, \dots, N\} \quad (4.41)$$

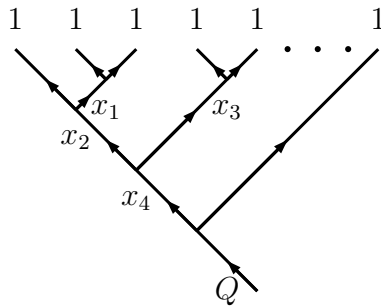


Figure 4.9: $SU(2)_4$ chain in the dimerized basis.

for some $N > 1$ such that

$$a_i \times j = a_k \times j \quad i \neq k \quad (4.42)$$

Fortunately such a model exists, is well known and has only three types of anyons which we will need to deal with.

4.4 $SU(2)_4$ Anyon Chain

Fibonacci anyons are part of a larger class of $SU(2)_k$ anyons. The $SU(2)_k$ models are 'q-deformed' versions of $SU(2)$ [7]. These models have anyonic charges $\mathcal{C} = \{0, \frac{1}{2}, \dots, \frac{k}{2}\}$ and have fusion rules

$$j_1 \times j_2 = \sum_{j=|j_1-j_2|}^{\min\{j_1+j_2, k-j_1-j_2\}} j \quad (4.43)$$

As $k \rightarrow \infty$ these fusion rules become the usual tensor product rules for $SU(2)$. The general form of the F-matrices are given in [71]. For $k = 3$ one can identify the τ of the Fibonacci model with the $j = 1$ anyon in the $SU(2)_3$ model.

The model we are particularly interested in is a chain of $SU(2)_4$ anyons. We consider a chain of incoming anyons of type 1 set up identically to the Fibonacci chain we looked at in the previous section. Since the anyons we are fusing are all of type 1 we need only consider the integer labels of $SU(2)_4$. We

are effectively working with a model with $\mathcal{C} = \{0, 1, 2\}$ and fusion rules

$$\begin{aligned} 1 \times 1 &= 0 + 1 + 2 \\ 1 \times 2 &= 1 \\ 2 \times 2 &= 0 \end{aligned} \tag{4.44}$$

0 is the identity particle here so fusion with it is trivial. The only F-matrix with dimension greater than 1 is

$$[F_1^{1,1,1}] = \begin{pmatrix} \frac{1}{2} & \frac{-1}{\sqrt{2}} & \frac{1}{2} \\ \frac{-1}{\sqrt{2}} & 0 & \frac{1}{\sqrt{2}} \\ \frac{1}{2} & \frac{1}{\sqrt{2}} & \frac{1}{2} \end{pmatrix} \tag{4.45}$$

which acts on the local Hilbert space, $\{|101\rangle, |111\rangle, |121\rangle\}$. We notice a few things from the fusion rules and F-matrices. Firstly, fusing 0 or 2 with 1 gives the same result. Secondly, chains with $Q = 0$ and $Q = 2$ both have the requirement that $x_{L-2} = 1$. This tells us that for each state with $Q = 0$ there is a corresponding state with all the same labels except $Q = 2$. The Hilbert space is the same size in both sectors, providing at least two potential symmetry sectors for a zero mode to map between. We also notice

$$[F_1^{111}]_{0,0} = [F_1^{111}]_{0,2} = [F_1^{111}]_{2,0} = [F_1^{111}]_{2,2} = \frac{1}{2} \tag{4.46}$$

which makes it likely that terms in the perturbative expansion of H which depend on Q will be the same for $Q = 0$ and $Q = 2$. There is a potential issue which could be caused by the fact that

$$[F_1^{111}]_{0,1} = [F_1^{111}]_{1,0} = -[F_1^{111}]_{2,1} = -[F_1^{111}]_{1,2} = -\frac{1}{\sqrt{2}} \tag{4.47}$$

and some other 1 dimensional F-matrices have their sign changed when swap-

ping a 0 for a 2 such as

$$[F_1^{121}]_{1,1} = -[F_1^{101}]_{1,1} = -1 \quad (4.48)$$

so the sign of Q dependent terms in the expansion of h_{L-1} could change depending on whether $Q = 0$ or $Q = 2$. However in the Fibonacci chain F-symbols appeared in terms like

$$[F_\tau^{\tau\tau\tau}]_{1,b} [F_\tau^{\tau\tau\tau}]_{b,\tau}^\dagger \quad (4.49)$$

or as square terms so the minus signs in the F-symbols may be squared wherever they appear.

For this model we take $E_0 < E_1 < E_2$. In this regime the ground states of the unperturbed system are

$$|GS\rangle = |010101\dots 01Q\rangle \quad Q \in \{0, 1, 2\} \quad (4.50)$$

This time we have a threefold degenerate ground state. In the ground state each intermediate charge on the spine of the tree, x_{2i} , is fixed to be 1. After what we saw in the Fibonacci case we would expect the ground states to remain topologically degenerate in the perturbed system. As before we expand h_{L-1} and test for Q dependence. The first order correction to h_{L-1} acting on a ground state is

$$\langle GS | h_{L-1} | GS \rangle = \sum_{b'} E_{b'} [F_Q^{101}]_{1,1}^2 [F_1^{111}]_{0,b'} \quad (4.51)$$

but

$$[F_Q^{101}]_{1,1}^2 = 1 \quad \forall Q \quad (4.52)$$

so as expected the first order correction is independent of Q . The second order

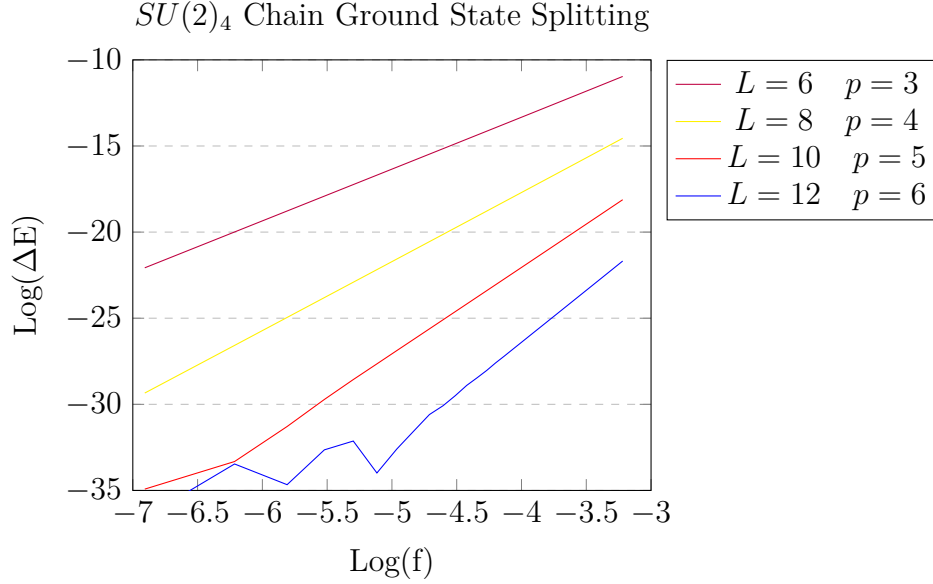


Figure 4.10: Splitting of the $SU(2)_4$ ground state, ΔE , grows proportionally to f^p where $p \propto L$. Here we set $E_0 = 0$, $E_1 = \frac{1}{\sqrt{2}}$, $E_2 = 1$.

correction is

$$\sum_{i=0}^2 \langle GS | h_{L-1} | m_i \rangle \langle m_i | h_{L-1} | GS \rangle \quad (4.53)$$

$$m_i = |010101\dots 11iQ\rangle$$

As in the Fibonacci chain the Q dependence of this term will come from

$$\sum_y [F_Q^{111}]_{y1}^2 = 1 \quad (4.54)$$

which again is true by unitarity of the F-matrices. The second order correction is therefore independent of Q . Performing the same numerical calculations that we did for the Fibonacci chain we see that the ground states are topologically degenerate in the perturbed system and so the system should have at least a weak zero mode. We wish to see if the system has a strong zero mode so we now check the splitting of the excited states. Let us consider the excited states of the unperturbed chain

$$|\phi_{Q1}\rangle = |010101\dots 111Q\rangle \quad (4.55)$$

$$|\phi_{Q2}\rangle = |010101\dots 121Q\rangle$$

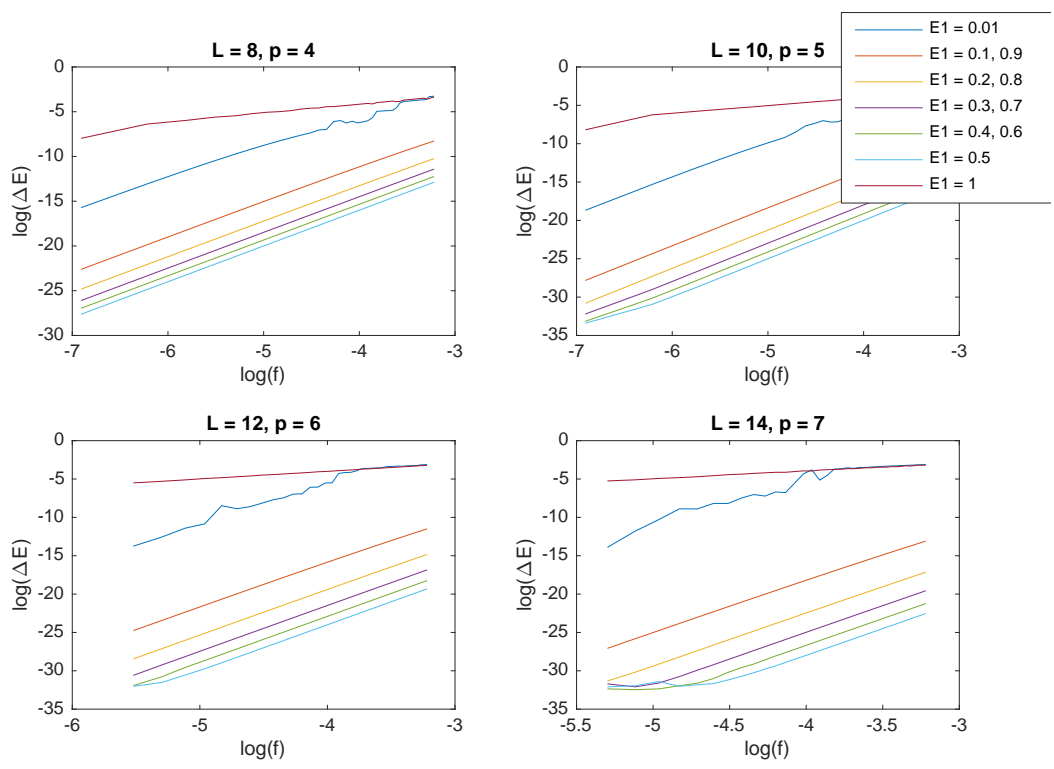


Figure 4.11: Plots of the \log of the maximum splitting of eigenstates with $Q = 0$ and $Q = 2$. Each line in the plot corresponds to a different value of $E1$. In each plot $E0 = 0$, $E2 = 1$ and $E1$ is varied from 0 to 1. At the top of each plot, length of the chain and the slope of the lines in the plot are given. We see as L grows the \log of the splitting of each eigenstate grows proportionally to $\log(f)$, showing that $Q = 0$ and $Q = 2$ eigenstates remain topologically degenerate throughout the spectrum. $p = 1$ lines in each plot show resonance points exist at $E1 = E0$ and $E1 = E2$ but, remarkably, no others.

The first order corrections of h_{L-1} acting on these states is given by

$$\begin{aligned} \langle \phi_{Q1} | H_{L-1} | \phi_{Q1} \rangle &= \sum_{a,b} E_b [F_Q^{111}]_{1a}^2 [F_a^{111}]_{1b}^2 \\ \langle \phi_{Q2} | H_{L-1} | \phi_{Q2} \rangle &= \sum_b E_b [F_Q^{121}]_{11}^2 [F_1^{111}]_{1b}^2 \end{aligned} \quad (4.56)$$

$[F_Q^{121}]_{1,1}^2 = 1$ for any Q so $\langle \phi_{Q2} | h_{L-1} | \phi_{Q2} \rangle$ is independent of Q . However evaluating the other correction explicitly we get

$$\begin{aligned} \langle \phi_{01} | H_{L-1} | \phi_{01} \rangle &= \frac{E_0}{2} + \frac{E_2}{2} \\ \langle \phi_{21} | H_{L-1} | \phi_{21} \rangle &= \frac{E_0}{2} + \frac{E_2}{2} \\ \langle \phi_{11} | H_{L-1} | \phi_{11} \rangle &= E_1 \end{aligned} \quad (4.57)$$

Similar to before, extra degeneracy on the spine of the chain arises due to the presence of a 1 excitation. We don't see this for a 2 excitation since $x_{2i+1} = 2$ always fixes the label x_{2i+2} . However all is not lost. While this extra degeneracy

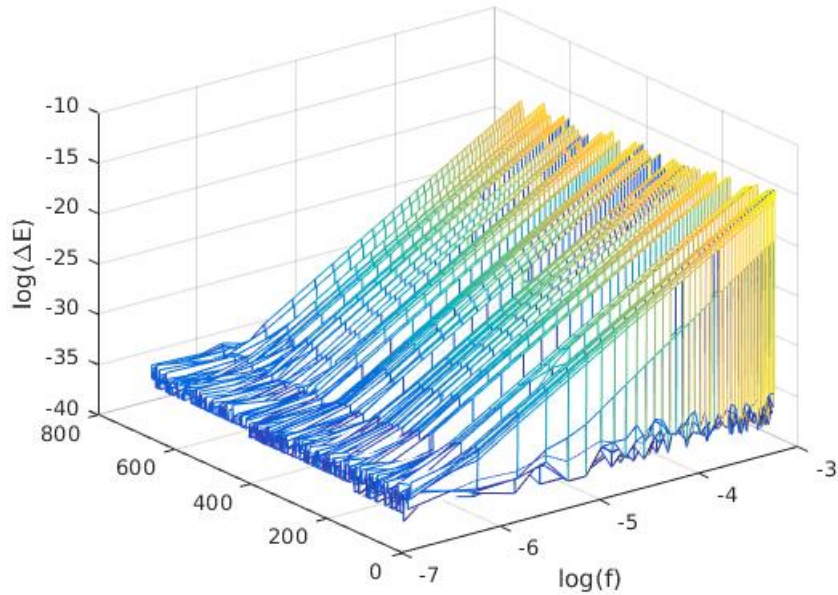


Figure 4.12: Log of the splitting of all $Q = 0$ and $Q = 2$ eigenstates of an $L = 12$ chain with $E_1 = \frac{1}{3}$ plotted against $\log(f)$. The splitting grows as f^6 as expected.

splits the degeneracy of $Q = 0/2$ states with $Q = 1$ states at first order, the first order correction does not split the $Q = 0$ and $Q = 2$ sectors. We collected numerical data on the splitting of states with $Q = 0$ with the corresponding identical states with $Q = 2$. We allowed E_1 to vary from 0 to 1 and we set $E_0 = 0$ and $E_2 = 1$. We plotted the maximum splitting of $Q = 0$ and $Q = 2$ states for each value of E_1 in Figure 4.11. The logic behind this is that if the maximum splitting scales exponentially to zero with increasing system size then all splittings must also scale exponentially to zero at the slowest. We also plotted the splitting of all 683 eigenstates in the $Q = 0/2$ sectors on a chain of length 12 and $E_1 = \frac{1}{3}$ in Figure 4.12.

Our numerics suggest that states in the 0 and 2 sectors remain topologically degenerate throughout the entire spectrum, hinting at the existence of a strong zero mode in this chain. We would very much like to be able to construct this zero mode using an iterative process similar to what has been shown for the Ising chain.

To do this we will make use of the fact that an $SU(2)_4$ anyon chain can be written as a D_3 symmetric XXZ spin chain [71, 72]. This is encouraging as

XYZ spin chains have already been shown to possess strong zero modes [73]. So without further ado let us plough ahead and try to explicitly construct this anyonic zero mode.

4.5 Constructing the Zero Mode

In this section we will construct the strong zero mode suggested to exist by the numerical work in the previous section. Following the work detailed in [71] we map the Hamiltonian of the $SU(2)_4$ chain to that of a staggered XXZ chain. Staggered or dimerized XXZ chains, as they are sometimes referred to in the literature, are known to possess edge zero modes as described in [74]. We then use the methods outlined in [33] to construct the zero mode in terms of spin operators. These operators can then be mapped back to the anyon formalism, giving us the form of the anyonic strong zero mode. We also perform this procedure for a system more similar to that described in [73] which possesses strong zero modes which we can easily write the general n^{th} order term for, allowing us to say exactly when the zero mode is normalisable.

We start with a brief summary of how to map between the $SU(2)_4$ anyon chain and the XXZ spin chain. This is done in more detail in [71]. The two models are equivalent up to the size of the Hilbert space, as shown below, because of the underlying D_3 symmetry in both. The group D_3 is the symmetry group of a triangle whose generators are

$$D_3 = \{\sigma, \tau | \sigma^3 = \tau^2 = \sigma\tau\sigma\tau = 1\} \quad (4.58)$$

where σ is a rotation and τ a flip. These generators can be represented graphically as

$$\begin{array}{ccc}
 \tau \begin{array}{c} \triangle \\ 2 \\ 1 \quad 3 \end{array} & = & \begin{array}{c} \triangle \\ 2 \\ 3 \quad 1 \end{array} \\
 \sigma \begin{array}{c} \triangle \\ 2 \\ 1 \quad 3 \end{array} & = & \begin{array}{c} \triangle \\ 3 \\ 2 \quad 1 \end{array}
 \end{array} \quad (4.59)$$

This group has three irreducible representations, say Π_+ , Π_- and Π_2 . Two of the representations are one dimensional and are given by

$$\Pi_{\pm}(\sigma) = 1 \quad \Pi_{\pm}(\tau) = \pm 1 \quad (4.60)$$

The remaining representation is two dimensional

$$\Pi_2(\sigma) = \begin{pmatrix} e^{\frac{2\pi i}{3}} & 0 \\ 0 & e^{-\frac{2\pi i}{3}} \end{pmatrix} \quad \Pi_2(\tau) = \begin{pmatrix} 0 & 1 \\ 1 & 0 \end{pmatrix} \quad (4.61)$$

We associate a vector space, V_a , with each Π_a . These spaces have the same fusion rules as the integer spins of the $SU(2)_4$ anyon model

$$\begin{aligned} V_- \otimes V_- &\cong V_+ \\ V_- \otimes V_2 &\cong V_2 \\ V_2 \otimes V_2 &\cong V_+ \oplus V_- \oplus V_2 \end{aligned} \quad (4.62)$$

and fusion with V_+ is trivial. To construct the anyon model V_+ , V_- and V_2 are identified with the 0, 2 and 1 anyons respectively. This leads to the discrepancy in the size of the Hilbert spaces of the two models. Every state in the anyonic Hilbert space which ends in a 1 anyon is identified with a 2 dimensional vector space. So for each such state in the anyon model there are 2 corresponding states in the spin model.

The Hilbert space for the spin model consists of L spin- $\frac{1}{2}$ particles coupled to a \mathbb{C}^4 space which acts as a particle reservoir

$$[V_2 \oplus V_+ \oplus V_-] \otimes V_2^L \quad (4.63)$$

A state in this Hilbert space is labelled by the total D_3 charge of the spins and an extra label indicating the internal state in the global D_3 representation acting on all the particles. This gives an identical structure to the anyon fusion tree. The \mathbb{C}^4 space is not needed to see the strong zero mode so we project

onto the V_+ component of the space, so the dimension of the Hilbert space is 2^L . The Hilbert space for the anyon model is as described in the previous section.

To express an operator in both models it must also possess an underlying D_3 symmetry. For an operator written in the anyon formalism this means both the first and final labels of the chain must be unchanged after we apply the operator whereas in the spin formalism the operator must commute with the group action of D_3 , meaning the overall D_3 label is conserved. The Hamiltonian does not change these labels and so can be expressed in the spin formalism. This turns out to be straightforward as the Hamiltonian is a sum of projection operators. Recall that the Hamiltonian is a sum of local Hamiltonians

$$H = \sum_i h_i \quad (4.64)$$

where h_i changes to a basis where the i^{th} and $(i+1)^{\text{th}}$ anyons fuse, assigns energy E_j to a fusion to the j anyon and changes back to the original basis. Taking the staggering we used in the last section into account we can write the $SU(2)_4$ Hamiltonian as

$$H = f \sum_{i=1,3,5\dots} (E_1 P_i^1 + P_i^2) + J \sum_{i=2,4,6\dots} (E_1 P_i^1 + P_i^2) \quad (4.65)$$

where P_i^j projects onto the j fusion channel for the i^{th} and $(i+1)^{\text{th}}$ incoming anyons, recalling that we set $E_0 = 0$ and $E_2 = 1$. These projectors can be

written in the standard basis as

$$\begin{aligned}
P_i^0 &= n_{i-2}^0 n_i^0 + n_{i-2}^2 n_i^2 + \frac{1}{4} n_{i-2}^1 n_i^1 \begin{pmatrix} 1 & -\sqrt{2} & 1 \\ -\sqrt{2} & 2 & -\sqrt{2} \\ 1 & -\sqrt{2} & 1 \end{pmatrix} \\
P_i^1 &= n_{i-2}^0 n_i^1 + n_{i-2}^1 n_i^0 + n_{i-2}^2 n_i^1 + n_{i-2}^1 n_i^2 + \frac{1}{2} n_{i-2}^1 n_i^1 \begin{pmatrix} 1 & 0 & -1 \\ 0 & 0 & 0 \\ -1 & 0 & 1 \end{pmatrix} \\
P_i^2 &= n_{i-2}^0 n_i^2 + n_{i-2}^2 n_i^0 + \frac{1}{4} n_{i-2}^1 n_i^1 \begin{pmatrix} 1 & \sqrt{2} & 1 \\ \sqrt{2} & 2 & \sqrt{2} \\ 1 & \sqrt{2} & 1 \end{pmatrix}
\end{aligned} \tag{4.66}$$

where $n_i^j = \delta_{x_i, j}$. The 3×3 matrices act on the subspace $|x_{i-2}, x_{i-1}, x_i\rangle \in \{|101\rangle, |111\rangle, |121\rangle\}$.

We can directly map these projectors to two site projectors in the spin model.

$$\begin{aligned}
P^0 &\leftrightarrow \tilde{P}^+ \\
P^1 &\leftrightarrow \tilde{P}^2 \\
P^2 &\leftrightarrow \tilde{P}^-
\end{aligned} \tag{4.67}$$

where \tilde{P}^a is the projector onto the space V_a for the fusion of two V_2 spaces.

These can be written

$$\begin{aligned}
\tilde{P}^+ &= \frac{1}{2} (|\uparrow\downarrow\rangle + |\downarrow\uparrow\rangle) (\langle\uparrow\downarrow| + \langle\downarrow\uparrow|) \\
\tilde{P}^- &= \frac{1}{2} (|\uparrow\downarrow\rangle - |\downarrow\uparrow\rangle) (\langle\uparrow\downarrow| - \langle\downarrow\uparrow|) \\
\tilde{P}^2 &= |\uparrow\uparrow\rangle \langle\uparrow\uparrow| + |\downarrow\downarrow\rangle \langle\downarrow\downarrow|
\end{aligned} \tag{4.68}$$

Written in the spin formalism the local Hamiltonian is now

$$E_1 P^1 + P^2 = E_1 \tilde{P}^2 + \tilde{P}^- = \begin{pmatrix} E_1 & 0 & 0 & 0 \\ 0 & \frac{1}{2} & -\frac{1}{2} & 0 \\ 0 & -\frac{1}{2} & \frac{1}{2} & 0 \\ 0 & 0 & 0 & E_1 \end{pmatrix} \quad (4.69)$$

which can be written in terms of Pauli operators as

$$-\frac{1}{4}(\sigma^x \otimes \sigma^x + \sigma^y \otimes \sigma^y) + \left(\frac{E_1}{2} - \frac{1}{4}\right)\sigma^z \otimes \sigma^z + \left(\frac{E_1}{2} + \frac{1}{4}\right)\mathbb{I}_{4 \times 4} \quad (4.70)$$

showing that the staggered anyon chain is indeed equivalent to a staggered XXZ chain.

This makes it possible to construct a strong zero mode using the methods in [33]. We write the Hamiltonian as

$$H = H_0 + fV \quad (4.71)$$

and as in [28] we start with an operator, $\psi^{(0)}$ such that

$$[H_0, \psi^{(0)}] = 0 \quad (4.72)$$

then try to iteratively construct a strong zero mode for the full Hamiltonian.

If we have an operator

$$\psi = \psi^{(0)} + f\psi^{(1)} + \dots + f^L\psi^{(L)} \quad (4.73)$$

such that

$$[H_0, \psi^{(i+1)}] = -[V, \psi^{(i)}] \quad (4.74)$$

then

$$[H, \psi] = \mathcal{O}(f^{L+1}) \quad (4.75)$$

which is the commutation relation of a strong zero mode with the Hamiltonian. The XXZ Hamiltonian we wrote above has a \mathbb{Z}_2 symmetry under flipping the spin at every site

$$S = \prod_i \sigma_i^x \quad (4.76)$$

For the Hamiltonian above we can brute force calculate the first few terms of a zero mode operator which satisfies 4.75. The method to do this, fully described in [33], involves using super-operators [75] or operators which act on operators to rewrite 4.74 as a degenerate perturbation theory problem. The Hamiltonian is rewritten in terms of super-operators, $\mathcal{H}_0 = [H_0, \cdot]$ and $\mathcal{V} = [V, \cdot]$. These commutators act on a Hilbert space which is isomorphic to a tensor product of two copies of the original Hilbert space. For example, for the chiral clock model, the super-operators act on states

$$|i_1, i_2, \dots, i_L\rangle |j_1, j_2, \dots, j_L\rangle := |i_1, i_2, \dots, i_L\rangle \langle j_1, j_2, \dots, j_L| \quad (4.77)$$

where the i_m and j_m label the clock value at each site of the chain as usual. In this basis, given an operator O , we have

$$[O, \cdot] = O \otimes \mathbb{1} - \mathbb{1} \otimes O^T \quad (4.78)$$

where O^T is the transpose of O . Using these super-operators 4.74 can be rewritten as

$$\begin{aligned} \mathcal{P}_0 \mathcal{V} \psi_p^{(k)} &= -\mathcal{P}_0 \mathcal{V} \psi_q^{(k)} \\ \mathcal{H}_0 \psi_q^{(k+1)} &= -\mathcal{Q}_0 \mathcal{V} (\psi_q^{(k)} + \psi_p^{(k)}) \end{aligned} \quad (4.79)$$

where $\psi_p^{(k)} = \mathcal{P}_0 \psi^{(k)}$, $\psi_q^{(k)} = \mathcal{Q}_0 \psi^{(k)}$, \mathcal{P}_0 is the projector onto the null space of \mathcal{H}_0 , $null(\mathcal{H}_0)$ and $\mathcal{Q}_0 = 1 - \mathcal{P}_0$. Solving this for the first two terms of the zero

mode we get

$$\begin{aligned}\psi^{(0)} &= z_1 \\ \psi^{(1)} &= \left(\frac{E}{1-E^2}\right)(x_1x_2 + y_1y_2)z_3 + \left(\frac{1}{1-E^2}\right)(x_1x_3 + y_1y_3)z_2\end{aligned}\tag{4.80}$$

where $E = 1 - 2E_1$ and we have switched notation for the Pauli matrices to $a_i = \sigma_i^a$ for convenience. The second order term already contains many terms and several correction terms like those mentioned in [73]. These terms arise in the following scenario. Say we have

$$[H, \psi^{(0)} + f\psi^{(1)} + \dots + f^{i-1}\psi^{(i-1)}] = -[V, \tilde{\psi}^{(i)}]\tag{4.81}$$

where we call $\tilde{\psi}^{(i)}$ a putative i^{th} order correction. Problems arise when $[H, \psi^{(i)}] = A$ for some operator, A , but any potential $(i+1)^{\text{th}}$ order correction, $\psi^{(i+1)}$, such that $[V, \psi^{(i+1)}]$ contains A , $[V, \psi^{(i+1)}]$ also contains another operator, B , which, crucially, does not appear in $[H, \tilde{\psi}^{(i)}]$. To get around this, we add a term, C , that commutes with V such that there exists a $\psi^{(i+1)}$ such that

$$[H, \psi^{(i)} = \tilde{\psi}^{(i)} + C] = -[V, \psi^{(i+1)}]\tag{4.82}$$

Since C commutes with V , we can add such a function to the zero mode at any order and its effects will not be seen until the next order so these corrections ensure the zero mode commutes with the Hamiltonian up to the correct order.

Even without writing the general n^{th} order term in the zero mode, the form of $\psi^{(0)}$ has an implication for the zero mode in the anyon chain. A single σ^z operator cannot be written in terms of a finite number of two site projectors, meaning the zero mode can only be mapped exactly to the anyon chain if the chain is half-infinite i.e. we can see one end of the chain but there are an infinite number of sites. If we have a half-infinite chain then σ_i^z acting on the

spin chain has an equivalent operator in the anyon formalism given by

$$\begin{aligned}
z_i &= \prod_{i=1}^{\infty} (z_i \otimes z_{i+1}) \\
&= \prod_{i=1}^{\infty} P_i^1 - (P_i^0 + P_i^2)
\end{aligned} \tag{4.83}$$

The other terms that appear in the early terms of the zero mode are of the form $x \otimes x + y \otimes y$ which can be mapped directly to the anyon formalism as it is expressible in terms of the 2 site projectors.

$$(x \otimes x) + (y \otimes y) = \tilde{P}^+ - \tilde{P}^- \tag{4.84}$$

Interestingly, there is no equivalent operator for the symmetry operator, S , in the anyon formalism. It can be shown that S does not commute with the group action. Since S flips the spin at every site then it acts as $\sigma^x \otimes \sigma^x$ on each pair of sites which in matrix form is

$$\begin{pmatrix}
0 & 0 & 0 & 1 \\
0 & 0 & 1 & 0 \\
0 & 1 & 0 & 0 \\
1 & 0 & 0 & 0
\end{pmatrix} \tag{4.85}$$

Clearly this cannot be written in terms of the projectors in 4.68 as none of those can send $|\uparrow\uparrow\rangle$ to $|\downarrow\downarrow\rangle$ and vice versa. This makes sense as this alternates between the internal states of the two dimensional representation which we do not see in the anyon formalism. However the matrix

$$\begin{pmatrix}
0 & 0 & 0 & 0 \\
0 & 0 & 1 & 0 \\
0 & 1 & 0 & 0 \\
0 & 0 & 0 & 0
\end{pmatrix} \tag{4.86}$$

can be expressed as $\tilde{P}^+ - \tilde{P}^-$. So the symmetry operator acting on this subspace can be written

$$\prod_{i=1}^{\frac{L}{2}} P_i^0 - P_i^2 \quad (4.87)$$

This operator only acts non-trivially in the anyon chain written in the standard basis when $x_i \in \{0, 2\}$ for every odd value of i . For these states it is an identity when the last label is 0 and the state is multiplied by -1 when the last label is 2. Recall that in the last section we saw topological degeneracy between states ending in 0 or 2 and only differing by the last label. It seems logical to extend S so that every state with $x_{L-1} = 0, 2$ is an eigenstate of S with eigenvalue ± 1 .

Let us take another look at 4.83 for $i = 1$ to see how the zero mode behaves in the anyon chain. When $f = 0$ this operator should be an exact zero mode so we should see that

$$\begin{aligned} [H, \sigma_1^z] &= 0 \\ \{S, \sigma_1^z\} &= 0 \end{aligned} \quad (4.88)$$

For a finite chain of length L we cannot write σ_1^z exactly but instead write

$$Z = \prod_{i=1}^{L-1} P_i^1 - (P_i^0 + P_i^2) \quad (4.89)$$

which is actually equivalent to a σ^z acting at each end of the chain but seeing how this operator acts should give us some insight into the half infinite case. Using 4.66 we see that this operator acting on a state $|x_1 x_2 \dots x_{L-1}\rangle$ in the standard basis has the effect of flipping all labels $x_i = 0$ to $x_i = 2$ and vice versa up to a sign change. In the dimerized basis it has the same effect except the flip only occurs at labels x_i for even values of i . This operator commutes with the Hamiltonian for $f = 0$ but also commutes with S . The zero mode should anti-commute with S but Z is only equivalent to the zero mode for the half infinite chain. However we observe something interesting if we examine what Z does in the half-infinite chain. Before we do that it is prudent to

introduce the topological symmetry operator [47, 76]. This operator is usually written about in the context of closed anyon chains like those in [59]. They can be depicted as

$$(4.90)$$

The topological symmetry operator creates a charge, l , inside the spine of the fusion tree. An F-move is then applied to fuse l into the spine of the chain. Further F-moves move l around the chain, past each fusion vertex before a final F-move removes l from the chain. This operator is usually denoted Y_l and its matrix elements are given by

$$\langle x'_0, x'_1, \dots, x'_{L-1} | Y_l | x_0, x_1, \dots, x_{L-1} \rangle = \prod_{i=0}^{L-1} (F_{x'_{i+1}, x'_i}^{j x_i l}) \quad (4.91)$$

This operator commutes with local projection operators. We can perform a similar construction for the open anyon chains we have been working with up to now. As an example we take a chain of length 6 and an anyon of type l as shown below.

$$(4.92)$$

We can use 2.19 to fuse l into the spine of the chain before and after each

fusion vertex which gives

$$\sum_{c,d,e,f} \sqrt{\frac{d_c d_d d_e d_f}{d_l^4 d_j d_{x_2} d_{x_4} d_Q}}$$

(4.93)

We then remove all the bubbles using F-moves. For example, we can change the above diagram to

$$\sum_{c,d,e,f} (F_d^{ljx_1})_{x'_2, x_2} \sqrt{\frac{d_c d_d d_e d_f}{d_l^4 d_j d_{x_2} d_{x_4} d_Q}}$$

(4.94)

which can be simplified further using 2.15 to get

$$\sum_{c,d,e,f} (F_d^{ljx_1})_{x'_2,x_2} \sqrt{\frac{d_d d_e d_f}{d_l^3 d_{x_2} d_{x_4} d_Q}} \text{Diagram} \quad (4.95)$$

We remove the other bubbles in the same way and are left with

$$\sum_{c,d,e,f} \sqrt{\frac{d_f}{d_l d_Q}} (F_d^{ljx_1})_{c,x_2} (F_e^{lx_2x_3})_{d,x_4} (F_f^{lx_4j})_{e,Q} \text{Diagram} \quad (4.96)$$

For a chain of length L the matrix elements of this operator, which we will refer to as Y_l^O , are

$$\langle x'_0, x_1, x'_2, x_3, \dots, x_{L-3}, x'_{L-2}, Q' | Y_l^O | x_0, \dots, Q \rangle = \prod_{i=0,2,4,\dots}^{L-2} \sqrt{\frac{d_{Q'}}{d_l d_Q}} (F_{x'_{i+2}}^{lx_i x_{i+1}})_{x'_i, x_{i+2}} \quad (4.97)$$

where $x_0 = j$ and we refer to the final incoming anyon as x_{L-1} and Q still labels the final fusion result of the chain. Now let us consider this operator for the $SU(2)_4$ chain with $l = 2$. The matrix elements of Y_2^O are given by

$$\langle x'_0, x_1, x'_2, x_3, \dots, x_{L-3}, x'_{L-2}, Q' | Y_2^O | x_0, \dots, Q \rangle = \prod_{i=0,2,4,\dots}^{L-2} (F_{x'_{i+2}}^{2x_i x_{i+1}})_{x'_i, x_{i+2}} \quad (4.98)$$

and $x'_i = x_i \times 2$. Applying this operator will flip every 0 label on the spine of the fusion tree, including Q , to a 2 and vice versa. Additionally, each F-symbol which appears in the matrix elements of Y_2^O is either 1 or -1. The only negative F-symbol which can appear here is

$$(F_1^{211})_{11} = -1 \tag{4.99}$$

so the state will be multiplied by -1 for each label $x_i = 1$ where i is odd and $x_{i-1} = x_{i+1} = 1$. An additional factor of -1 is picked up if $x_{L-2} = Q = 1$. The effect of the operator is almost the same in the standard basis. In that basis, each label $x_i \in \{0, 2\}$ is flipped and the state is multiplied by -1 for each pair of consecutive 1 labels i.e. each pair $x_i = x_{i+1} = 1$ including if $x_{L-2} = Q = 1$. Interestingly, this is exactly how Z acts on the half-infinite chain. We will illustrate this with an example. Consider the first 13 sites of a chain in the dimerized basis as shown below.

$$|011111211000\dots\rangle = \begin{array}{cccccccccccccccc} & 1 & 1 & 1 & 1 & 1 & 1 & 1 & 1 & 1 & 1 & 1 & 1 & 1 & 1 & 1 & 1 & 1 \\ & \diagdown & / & \diagdown & / & \diagdown & / & \diagdown & / & \diagdown & / & \diagdown & / & \diagdown & / & \diagdown & / & \diagdown & / \\ & & 0 & & 1 & & 1 & & 2 & & 1 & & & & & & & & 0 \\ & & & 1 & & & & & & & & & & & & & & & & \\ & & & & 1 & & & & & & & & & & & & & & & \\ & & & & & 1 & & & & & & & & & & & & & & \\ & & & & & & 0 & & & & & & & & & & & & & \\ & & & & & & & & & & & & & & & & & & & \dots \\ & & & & & & & & & & & & & & & & & & & \dots \end{array} \tag{4.100}$$

and we act on this state with Z . To do this we first need to know how $P_i = P_i^1 - P_i^0 - P_i^2$ acts at each site. Clearly P_i is diagonal for i even. The first projector, P_1 , only depends on the labels, x_1 and x_2 . It acts on these

labels as

$$\begin{aligned}
 |01\rangle &\rightarrow -|21\rangle \\
 |10\rangle &\rightarrow |10\rangle \\
 |11\rangle &\rightarrow -|11\rangle \\
 |12\rangle &\rightarrow |12\rangle \\
 |21\rangle &\rightarrow -|01\rangle
 \end{aligned}
 \tag{4.101}$$

For $i \neq 1$ and odd, P_i acts on 5 labels

$$\tag{4.102}$$

Acting on these labels, P_i does the following:

- If x_{i-2} , x_{i-1} or x_i are 0 or 2, then they are flipped.
- If $x_{i-3} = 1$ and $x_{i+1} \in \{0, 2\}$ or vice versa and $x_{i-1} = 1$ the state is multiplied by 1. Otherwise the state is multiplied by -1.

Acting on our sample state with Z will give

$$\tag{4.103}$$

If we extended the chain, the final 0 label would be flipped and the final incoming 2 label would be flipped back to 0. It can be seen from this that in

the half-infinite chain, only labels on the spine will be flipped. So Z and Y_2^O flip the same labels in the half-infinite chain and only differ in their effect on the final label in the finite chain. Remember that Y_2^O applies a minus sign for each sequence of labels $x_{i-1} = x_i = x_{i+1} = 1$ where i is odd. In our sample state there are 2 such sequences and the result after acting with Z is positive. We can change the overall sign by changing the number of these sequences. For example, consider the states

$$\begin{aligned}
& |011111211101\dots\rangle \\
& |011110221101\dots\rangle \\
& |011011211000\dots\rangle
\end{aligned} \tag{4.104}$$

These have 3, 1 and 0 such sequences respectively. After acting with Z , the first two will pick up a minus sign while the third will be positive. The operators, Z and Y_l^O , act on the half-infinite chain in the same way. So we might expect that Y_l^O is an exact zero mode with $f = 0$. We see that this is indeed the case as in the dimerized basis, Y_l^O does not change labels x_i for i odd so commutes with the Hamiltonian when $f = 0$. This operator clearly anti-commutes with S and so is an exact zero mode when $f = 0$. With this in mind we can now re-write 4.80 in terms of anyonic operators.

$$\begin{aligned}
\psi^{(0)} &= Y_2^O \\
\psi^{(1)} &= \left(\frac{E}{1-E^2}\right)(P_1^0 - P_1^2)Y_{2,2}^O + \left(\frac{1}{1-E^2}\right)(P_{1,3}^0 - P_{1,3}^2)Y_{2,1}^O
\end{aligned} \tag{4.105}$$

We introduced some new notation here. The projector, $P_{j,k}^i$, indicates we are projecting onto the i fusion channel for the incoming anyons in positions j and k which may not be nearest neighbours. To do this we braid one of the anyons, say the one in position k , to position $j + 1$, then apply the usual projector, P_j^i and then perform the inverse braid operators to return the anyon to its original position. The operator, $Y_{2,i}^O$, is the same as Y_2^O except we initially fuse the additional 2 label with the label x_i rather than with the first incoming label as shown below. It is clear that if Y_2^O is equivalent to σ_1^z then $Y_{2,i}^O$ is

equivalent to σ_{i+1}^z . The matrix elements in the standard basis are given by

$$\langle x'_0, x'_1, x'_2, x'_3, \dots, x'_{L-3}, x'_{L-2}, Q' | Y_{2,i}^O | x_0, \dots, Q \rangle = \prod_{j=i}^{L-2} (F_{x'_j, x'_{j+1}}^{lx'_j 1})_{x'_j, x'_{j+1}} \quad (4.106)$$

So rather than states $|x\rangle_0 = |x_1, x_2, \dots, 0\rangle$ and $|x_1, x_2, \dots, 2\rangle$ being topologically degenerate as we initially suspected, $|x\rangle_0$ and $Y_2^O|x\rangle_0$ are topologically degenerate.

4.6 Strong Zero Mode in Modified XXZ Chain

In this subsection we alter the Hamiltonian from above and instead consider $H = H_0 + fV$ with

$$\begin{aligned} H_0 &= - \sum_{i=1}^L z_{2i-1} z_{2i} + z_{2i} z_{2i+1} \\ V &= \sum_{i=1}^L x_{2i-1} x_{2i} + y_{2i-1} y_{2i} \end{aligned} \quad (4.107)$$

This is similar to the Hamiltonian for the XXZ chain given in [73] with the exception that here, increasing the perturbing parameter only introduces σ^x and σ^y terms at alternating sites rather than at every site. In the anyon formalism, this Hamiltonian is written

$$H = \sum_{i=1}^{L-1} -P_{2i-1}^1 + P_{2i-1}^0(1+f) + P_{2i-1}^2(1-f) + (-P^1 + P^0 + P^2)_{2i} \quad (4.108)$$

On even sites this assigns energy -1 to a fusion to a 1 and assigns 1 to a fusion to 0 or 2. The Hamiltonian acts similarly on odd sites except fusion to 0 and 2 are now assigned values of $1+f$ and $1-f$ respectively.

In [33] it was shown that for a large class of models the only possible starting point for the zero mode expansion such that

$$Q\psi^{(0)} = -\psi^{(0)}Q \quad (4.109)$$

is given by

$$\psi^{(0)} = z_1 \quad (4.110)$$

For example, this is the case in the Ising chain and gives a zero mode localised at each edge and no more. For this Hamiltonian, however, there exist multiple possible starting points such that 4.109 is true. These starting points are given by

$$\psi^{(0)} = (z_1)^{i_1} (z_2)^{i_1+1} A_2^{i_2} A_3^{i_3} \cdots A_{L-1}^{i_{L-1}} A_L^{i_L} \quad (4.111)$$

where $i_k = 0, 1$ and

$$A_k = z_{2k-1}z_{2k} \quad \text{or} \quad z_{2k-1} + z_{2k} \quad (4.112)$$

For example, some possible starting points are

$$z_1 \quad z_2 \quad z_2(z_5 + z_6)z_{11}z_{12} \quad (4.113)$$

A different zero mode expansion can be found for each of these starting points but let us consider

$$\psi^{(0)} = z_1 \quad (4.114)$$

From this starting point we can write a general k^{th} order term for the zero mode expansion.

$$\psi^{(k)} = \prod_{j=1}^k (x_{2j-1}x_{2j} + y_{2j-1}y_{2j})z_{2k+1} \quad (4.115)$$

which in the anyon formalism is

$$\prod_{j=1}^k (P^0 - P^2)_{2j-1} Y_{2,2k+2}^O \quad (4.116)$$

We can see that this expansion satisfies 4.74 as

$$[V, \psi^{(k-1)}] = -[H_0, \psi^{(k)}] = 2i \prod_{j=1}^{k-1} (x_{2j-1}x_{2j} + y_{2j-1}y_{2j})(x_{2k-1}y_{2k} - y_{2k-1}x_{2k}) \quad (4.117)$$

The full expansion of the zero mode can be written for any of the starting points. To do this, we note that

$$[H_0, A_k] = [V, A_k] = 0 \quad \forall k \quad (4.118)$$

regardless of which of the two possible forms A_k takes. This means that for

$$\psi^{(0)} = (z_1)^{i_1} (z_2)^{i_1+1} A_2^{i_2} A_3^{i_3} \cdots A_{L-1}^{i_{L-1}} A_L^{i_L} \quad (4.119)$$

we can write the general k^{th} order term as

$$\psi^{(k)} = (-1)^{i_1+1} \prod_{j=1}^k (x_{2j-1}x_{2j} + y_{2j-1} + y_{2j}) z_{2k+1} A_2^{i_2} A_3^{i_3} \cdots A_{L-1}^{i_{L-1}} A_L^{i_L} \quad (4.120)$$

The factor of $(-1)^{i_1+1}$ comes from the fact that

$$[V, z_2] = -[V, z_1] \quad (4.121)$$

If at least one of the A_k in the expression for the starting point are given by $z_{2k-1} + z_{2k}$ then we can construct an exact strong zero mode. If we assume k is the lowest number for which

$$A_k = z_{2k-1} + z_{2k} \quad (4.122)$$

then $\psi^{(k-1)}$ is the highest order non-zero term in the expansion of the zero

mode. To see this we write

$$\begin{aligned}
\psi^{(k-1)} &= (-1)^{i_1+1} \prod_{j=1}^{k-1} (x_{2j-1}x_{2j} + y_{2j-1} + y_{2j}) z_{2k-1} A_2^{i_2} A_3^{i_3} \cdots A_k \cdots A_{L-1}^{i_{L-1}} A_L^{i_L} \\
&= (-1)^{i_1+1} \prod_{j=1}^{k-1} (x_{2j-1}x_{2j} + y_{2j-1} + y_{2j}) A_2^{i_2} A_3^{i_3} \cdots z_{2k-1} (z_{2k-1} + z_{2k}) \cdots A_{L-1}^{i_{L-1}} A_L^{i_L} \\
&= (-1)^{i_1+1} \prod_{j=1}^{k-1} (x_{2j-1}x_{2j} + y_{2j-1} + y_{2j}) A_2^{i_2} A_3^{i_3} \cdots (1 + z_{2k-1}z_{2k}) \cdots A_{L-1}^{i_{L-1}} A_L^{i_L}
\end{aligned} \tag{4.123}$$

However, this gives

$$[V, \psi^{(k-1)}] = 0 \tag{4.124}$$

and so the expansion of the zero mode terminates here, making this an exact zero mode. Interestingly these exact zero modes correspond to when each term in the zero mode has an underlying D_3 symmetry so the zero mode can be mapped exactly to the anyon formalism even for a finite chain.

While we have been using the term "zero mode" throughout this section we should really be more careful as we should confirm that these expansions converge before we can call these operators zero modes. Let us consider the normalisation of the zero mode with $\psi^{(0)} = z_1$. Each $\psi^{(k)}$ in this expansion is self-adjoint so

$$\psi^\dagger \psi = \psi^2 = \sum_{k=0}^{2L} f^k \sum_{j=0}^k \psi^{(k-j)} \psi^{(j)} \tag{4.125}$$

It can be seen from 4.115 that

$$\{\psi^{(k)}, \psi^{(j)}\} = 0 \quad k \neq j \tag{4.126}$$

which gives

$$\psi^2 = \sum_{j=0}^L f^{2j} (\psi^{(j)})^2 \tag{4.127}$$

Squaring the general term in 4.115 we see

$$(\psi^{(k)})^2 = 2^k \prod_{j=1}^k (1 - z_{2j-1}z_{2j}) = 2^k \prod_{j=1}^k 2\tilde{P}_{2j-1,2j}^+ + 2\tilde{P}_{2j-2,2j}^- \tag{4.128}$$

This means there will be terms 2^{2k} on the diagonal. This means ψ^2 should converge in the $L \rightarrow \infty$ limit if and only if the series

$$\sum_{j=0}^{\infty} (2f)^{2j} \quad (4.129)$$

converges which it does if and only if $f < \frac{1}{2}$. This gives the range of parameters for which the system is in a topological regime. In the limit $L \rightarrow \infty$ we have

$$\psi^2 = 1 + \sum_{k=1}^{\infty} (2f)^{2k} \prod_{j=1}^k (\tilde{P}^+ + \tilde{P}^-)_{2j-1, 2j} \quad (4.130)$$

This is in contrast to the XYZ strong zero mode written in [73] and the strong zero modes in the quantum Ising chain as in both of those cases $\psi^2 \propto 1$ but in this case, while ψ^2 is diagonal, the values on the diagonal can vary. In particular, in the standard basis, $\psi^2 = 1$ when acting on the subset of states where $x_i = 1$ for any odd i . When acting on the subset of states where $x_i \in \{0, 2\}$ for all odd i , we have $\psi^2 = 1 + \sum_{k=1}^{\infty} (2f)^{2k}$. To see this, we consider how the product in 4.130 acts on a state in the standard basis as in figure 4.1. Every product in 4.130 begins with $(P^0 + P^2)_1$. In the standard basis this is simply

$$(P^0 + P^2)_1 = \delta_{x_1,0} + \delta_{x_1,2} \quad (4.131)$$

The operator, $(P^0 + P^2)_3$ is not diagonal but it is when acting only on the space where $x_1 \in \{0, 2\}$. We have

$$(P^0 + P^2)_3 (P^0 + P^2)_1 = \delta_{x_1,0} \delta_{x_3,0} + \delta_{x_1,0} \delta_{x_3,2} + \delta_{x_1,2} \delta_{x_3,0} + \delta_{x_1,2} \delta_{x_3,2} \quad (4.132)$$

Similarly

$$\begin{aligned} \prod_{j=1}^k (P^0 + P^2)_{2j-1} |x_1, x_2, \dots, Q\rangle &= |x_1, x_2, \dots, Q\rangle \quad \text{if } x_1, x_3, \dots, x_{2k-1} \in \{0, 2\} \\ &= 0 \quad \text{otherwise} \end{aligned} \quad (4.133)$$

4.7 Conclusion

In this chapter we calculated a nearest neighbour interaction Hamiltonian for a Tambara-Yamagami chain. By introducing a staggering of the interaction strengths we realised that this chain is identical to a \mathbb{Z}_n chiral clock model. This led to an interest in investigating anyon chains for strong zero modes.

We found that a Fibonacci anyon chain did not possess strong zero modes due to a resonance from the degeneracy in the fusion tree but we found numerical evidence for a strong zero mode in an $SU(2)_4$ chain. We were able to construct this zero mode using the methods in [33] after using a transformation between $SU(2)_4$ chains and XXZ spin chains. We also constructed a modified chain with many strong zero modes which could be constructed exactly. We finished by constructing the $SU(2)_4$ strong zero mode in the diagrammatic notation. This was made possible by the realisation that σ^z applied to the first site of the spin chain is equivalent to fusing an extra 2 label into each label on the spine of the fusion tree.

We now move away from the topic of strong zero modes and venture forth into the world of tight binding anyon models.

Chapter 5

Anyonic Tight Binding

In this chapter we construct a tight binding model of non-abelian anyons on a torus. To do this we review a construction of abelian anyons on a torus, as well as a construction of fusion trees on a torus. We then construct a rectangular lattice model for anyons on the torus. While we construct our model on a torus, we note that the same principles apply to constructing these models on other surfaces, for example, on a cylinder [77].

For comparison to the results we obtain from the anyonic system, let us first review a solution of a spinless fermion hopping model with periodic boundary conditions.

5.1 Tight Binding Model of Spinless Fermions

We consider a 2D, $L_x \times L_y$ rectangular lattice occupied by spinless fermions. We impose periodic boundary conditions. The Hamiltonian in the second quantisation formalism is

$$H = -t \sum_{\langle i,j \rangle} (c_j^\dagger c_i + c_i^\dagger c_j) \quad (5.1)$$

where c_j^\dagger , c_j are the usual fermionic creation and annihilation operators. The Hamiltonian is currently written in position space but is actually diagonal in momentum space. We can write the creation and annihilation operators in

momentum space

$$\begin{aligned} c_j^\dagger &= \frac{1}{L_x L_y} \sum_{\mathbf{k}} e^{-i\mathbf{k}\cdot r_j} c_{\mathbf{k}}^\dagger \\ c_j &= \frac{1}{L_x L_y} \sum_{\mathbf{k}} e^{i\mathbf{k}\cdot r_j} c_{\mathbf{k}} \end{aligned} \quad (5.2)$$

where r_j is the vector detailing the lattice position labeled by j and \mathbf{k} are the momentum vectors. We can write the Hamiltonian in momentum space using the above relations. First we rewrite the Hamiltonian as

$$H = -\frac{t}{2} \sum_j \sum_{\delta} (c_j^\dagger c_{j+\delta} + c_{j+\delta}^\dagger c_j) \quad (5.3)$$

where δ are the vectors which indicate the lattice spacing in the x and y directions. The operator, $c_{j+\delta}^\dagger$, creates a fermion at the lattice site, $r_j + \delta$. In momentum space the Hamiltonian is written

$$\begin{aligned} H &= -\frac{t}{2L_x L_y} \sum_j \sum_{\delta, \mathbf{k}, \mathbf{k}'} (e^{-i\mathbf{k}\cdot r_j} e^{i\mathbf{k}'\cdot (r_j+\delta)} c_{\mathbf{k}}^\dagger c_{\mathbf{k}'} + e^{i\mathbf{k}'\cdot r_j} e^{-i\mathbf{k}\cdot (r_j+\delta)} c_{\mathbf{k}}^\dagger c_{\mathbf{k}'}) \\ &= -\frac{t}{2} \sum_{\delta, \mathbf{k}} (e^{i\mathbf{k}\cdot\delta} + e^{i\mathbf{k}\cdot\delta}) c_{\mathbf{k}}^\dagger c_{\mathbf{k}} \\ &= -t \sum_{\delta, \mathbf{k}} \cos(\mathbf{k} \cdot \delta) c_{\mathbf{k}}^\dagger c_{\mathbf{k}} \end{aligned} \quad (5.4)$$

where we have used that

$$\sum_r e^{i(\mathbf{k}-\mathbf{k}')\cdot r} = \sum_j e^{i(\mathbf{k}-\mathbf{k}')\cdot r_j} = L_x L_y \delta_{\mathbf{k}, \mathbf{k}'} \quad (5.5)$$

For a 2D rectangular lattice

$$\delta \in \{(1, 0), (-1, 0), (0, 1), (0, -1)\} \quad (5.6)$$

so the Hamiltonian is

$$-2t \sum_{\mathbf{k}} [\cos(k_x) + \cos(k_y)] c_{\mathbf{k}}^\dagger c_{\mathbf{k}} \quad (5.7)$$

where

$$k_x = \frac{2\pi n}{L_x}, \quad k_y = \frac{2\pi m}{L_y} \quad n, m \in \mathbb{Z} \quad (5.8)$$

This gives all of the single particle energies and eigenstates of the system. The multi-particle energies are all possible sums of the single particle energies while eigenstates are anti-symmetrized tensor products of single particle eigenstates with the condition that no two particles have the same single particle eigenstate. This is due to the Pauli exclusion principle. So we see that the system is easily solvable due to a single particle translation symmetry in each direction. We will now go on to construct the equivalent anyon tight binding model where this is not the case.

5.2 Anyons on a Torus

In this section we provide a mathematical description of a system of anyons on a torus. The description of abelian anyons on a torus is based on the material in [77–80] while the equivalent description of non-abelian anyons is based on [50].

5.2.1 Abelian Anyons

We consider a system of N indistinguishable hard-core particles on a torus T . The configuration space of this system is given by

$$\mathcal{Q} = (T^N - \Delta)/S_N \quad (5.9)$$

where Δ , known as the diagonal, is the set of all vectors in T^N where the positions of two or more particles coincide. We remove this as we stated that the particles are hard-core. Taking a quotient by S_N , the permutation group of N particles, makes states which only differ by a permutation of the particles equivalent, enforcing that the particles are indistinguishable. Moving a particle along a closed loop in \mathcal{Q} must transform the wave-function of the

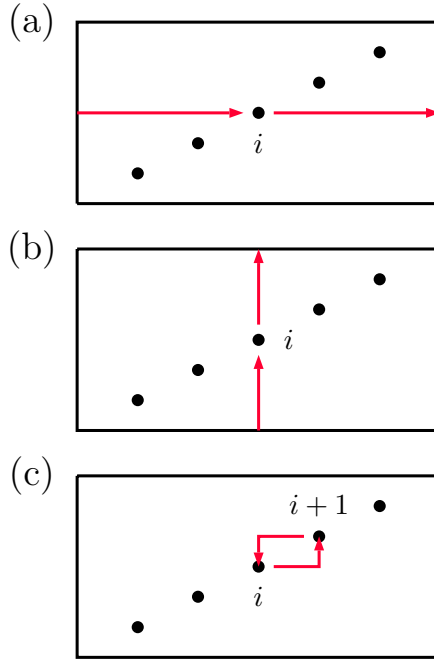


Figure 5.1: The effect of braid group generators on particles on a torus. (a)+(b) Generators $\{\tau_i\}$ and $\{\rho_i\}$ take the i^{th} particle around one of the non-contractible torus loops. (c) A local exchange of the i^{th} and $i+1^{\text{th}}$ particles due to σ_i .

system according to a unitary representation of $\pi_1(\mathcal{Q})$, the fundamental group of \mathcal{Q} . The fundamental group of a space is the group of all equivalence classes of all loops in the space. Two loops are in the same equivalence class if they can be smoothly deformed into each other. The fundamental group of \mathcal{Q} is the fundamental group of the torus with N punctures. This is known to be the N -string braid group of T , $\mathcal{B}_N(T)$. The generators of this group can be written

$$\{\tau_i, \rho_i, \sigma_k; i = 1, 2, \dots, N; k = 1, 2, \dots, N-1\} \quad (5.10)$$

The generators $\{\tau_i\}$ and $\{\rho_i\}$ take the particle i around one of the non-contractible loops of the torus without encircling any other particles as shown in Figure 5.1. The generators $\{\sigma_k\}$ perform a local exchange of the particles k and $k+1$. The torus braid group is discussed in greater detail in [81]. Here we only mention the properties of the torus braid group which are necessary to understand the research in this thesis.

The local braid generators, $\{\sigma_k\}$, are the same as those on the plane and

so they satisfy the relations

$$\sigma_i \sigma_j = \sigma_j \sigma_i \quad (i \neq j \pm 1) \quad (5.11)$$

$$\sigma_{i+1} \sigma_i \sigma_{i+1} = \sigma_i \sigma_{i+1} \sigma_i$$

The generators, $\{\tau_i\}$ and $\{\rho_i\}$ satisfy

$$\tau_{i+1} = \sigma_i^{-1} \tau_i \sigma_i^{-1} \quad (5.12)$$

$$\rho_{i+1} = \sigma_i \rho_i \sigma_i$$

$$\sigma_i^2 = \tau_{i+1}^{-1} \rho_i \tau_{i+1} \rho_i^{-1} \quad (5.13)$$

To describe abelian anyons on a plane one usually uses a 1D representation of the braid group such that

$$\sigma_k = e^{i\theta} \quad \forall k \quad (5.14)$$

where θ is the statistical angle of the anyons. For $\theta = 0/\pi$ we get the usual Bose/Fermi exchange statistics. For a 1D representation of $\mathcal{B}_N(T)$, equation 5.13 gives

$$e^{2i\theta} = 1 \quad (5.15)$$

which only allows for Bose and Fermi statistics. To allow for the more exotic exchange statistics that exist in planar systems, we instead use an M dimensional representation of $\mathcal{B}_N(T)$ and say

$$\sigma_k = e^{i\theta} \mathbb{1}_{M \times M} \quad (5.16)$$

with $\mathbb{1}_{M \times M}$ the $M \times M$ identity matrix. This gives an M component wave-function

$$|\psi\rangle = \sum_{s, x_1, x_2, \dots, x_N} \psi(s, x_1, \dots, x_N) |s, x_1, \dots, x_N\rangle \quad (5.17)$$

where x_i are the position vectors of each particle and $s \in \{1, 2, 3, \dots, M\}$ is the "sheet index" which labels the M components of the wave-function. To derive restrictions on the allowed exchange statistics for this system we first derive,

using the equations above, that

$$\begin{aligned}\tau_i \rho_j &= e^{2i\theta} \rho_j \tau_i & i \neq j \\ \tau_i \rho_i &= e^{-2i\theta(N-1)} \rho_i \tau_i\end{aligned}\tag{5.18}$$

Taking a determinant of 5.18 yields

$$e^{2i\theta M} = 1\tag{5.19}$$

while 5.12 and 5.18 can be used together to show

$$e^{2i\theta N} = 1\tag{5.20}$$

The statistics of abelian anyons on a torus are restricted both by the dimension of the representation of $\mathcal{B}_N(T)$ being used as well as by the number of anyons on the torus. To ensure that we use an irreducible representation of $\mathcal{B}_N(T)$ we set M to be the lowest integer such that 5.19 is true. In general we will have $\theta = \frac{p}{q}\pi$ for p, q mutually prime integers and $M = q$. The possible statistical angles for abelian anyons on a torus are then

$$\theta = \frac{n\pi}{G} \quad 0 \leq n \leq 2G - 1\tag{5.21}$$

where G is the greatest common divisor of M and N . This is equivalent to saying that abelian anyons on a torus must fuse to the vacuum. Now we still need to write a representation for τ_i and ρ_i . The relations 5.12 give expressions for τ_{i+1} and ρ_{i+1} in terms of τ_i and ρ_i so to fix the representation of the braid group we need only define representations of τ_1 and ρ_1 . A choice

of representation which satisfies all of the above relations is

$$\tau_1 = \begin{pmatrix} 0 & 1 & 0 & 0 & \dots & 0 \\ 0 & 0 & 1 & 0 & \dots & 0 \\ 0 & 0 & 0 & 1 & \dots & 0 \\ \dots & \dots & \dots & \dots & \dots & \dots \\ 0 & 0 & 0 & 0 & \dots & 1 \\ 1 & 0 & 0 & 0 & \dots & 0 \end{pmatrix}, \quad \rho_1 = \begin{pmatrix} c & 0 & 0 & 0 & \dots & 0 \\ 0 & c^2 & 0 & 0 & \dots & 0 \\ 0 & 0 & c^3 & 0 & \dots & 0 \\ \dots & \dots & \dots & \dots & \dots & \dots \\ 0 & 0 & 0 & \dots & c^{M-1} & 0 \\ 0 & 0 & 0 & \dots & 0 & c^M \end{pmatrix} \quad (5.22)$$

where $c = e^{2i\theta}$. With a representation of $\mathcal{B}_N(T)$ fixed, we have all we need to construct a tight binding Hamiltonian for abelian anyons on a torus. Before we do this, we will first present a similar theory for N non-abelian anyons on a torus.

5.2.2 Non-Abelian Anyons

In order to discuss non-abelian anyons on a torus, it is beneficial to return to the diagrammatic notation introduced earlier. We may construct a system of N anyons by starting from a system of N anyons on the sphere as in Figure 5.2. The sphere is punctured at the north and south poles and anyonic charges, a_n and a_s , are associated with the north and south poles respectively. These

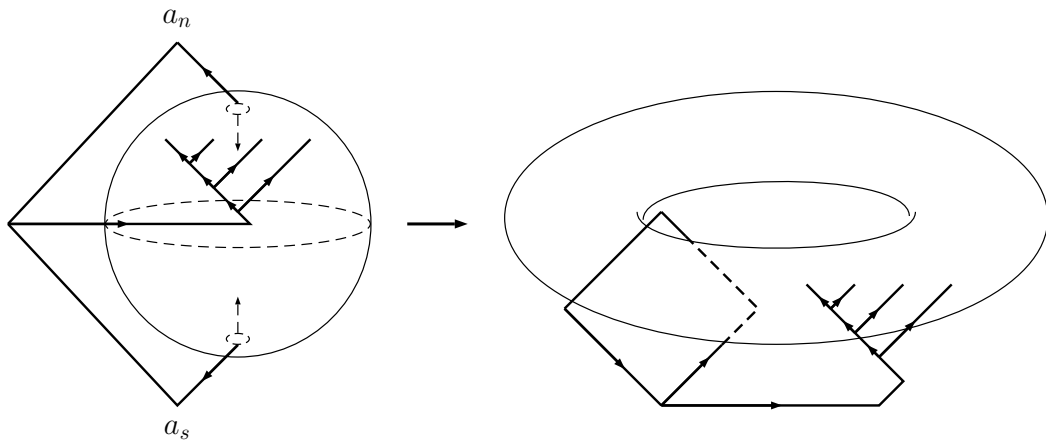
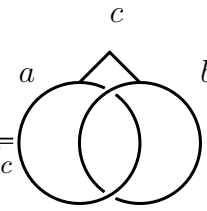


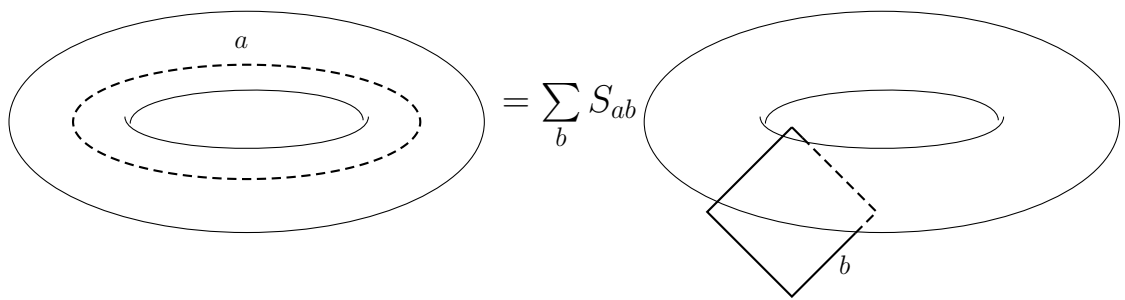
Figure 5.2: Constructing a fusion tree for N anyons on a torus in an outside basis starting from a fusion tree on a sphere.

indicates that the loop encloses a non-trivial loop of the torus and so does not result in a tadpole diagram.

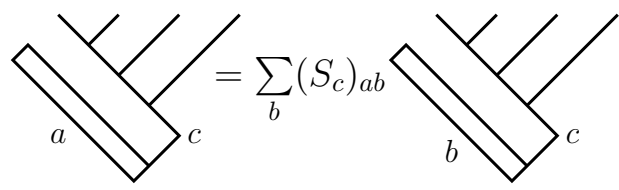
In 2.42 we evaluated the quantity

$$(S_c)_{ab} = \frac{1}{\mathcal{D}\sqrt{d_c}} \text{Diagram} \quad (5.24)$$


These matrices relate fusion trees constructed inside the torus to those constructed outside. If we consider a torus with no anyons on the surface then a fusion tree for this system consists solely of a charge encircling one of the non-trivial loops. The Hilbert space for this system has one state for each type of anyon in the theory we are studying provided the theory is modular. For example, if we consider Fibonacci anyons then the Hilbert space of a torus with no anyons on the surface is two dimensional with the states corresponding to a torus with no charge and a torus with a τ charge encircling one of the non-trivial loops. The inside and outside bases of a system with no anyons are related by the topological S-matrix

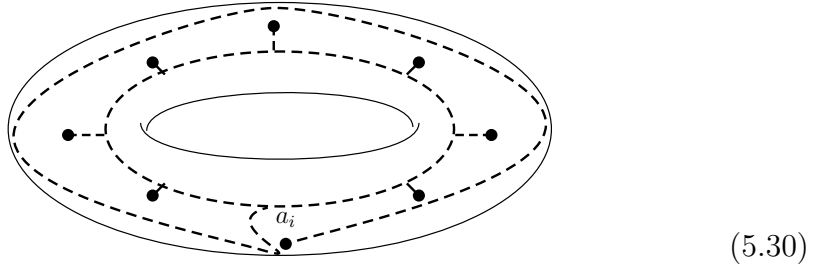
$$\text{Diagram 1} = \sum_b S_{ab} \text{Diagram 2} \quad (5.25)$$


For a system with N anyons this generalises to

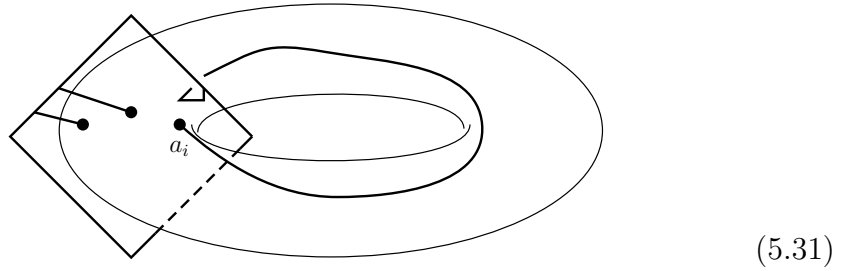
$$\text{Diagram 3} = \sum_b (S_c)_{ab} \text{Diagram 4} \quad (5.26)$$


where the left tree corresponds to an inside basis and the right to an outside

to a similar state. This looks like



This can not be written in terms of simple braid operations in the current basis. However we may use a sequence of F-moves to change to basis B_2 . After this we use $(S_c)_{ab}$ to change to an outside basis. Performing the inverse to the F-moves we just performed leaves us with a state written in basis B_1 in an outside basis. Applying τ_i to this state now has the i^{th} anyon perform a double exchange with the charge outside the torus.



We then apply the inverse of all the basis changes we performed to return to the original basis. This concludes the construction of the braid group generators for this system. We will construct one more operator which will aid in constructing a tight binding anyon model on a torus. This is the periodic translation operator, \tilde{T} , which translates each anyon around the torus by one site. Let us consider a fusion tree in basis B_1 constructed inside the torus.

Then

$$\tilde{T} \begin{array}{c} * \\ | \\ \text{---} \\ | \end{array} = \begin{array}{c} * \\ | \\ \text{---} \\ | \end{array} \quad (5.32)$$

This operator cannot be written in terms of local braid operations. Instead,

we consider an operator, \tilde{T}' , which cyclically permutes all of the labels, a_i and x_i .

$$\tilde{T}' = \text{Diagram} \quad (5.33)$$

We can redraw this operator as

$$\tilde{T}' = \text{Diagram} = [R_1^{a_N \bar{a}_N}]^{-1} \tilde{T} \quad (5.34)$$

So the operator \tilde{T} just cyclically permutes all of the indices of the fusion tree and the wave-function is multiplied by a phase $R_1^{a\bar{a}}$. The phase is derived by undoing the twist in a_N in the previous diagram.

$$\text{Diagram} = \text{Diagram} = R_{a\bar{a}}^1 \quad (5.35)$$

where $R_{a\bar{a}}^1 = [R_1^{a\bar{a}}]^{-1}$. We now possess all the tools required to construct a 2D tight binding anyon model on a torus.

5.3 The Model

In this section, we present a prescription for constructing a 2D hopping model of anyons on a torus. The rules for constructing this model for abelian anyons were derived by Hatsugai et al. [77, 79, 80]. Their work improved upon a previous prescription derived by Wen et al. [82], who constructed a similar model. We present our construction of the model for non-abelian anyons. A similar lattice construction following the diagrammatic calculus of Pfeifer et al. is seen in [83], however, in their construction, anyons are allowed to occupy the same lattice space and only fuse with other anyons on the same site. Here we have constructed a model where the anyons may not occupy the same lattice site and all anyons on the lattice fuse into a single fusion tree at all times. The model consists of an $L_x \times L_y$ lattice on the surface of a torus with N anyons on the lattice. For abelian anyons the Hilbert space consists of the tensor product of an $\binom{L_x \times L_y}{N}$ dimensional lattice space, one state for each choice of the anyons' positions, and an M dimensional topological space. For non-abelian anyons the Hilbert space is the tensor product of the lattice space and the space of all possible fusion trees in our chosen basis which can be formed from the N anyons. We apply periodic boundary conditions in both the horizontal and vertical directions since the lattice sits on a torus. The Hamiltonian is

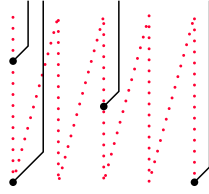
$$H = -t \sum_{\langle i,j \rangle} \Theta_{ij} (c_i^\dagger c_j + c_j^\dagger c_i) \quad (5.36)$$

where the sum is over all nearest neighbour pairs, i, j and $c_i^\dagger c_j$ annihilates an anyon at site j and creates an anyon of the same type at site i . The operator, Θ_{ij} , applies all of the effects of anyons exchanging or traversing non-trivial torus loops. To fix a convention for these effects we pick an ordering for the anyons as in [83, 84].



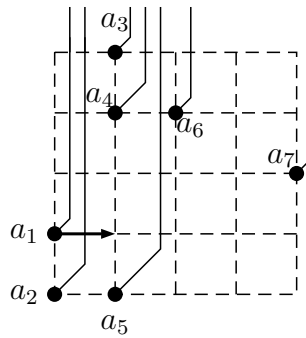
$$\begin{array}{ccccc}
 1 \bullet & 6 \bullet & \bullet & \bullet & \bullet \\
 2 \bullet & \bullet & \bullet & \bullet & \bullet \\
 3 \bullet & \bullet & \bullet & \bullet & \bullet \\
 4 \bullet & \bullet & \bullet & \bullet & 24 \bullet \\
 5 \bullet & \bullet & \bullet & \bullet & 25 \bullet
 \end{array} \quad (5.37)$$

Any move which changes the order of the anyons will cause anyons to braid. To visualise this, we insert a vertical branch cut, extending from each anyon.



(5.38)

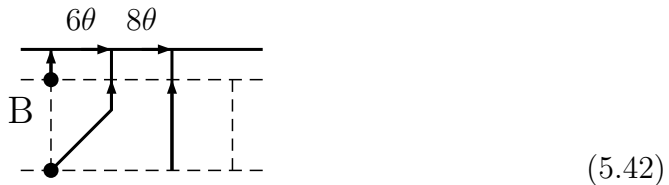
If an anyon passes through one of these cuts from left to right then we say that the anyons have braided clockwise. An anyon traversing one of these cuts from right to left induces a counter-clockwise braid. When an anyon moves its corresponding branch cut moves with it. Anyons which are swept by a moving branch cut are braided with the moving anyon as though they had traversed the branch cut. For example, consider the state



(5.39)

and we say a_1 hops one space to the right. We see that the first branch cut it encounters is the one associated with a_2 so those anyons are exchanged clockwise. The anyons, a_3 and a_4 are swept by the branch cut associated with a_1 so a_1 braids counter-clockwise with a_3 and then with a_4 . We also need to account for the effect of an anyon moving over a boundary and around a non-trivial torus loop. To do this, we first recall the construction of Hatsugai et al for abelian anyons before presenting our own construction for general anyon models. Appendix A shows that our construction is equivalent to the one of Hatsugai et al when we put \mathbb{Z}_n anyons on the lattice. Their construction involves joining all of the branch cuts to a base point, O , as in Figure 5.4. The $n\theta$ labels indicate that the horizontal lines act as branch cuts which have

The anyon must now be moved onto lattice site B .



This induces a phase shift of $e^{2i\theta}$ since the anyon must cross two branch cuts. The total phase shift due to this hop is $e^{-6i\theta}$. In general, the m^{th} anyon in the ordering hopping downward across the boundary causes a phase shift of $e^{i\theta(k-2m+2)}$ where k is the number of anyons that lie in the same column as the hopping anyon. This construction gives a representation of the $\{\rho_i\}$ generators. We now present a rule for anyons hopping horizontally over the boundary to give a representation of the $\{\tau_i\}$ generators. Since Rule C gives a diagonal representation of $\{\rho_i\}$, the representation of $\{\tau_i\}$ we derive should not be diagonal. To encode this we remember that the wave-function of this system includes a sheet index, s , as in 5.17. We say that an anyon hopping horizontally to the right across the boundary decreases this sheet index by one. To calculate the phase shift, if any, applied to the wave-function we consider the case where the anyon in position A in Figure 5.4 hops to the right repeatedly until it arrives back in its original position. During its journey, the anyon braids with each of the others counter-clockwise, resulting in an extra phase of $e^{i\theta(N-1)}$. To account for this extra phase factor, when an anyon moves across the boundary from left to right, the sheet index is reduced by one and the wave-function gains an extra phase of $e^{-i\theta(N-1)}$. This rule is called Rule B in [79]. Rule B and Rule C are consistent in that each give identical results applied to systems with periodic boundary conditions in one direction only i.e. on an annulus/cylinder.

The construction is similar for non-abelian anyons. As before, we consider a lattice with N anyons with periodic boundary conditions and an ordering imposed on the anyons. Each anyon has a vertical branch cut associated with it as before. Our choice of branch cuts is merely a gauge choice. We

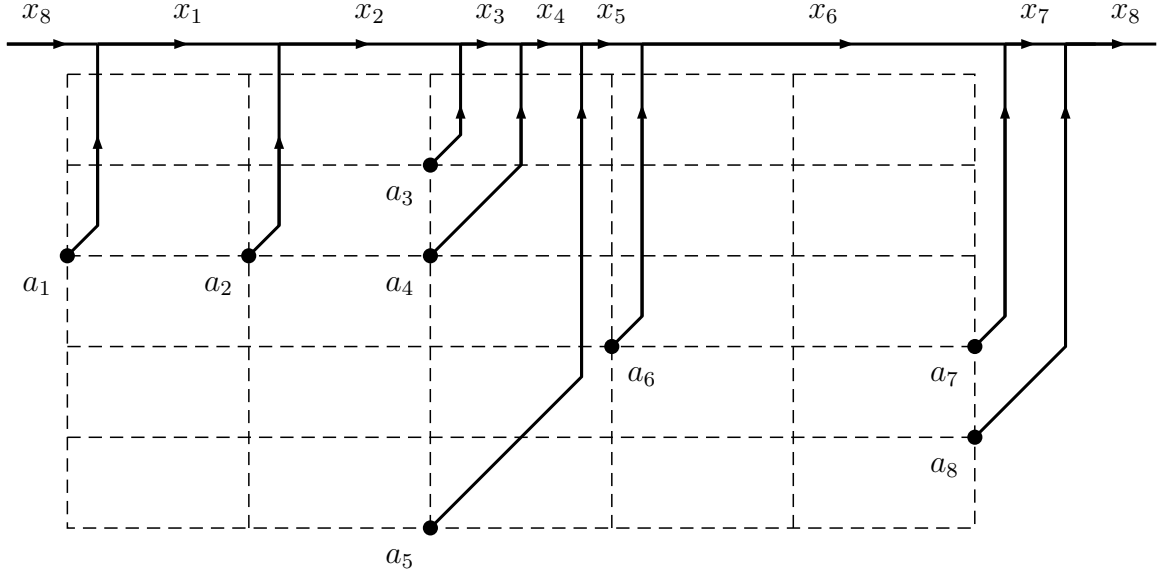
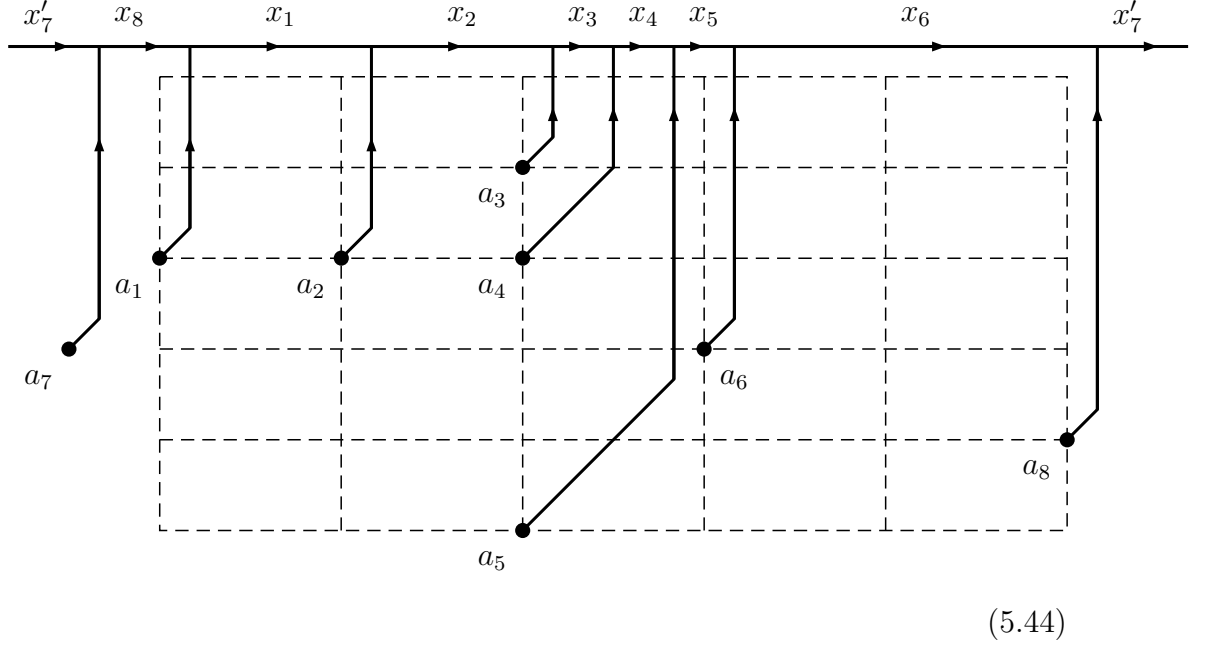


Figure 5.5: Non-Abelian anyons in basis B_1 in an inside basis.

present a brief argument for this in Appendix B. Local braids are applied in the same way as the abelian case. When an anyon passes through a branch cut a local braid operator, σ_i or σ_i^\dagger , is applied to the fusion space for counter-clockwise/clockwise braids respectively. The difference between abelian and non-abelian systems is that for non-abelian systems, the local braid operators do not commute with each other in general so care must be taken to apply braids in the correct order. To show the effects of an anyon hopping across a boundary, we consider a system in basis B_1 inside the torus as in Figure 5.5. The process of constructing the $\{\rho_i\}$ generators is completely identical to Rule C. For example, if a_5 hops downward, it first crosses the line labelled x_4 , then braids with a_4 and a_3 in that order. When a_5 crosses x_4 we say it has performed a double exchange with the loop inside the torus and so the wave-function is multiplied by $([R_{x_5}^{a_5 x_4}][R_{x_5}^{x_4 a_5}])^{-1}$. The minus sign in the power indicates the anyon performs a double clockwise braid with the inside loop. This direction of braiding is fixed by our choice of branch cut and ensures a translational symmetry in the model. We then apply the operator $\sigma_3 \sigma_4$ to the fusion space. In general, an anyon a_n hopping downward across the boundary causes the fusion space to be acted on by

$$([R_{x_n}^{a_n x_{n-1}}][R_{x_n}^{x_{n-1} a_n}])^{-1} (\sigma_{n-k} \sigma_{n-k+1} \dots \sigma_{n-1}) \quad (5.43)$$

where $\{a_{n-k}, a_{n-k+1}, \dots, a_{n-1}\}$ is the set of all anyons in the same column as a_n . To calculate the effect of an anyon hopping to the right across the boundary we consider a_7 in 5.5 moving to the right across the boundary. First, a_7 braids clockwise with a_8 and is then translated around the torus to a virtual site to the left of the lattice. This is done by applying the translation operator, \tilde{T} , leaving the lattice in a state



To move a_7 to the appropriate lattice site its branch cut sweeps a_1 counter-clockwise so a_7 braids counter-clockwise with a_1 . In general, an anyon, a_n , hopping to the right across the boundary causes the fusion space to be acted on by

$$\sigma_k \sigma_{k-1} \dots \sigma_1 \tilde{T} \sigma_{N-1}^\dagger \sigma_{N-2}^\dagger \dots \sigma_n^\dagger \quad (5.45)$$

where $\{a_1, a_2, \dots, a_k\}$ is the set of all anyons in the leftmost column of the lattice which are earlier in the ordering than the site which a_n hops to. The above construction results in a translation symmetry in each direction as will be discussed in the next section. The above braiding and boundary effects are all included in Θ_{ij} in the Hamiltonian.

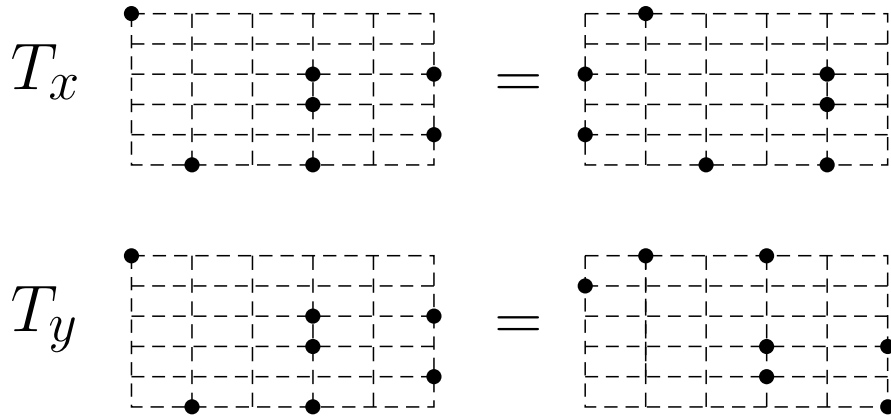


Figure 5.6: Action of T_x and T_y

5.4 Translation Symmetry

In this section we demonstrate the translation symmetry of this system. These symmetries are generated by the centre of mass momentum operators in each direction, T_x and T_y , which translate each anyon in the system one lattice space to the right and one lattice space downward respectively. This is in contrast to a tight binding model of bosons or fermions where there is translation symmetry in each direction for each individual particle which gives a simple solution for the model. In the anyonic case, this symmetry allows us to divide the spectrum into $L_x \times L_y$ non-degenerate spectra with L_x and L_y the lattice width and height respectively. We now show that T_x and T_y commute with each other and the Hamiltonian, allowing all three to be diagonalised simultaneously.

5.4.1 $[T_x, T_y] = 0$

Clearly $T_x T_y$ and $T_y T_x$ have the same effect on the lattice space as both operators shift every anyon one space to the right and one space downward. To show how these operators act on the fusion space we consider a state

$$|\psi\rangle = \begin{array}{cccccccc} & a_1 & a_2 & a_3 & \dots & a_{N-2} & a_{N-1} & a_N \\ & | & | & | & & | & | & | \\ x_N & x_1 & x_2 & \dots & x_{N-2} & x_{N-1} & x_N & \end{array} = |x_1, \dots, x_N\rangle \quad (5.46)$$

For any models we consider we take $a_i = j$ for all i where j is some anyon type. Say $\{a_{i_1}, \dots, a_{i_k}\}$ is the set of anyons on the bottom row of the lattice. These are the anyons which will perform a loop of the torus upon application of T_y . Similarly we say $\{a_l, a_{l+1}, \dots, a_N\}$ is the set of anyons on the rightmost column of the lattice. These anyons perform a loop of the torus upon application of T_x . The lattice space looks like

$$(5.47)$$

We now act on this state with T_x and T_y .

$$\begin{aligned} T_x |\psi\rangle &= (R_1^{j\bar{j}})^{N-l+1} C^{N-l+1} |\psi\rangle \\ &= (R_1^{j\bar{j}})^{N-l+1} |x_l, x_{l+1}, \dots, x_N, x_1, \dots, x_{l-1}\rangle \end{aligned} \quad (5.48)$$

since each anyon that crosses the boundary causes the labels of the fusion tree to be shifted one place and the wavefunction picks up a phase of $R_1^{j\bar{j}}$. The operator, C , cyclically permutes the fusion labels by one place. This operator has the relation with the local braid operators

$$\sigma_n C^m = C^m \sigma_{(n-m) \bmod N} \quad (5.49)$$

Acting with T_y on $|\psi\rangle$ gives

$$T_y |\psi\rangle = \left[\prod_{s=1}^k ([R_{x_{i_s}}^{a_{i_s} x_{i_s-1}}] [R_{x_{i_s}}^{x_{i_s-1} a_{i_s}}])^{-1} \right] \sigma |\psi\rangle \quad (5.50)$$

where σ implements any braids that occur when an anyon crosses the boundary.

Acting with the products of the translation operators we get

$$\begin{aligned} T_x T_y |\psi\rangle &= (R_1^{j\bar{j}})^{N-l+1} \left[\prod_{s=1}^k ([R_{x_{i_s}}^{a_{i_s} x_{i_s-1}}] [R_{x_{i_s}}^{x_{i_s-1} a_{i_s}}])^{-1} \right] C^{N-l+1} \sigma |\psi\rangle \\ T_y T_x |\psi\rangle &= (R_1^{j\bar{j}})^{N-l+1} \left[\prod_{s=1}^k ([R_{x_{i_s}}^{a_{i_s} x_{i_s-1}}] [R_{x_{i_s}}^{x_{i_s-1} a_{i_s}}])^{-1} \right] \sigma' C^{N-l+1} |\psi\rangle \end{aligned} \quad (5.51)$$

where σ' is the same sequence of braids as σ but each σ_i in the sequence is replaced by $\sigma_{i+N-l+1}$. Using 5.49 we see that T_x and T_y commute.

5.4.2 $[H, T_x] = [H, T_y] = 0$

Say H_{a_m} is the Hamiltonian component which acts on the anyon, a_m . In particular we say this is the Hamiltonian component which hops a_m to the right and downward. If the translation operators commute with H_{a_m} it follows that they commute with H . Clearly $[H_{a_m}, T_x] = [H_{a_m}, T_y] = 0$ if a_m is not on the bottom row or rightmost column of the lattice. We now consider the state ψ from the last section with the condition that a_N is in the bottom right corner of the lattice and $\{a_1, \dots, a_p\}$ is the set of anyons in the leftmost column of the lattice.

$$\quad (5.52)$$

We show that $[H_{a_N}, T_x] = [H_{a_N}, T_y] = 0$ and it follows that the Hamiltonian commutes with both translation operators. The operator, H_{a_N} , acts on the fusion space as

$$H_{a_N} |\psi\rangle = (R_1^{j\bar{j}}) \prod_{i=1}^p \sigma_{p-i+1} C |\psi\rangle + ([R_{x_N}^{j x_{N-1}}] [R_{x_N}^{x_{N-1} j}])^{-1} \prod_{i=l}^{N-1} \sigma_i |\psi\rangle \quad (5.53)$$

We now look at the product of T_x and H_{a_N}

$$\begin{aligned}
T_x H_{a_N} | \psi \rangle &= (R_1^{j\bar{j}})^{N-l+1} C^{N-l} \left[\prod_{i=1}^p \sigma_{p-i+1} \right] C | \psi \rangle \\
&\quad + (R_1^{j\bar{j}})^{N-l+1} ([R_{x_N}^{jx_{N-1}}] R_{x_N}^{x_{N-1}j})^{-1} C^{N-l+1} \prod_{i=l}^{N-1} \sigma_i | \psi \rangle \\
H_{a_N} T_x | \psi \rangle &= (R_1^{j\bar{j}})^{N-l+1} \left[\prod_{i=1}^p \sigma_{N-l+p-i+1} \right] C^{N-l+1} | \psi \rangle \\
&\quad + (R_1^{j\bar{j}})^{N-l+1} ([R_{x_N}^{jx_{N-1}}] R_{x_N}^{x_{N-1}j})^{-1} \left[\prod_{i=1}^{N-l} \sigma_i \right] C^{N-l+1} | \psi \rangle
\end{aligned} \tag{5.54}$$

Using 5.49 we see that $[H_{a_N}, T_x] = 0$. To show $[H_{a_N}, T_y] = 0$ it is useful to write these operators using the torus braid group notation as in 5.12. Similar to 5.49 we have

$$\tau_n C^m = C^m \tau_{(n-m) \bmod N} \tag{5.55}$$

since we can also view C as a shift of labels, $a_i \rightarrow a_{i+1}$. We rewrite T_y and H_{a_N} as

$$\begin{aligned}
T_y | \psi \rangle &= \sigma \left[\prod_{s=1}^k \tau_{i_s} \right] | \psi \rangle \\
H_{a_N} | \psi \rangle &= (R_1^{j\bar{j}}) \left[\prod_{i=1}^p \sigma_{p-i+1} \right] C | \psi \rangle + \left[\prod_{i=l}^{N-1} \sigma_i \right] \tau_N | \psi \rangle
\end{aligned} \tag{5.56}$$

Taking the product of these operators we get

$$\begin{aligned}
T_y H_{a_N} | \psi \rangle &= (R_1^{j\bar{j}}) \left[\prod_{i=1}^p \sigma_i \right] \tau_{p+1} \sigma'' \left[\prod_{s=1}^{k-1} \tau_{i_{s+1}} \right] \left[\prod_{i=1}^p \sigma_{p-i+1} \right] C | \psi \rangle + T_y | \psi \rangle \\
&= (R_1^{j\bar{j}}) \tau_1 \sigma'' \left[\prod_{s=1}^{k-1} \tau_{i_{s+1}} \right] C | \psi \rangle + T_y | \psi \rangle \\
H_{a_N} T_y | \psi \rangle &= (R_1^{j\bar{j}}) C \tau_N \sigma''' \left[\prod_{s=1}^{k-1} \tau_{i_s} \right] | \psi \rangle + T_y | \psi \rangle
\end{aligned} \tag{5.57}$$

where σ''' is the same sequence of braids as σ with the braids corresponding to τ_N removed. The sequence of braids, σ'' , is the same as σ''' with each σ_i in

the sequence replaced with σ_{i+1} . The expressions above are equal by 5.55 and so $[H_{a_N}, T_y] = 0$. We can now simultaneously diagonalise H , T_x and T_y . Next we will explicitly write the eigenvalues of the translation operators.

5.4.3 Eigenvalues of T_x and T_y

To find the eigenvalues of the translation operators we will first prove that

$$\begin{aligned} T_x^{L_x} &= (R_1^{j\bar{j}})^N \times \mathbb{1} \\ T_y^{L_y} &= (R_1^{j\bar{j}})^{-N} \times \mathbb{1} \end{aligned} \quad (5.58)$$

with $\mathbb{1}$ the identity matrix acting on the full Hilbert space. We first note that the operators above clearly return all anyons to their original positions, with each anyon traversing a non-trivial torus loop, so they act like the identity on the lattice space, meaning we need only investigate how they act on the fusion space. Acting on a fusion tree, $|x_1, \dots, x_N\rangle$ with $T_x^{L_x}$ we get

$$\begin{aligned} T_x^{L_x} |x_1, \dots, x_N\rangle &= (R_1^{j\bar{j}})^N C^N |x_1, \dots, x_N\rangle \\ &= (R_1^{j\bar{j}})^N |x_1, \dots, x_N\rangle \end{aligned} \quad (5.59)$$

Applying $T_y^{L_y}$ is slightly more complicated. Let us first consider the case where no two anyons share a column of the lattice. In this case, applying T_y does not cause any local braids and we can say

$$T_y^{L_y} |x_1, \dots, x_N\rangle = \left[\prod_{i=1}^N ([R_{x_i}^{j x_{i-1}}][R_{x_i}^{x_{i-1} j}])^{-1} \right] |x_1, \dots, x_N\rangle \quad (5.60)$$

where we say $x_0 = x_N$. Using the ribbon property, 2.34, this can be written in the form

$$\begin{aligned} & \left[\prod_{i=1}^N \frac{\theta_{x_i}}{\theta_j \theta_{x_{i-1}}} \right]^{-1} |x_1, \dots, x_N\rangle \\ &= \left(\frac{1}{\theta_j} \right)^{-N} |x_1, \dots, x_N\rangle \\ &= (R_1^{j\bar{j}})^{-N} |x_1, \dots, x_N\rangle \end{aligned} \quad (5.61)$$

Now we consider the case where multiple anyons may occupy the same column. Once again, for the sake of convenience, we revert to the notation from 5.12. In this notation, $T_y^{L_y}$ acting on the state where no two anyons share a column is given by

$$T_y^{L_y} |x_1, \dots, x_N\rangle = \prod_{i=1}^N \tau_i |x_1, \dots, x_N\rangle \quad (5.62)$$

Without loss of generality, let us now consider a state where the first k anyons occupy the same column. Then we can write

$$T_y^{L_y} |x_1, \dots, x_N\rangle = \left(\left[\prod_{i=1}^{k-1} \sigma_i \right] \tau_k \right)^k \left[\prod_{i=k+1}^N \tau_i \right] |x_1, \dots, x_N\rangle \quad (5.63)$$

The result, 5.58, holds if

$$\left(\left[\prod_{i=1}^{k-1} \sigma_i \right] \tau_k \right)^k = \prod_{i=1}^k \tau_i \quad k \geq 2 \quad (5.64)$$

This can be proven by induction. Consider $k = 2$

$$(\sigma_1 \tau_2)^2 = \sigma_1 \tau_2 \sigma_1 \tau_2 = \tau_1 \tau_2 \quad (5.65)$$

using 5.12. Assume the statement is true for $k = n$. Letting $k = n + 1$ we have

$$\begin{aligned} (\sigma_1 \dots \sigma_n \tau_{n+1})^{n+1} &= (\sigma_1 \dots \sigma_{n-1} \tau_n \sigma_n^\dagger)^{n+1} \\ &= (\sigma_1 \dots \sigma_{n-1} \tau_n) (\sigma_1 \dots \sigma_{n-2} \tau_{n-1} \sigma_n^\dagger \sigma_{n-1}^\dagger \sigma_n^\dagger) (\sigma_1 \dots \sigma_{n-1} \tau_n \sigma_n^\dagger)^{n-1} \\ &= (\sigma_1 \dots \sigma_{n-1} \tau_n) (\sigma_1 \dots \sigma_{n-1} \tau_n \sigma_n^\dagger \sigma_{n-1}^\dagger) (\sigma_1 \dots \sigma_{n-1} \tau_n \sigma_n^\dagger)^{n-1} \\ &= (\sigma_1 \dots \sigma_{n-1} \tau_n)^n (\sigma_n^\dagger \sigma_{n-1}^\dagger \dots \sigma_1^\dagger \sigma_1 \dots \sigma_{n-1} \tau_n \sigma_n^\dagger) \\ &= \left[\prod_{i=1}^{n+1} \tau_i \right] \end{aligned} \quad (5.66)$$

where we used the fact that σ_i and τ_j commute if neither of the anyons exchanged by σ_i are acted on by τ_j . Thus the result, 5.58 holds. This allows us

to write the eigenvalues of T_x and T_y as

$$\begin{aligned} P_x(A) &= \exp\left(\frac{2\pi i A}{L_x} + \frac{i \arg((R_1^{j\bar{j}})^N)}{L_x}\right) & A = 1, 2, 3, \dots, L_x \\ P_y(B) &= \exp\left(\frac{2\pi i B}{L_y} - \frac{i \arg((R_1^{j\bar{j}})^N)}{L_y}\right) & B = 1, 2, 3, \dots, L_y \end{aligned} \quad (5.67)$$

where $\arg(z)$ gives the argument of a complex number, z . This allows us to diagonalise the Hamiltonian in $L_x \times L_y$ momentum sectors with centre of mass momentum $K = \left(\frac{2\pi A}{L_x} + \frac{\arg((R_1^{j\bar{j}})^N)}{L_x}, \frac{2\pi i B}{L_y} - \frac{\arg((R_1^{j\bar{j}})^N)}{L_y}\right)$.

In the following section we will use the translation symmetry to solve the system with a single anyon on the lattice before examining the multi-particle system's level spacing statistics, (LSS). We will calculate LSS for systems of abelian anyons, systems of Fibonacci anyons and systems of Ising anyons.

5.5 Single Particle Solution and Level Statistics

First let us consider an $L_x \times L_y$ lattice on a torus containing a single anyon of type j . The fusion space of this model is simply the space of all diagrams



$$(5.68)$$

There is one such diagram for each anyon type, a , such that $a \times j = a + \dots$. The condition that fusion trees must satisfy the fusion rules of the model in question is analogous to the condition 5.21 for abelian anyons. In the previous section we wrote the Hamiltonian for this system as

$$H = -t \sum_{\langle i,j \rangle} \Theta_{ij}(c_i^\dagger c_j + c_j^\dagger c_i) \quad (5.69)$$

where Θ implemented braiding and boundary effects. However, since we don't need to consider braiding with only one anyon and crossing the boundary in either direction just adds a phase, we can write the single particle Hamiltonian in momentum space just as we did for spinless fermions. This gives

$$\begin{aligned} c_j^\dagger &= \frac{1}{L_x L_y} \sum_{\mathbf{k}} e^{-i\mathbf{k}\cdot\mathbf{r}_j} c_{\mathbf{k}}^\dagger \\ c_j &= \frac{1}{L_x L_y} \sum_{\mathbf{k}} e^{i\mathbf{k}\cdot\mathbf{r}_j} c_{\mathbf{k}} \\ H &= -t \sum_{\delta, \mathbf{k}} \cos(\mathbf{k}\cdot\delta) c_{\mathbf{k}}^\dagger c_{\mathbf{k}} \end{aligned} \quad (5.70)$$

For our 2D rectangular lattice we have

$$H = -2t \sum_{\mathbf{k}} [\cos(k_x) + \cos(k_y)] c_{\mathbf{k}}^\dagger c_{\mathbf{k}} \quad (5.71)$$

For a fermionic system we had

$$k_x = \frac{2\pi n}{L_x}, \quad k_y = \frac{2\pi m}{L_y} \quad n, m \in \mathbb{Z} \quad (5.72)$$

This is because the translation operators for fermions are such that

$$\begin{aligned} T_x^{L_x} &= \mathbb{1} \\ T_y^{L_y} &= \mathbb{1} \end{aligned} \quad (5.73)$$

However, for our system with a single anyon, 5.58 tells us

$$\begin{aligned} T_x^{L_x} &= (R_1^{j\bar{j}}) \times \mathbb{1} \\ T_y^{L_y} &= (R_1^{j\bar{j}})^{-1} \times \mathbb{1} \end{aligned} \quad (5.74)$$

meaning the momentum is now quantised as

$$k_x = \frac{2\pi n + \arg(R_1^{j\bar{j}})}{L_x}, \quad k_y = \frac{2\pi m - \arg(R_1^{j\bar{j}})}{L_y} \quad n, m \in \mathbb{Z} \quad (5.75)$$

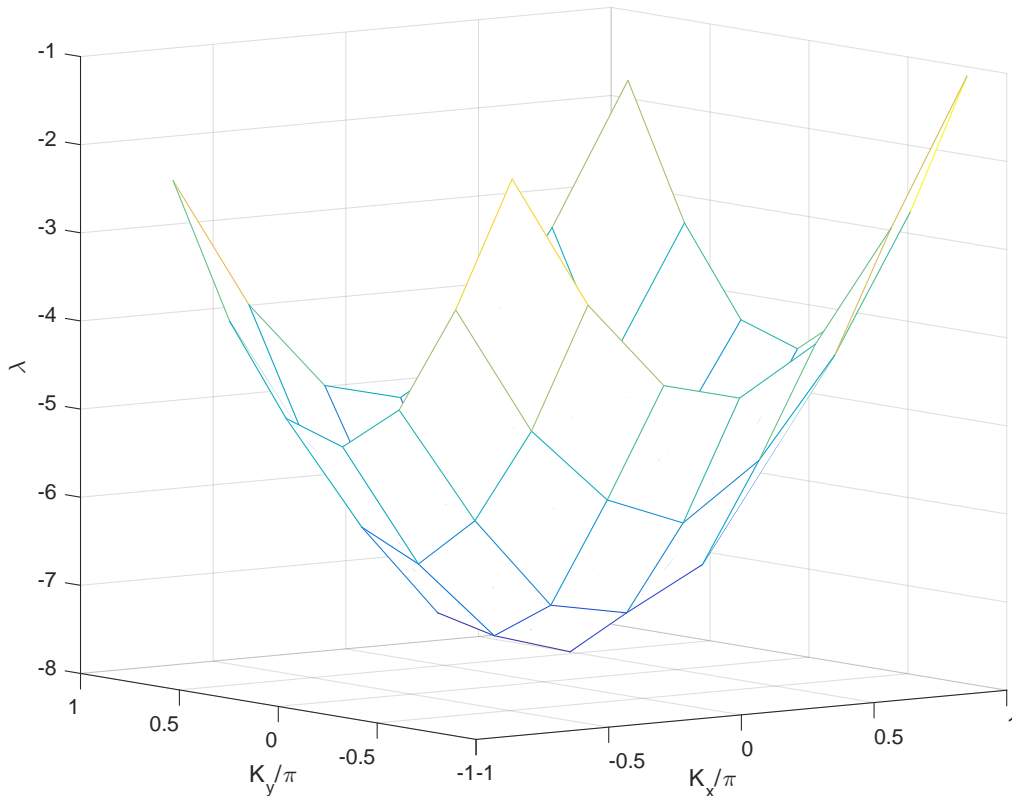


Figure 5.7: Surface plot of the lowest energy states in each momentum sector of a system of 2 Fibonacci anyons on a 7×7 lattice. The lowest eigenvalue here is -7.6530 , which is in the $(\frac{8\pi}{175}, -\frac{8\pi}{175})$ momentum sector. If we take the lowest eigenvalue of a system with a single anyon on the same lattice and double it, we get approximately -7.4899 , showing that two particle energies cannot be sums of single particle energies. The lowest energy eigenvalue of the single particle system lies in the $(\frac{4\pi}{35}, -\frac{4\pi}{35})$ momentum sector. Clearly, two anyons with this momentum cannot have their momenta added to give a centre of mass momentum $(\frac{8\pi}{175}, -\frac{8\pi}{175})$.

This gives single particle energies which are slightly shifted from the single fermion energies.

Things become much more complicated with multiple anyons. The eigenvalues of a multi-anyon Hamiltonian cannot be written as sums of single anyon eigenvalues. This is demonstrated in Figure 5.7. This leads us to investigating the level spacing statistics (LSS) of systems of multiple anyons. The LSS of a Hamiltonian are used to determine the integrability of a system. In general, an integrable system will display Poissonian statistics while a non-integrable system will have Wigner-Dyson statistics [85–88]. GOE (Gaussian Orthogonal Ensemble) statistics are usually present in a system with some non-unitary symmetry, such as time reversal symmetry, while GUE (Gaussian Unitary En-

semble) statistics indicate a lack of any such symmetry [89]. Many 1D anyon chain models studied so far have been shown to be integrable [59,90–95] while some recent work has shown a 1D tight-binding model of parafermions has GOE statistics [44].

We calculate the LSS using the ratio of consecutive level spacings [96,97]. These ratios, r_n , are calculated using

$$r_n = \frac{\min(s_n, s_{n-1})}{\max(s_n, s_{n-1})} \quad (5.76)$$

where $s_n = E_{n+1} - E_n$ is the level spacing between the $n + 1^{\text{th}}$ and n^{th} energy eigenvalues. For Poisson statistics the probability distribution of r_n is

$$P(r) = \frac{2}{(1+r)^2} \quad (5.77)$$

while the distributions for GOE and GUE statistics are given by

$$\begin{aligned} P(r) &\propto \frac{(r+r^2)}{(1+r+r^2)^{5/2}} && \text{(GOE)} \\ P(r) &\propto \frac{(r+r^2)^2}{(1+r+r^2)^4} && \text{(GUE)} \end{aligned} \quad (5.78)$$

up to normalisation. The statistics are only accurate if we first sort the spectrum into symmetry sectors and so we sort the spectrum into momentum sectors. We then calculate the LSS in each momentum sector separately and use all the statistics to find the final probability distribution.

We calculated the LSS for abelian anyons, Fibonacci anyons and Ising anyons on a torus as shown in figure 5.8. We found that a system of abelian anyons with statistical angle, $\theta = \frac{\pi}{3}$, displays GOE statistics, suggesting that this system is non-integrable but possesses some anti-unitary symmetry. We found this anti-unitary symmetry numerically for this system. The symmetry operator is given by $\mathcal{T} = \mathcal{U}\mathcal{K}$. \mathcal{K} is the complex conjugate operator where

$$\mathcal{K}|\psi\rangle = |\psi\rangle^* \quad (5.79)$$

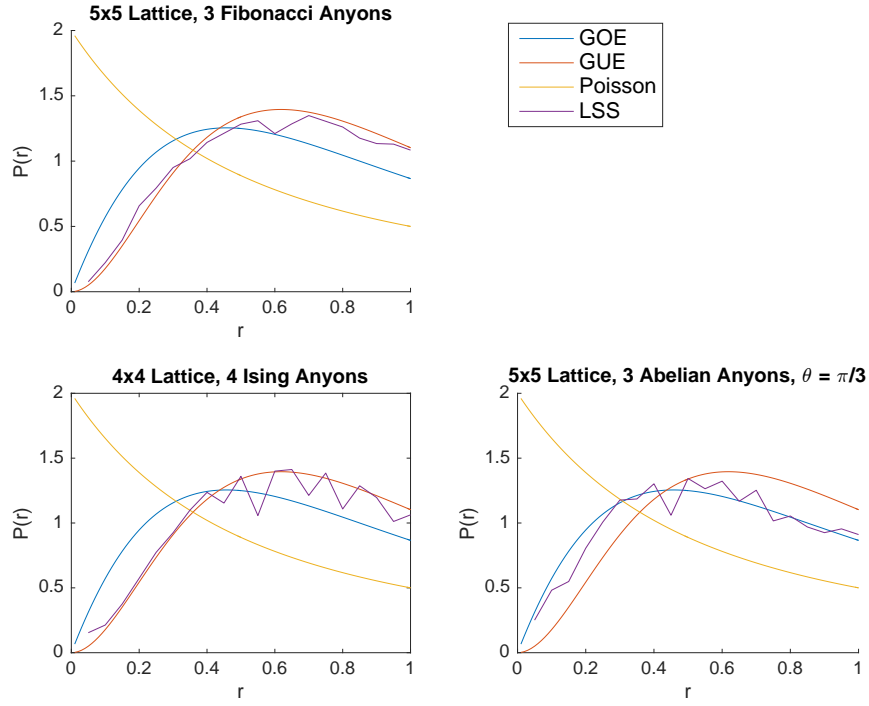
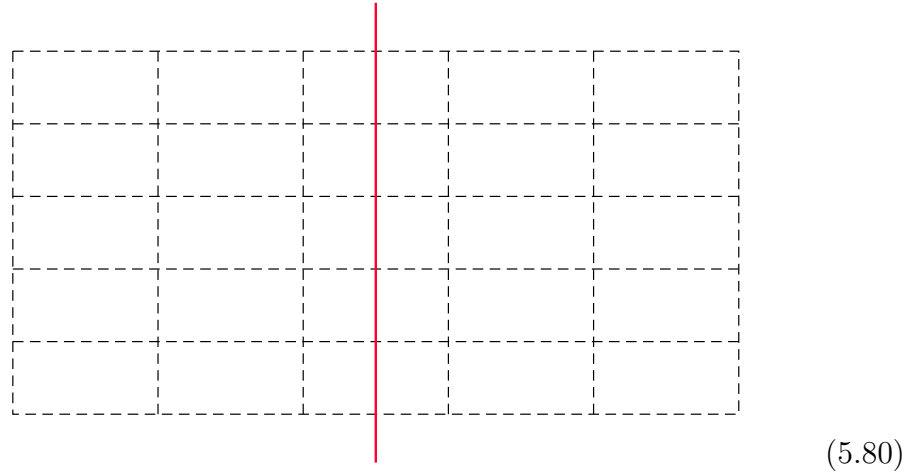


Figure 5.8: Level spacing statistics of three different systems. These systems are non-integrable, with abelian anyons with $\theta = \frac{\pi}{3}$ displaying GOE statistics. Fibonacci and Ising systems give GUE statistics.

\mathcal{U} is the unitary operator which flips the positions of the anyons in a state about the axis



Additionally, if $|\psi\rangle$ is a state with sheet index, 0, $\mathcal{U}|\psi\rangle$ has sheet index 2 and vice versa. Finally, if the anyons of a state are nearest neighbours and all in the same column, the state acquires no phase when acted on by \mathcal{U} . If no two anyons share a column, the state is multiplied by -1 . Otherwise the state picks up a phase of $e^{\frac{2\pi i}{3}}$. If $|\psi\rangle$ is a state with energy, E , and momentum, (k_x, k_y) , then

$\mathcal{T}|\psi\rangle$ has energy, E , and momentum, $(-k_x, -k_y)$. The system sizes checked for Fibonacci and Ising anyons in Figure 5.8 displayed GUE statistics, suggesting those systems are also non-integrable but possess no anti-unitary symmetry. We can see a similar symmetry to \mathcal{T} does not exist in general for non-abelian anyons since the quantisation of momentum in non-abelian systems means (k_x, k_y) and $(-k_x, -k_y)$ are rarely both good momentum sectors whereas they are always both good momentum sectors for abelian systems. For systems of $5n$ Fibonacci anyons, with n an integer, these momentum sectors exist but we found numerically that the spectra in these sectors are different, leading to GUE statistics in 5 anyon systems. Calculations were performed with small system sizes as we used exact diagonalisation to obtain full energy spectra. For example, a system of 3 Fibonacci anyons on a 5×5 lattice has a Hilbert space dimension of 9200. Nevertheless these small system sizes produced remarkably smooth statistics given the limitations.

5.6 Interactions and Entanglement

In this section we add local interactions between anyons to the hopping Hamiltonian. We subsequently cut the system into two cylindrical pieces, trace out one of them and calculate the reduced density matrix corresponding to a ground state of the system. We present some entanglement spectra for 4 Fibonacci anyons on a 5×4 lattice. We expect to see that these spectra are described by the conformal field theory spectrum of states on the edge of the cut [98]. In this case we naively expect to see the CFT spectrum related to a ring of Fibonacci anyons as detailed in [59].

To include anyon interactions to the model, we write the Hamiltonian as

$$H = -t \sum_{\langle i,j \rangle} \Theta_{ij}(c_i^\dagger c_j + c_j^\dagger c_i) + J \sum_{i=1}^N h_i \quad (5.81)$$

where h_i gives the interaction between the i^{th} anyon in the ordering and the anyons one space below it and one space to the right of it. We allow anyons to

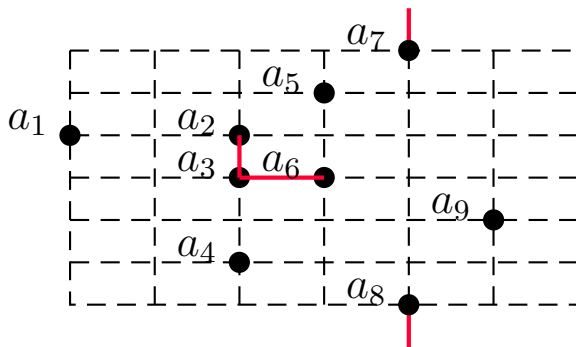
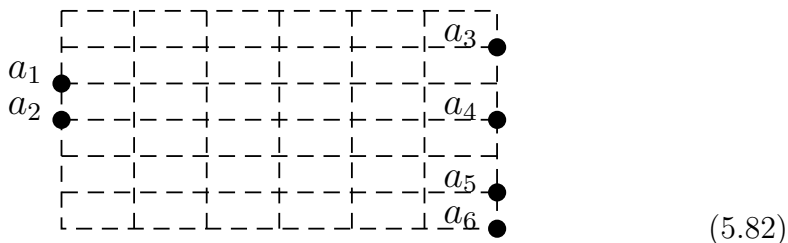


Figure 5.9: Anyons interact if they are nearest neighbours on the lattice. Here a_3 will interact with a_2 and a_6 while a_7 interacts with a_8 around one of the non-trivial torus loops.

interact if they are nearest neighbours on the lattice as in Figure 5.9. Anyons may also interact across the boundary. If two anyons are adjacent in the ordering, then their interaction is calculated as in Figure 4.2. If two anyons are not adjacent in the ordering but are nearest neighbours on the lattice, then we hop one of the anyons to a virtual site adjacent to the other, then the usual local interaction is applied and the anyon which hopped is returned to its original position. For example, say the lattice space of a state is given by

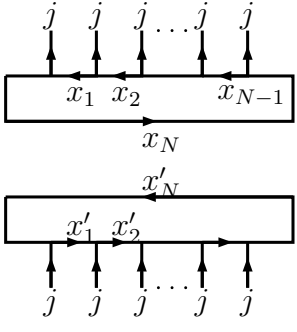


For a_4 to interact with a_2 , we hop it to the right, braiding clockwise with a_5 and a_6 . It then traverses the torus loop, braids counter-clockwise with a_1 and then we can apply a local interaction term to have it interact with a_2 . It must then return to its original position. This process acts on the fusion space as

$$\sigma_4 \sigma_5 C^\dagger \sigma_1^\dagger \tilde{h}_2 \sigma_1 C \sigma_5^\dagger \sigma_4^\dagger \quad (5.83)$$

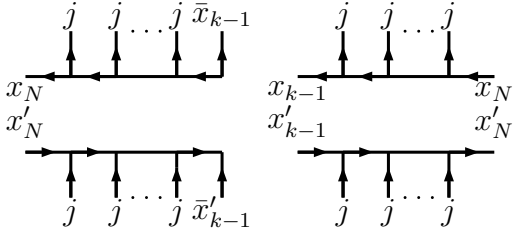
where \tilde{h}_2 is the local interaction term between the second and third anyons in the ordering. This interaction Hamiltonian has the same translational symmetry as the hopping Hamiltonian.

is given by

$$\rho = |\psi\rangle\langle\psi| = \sum_{\substack{\mathbf{l}_A, \mathbf{l}_B, \mathbf{x}, \\ \mathbf{l}'_A, \mathbf{l}'_B}} \psi_{\mathbf{l}_A, \mathbf{l}_B, \mathbf{x}} \psi_{\mathbf{l}'_A, \mathbf{l}'_B, \mathbf{x}'}^* |\mathbf{l}_A, \mathbf{l}_B\rangle\langle\mathbf{l}'_A, \mathbf{l}'_B, \mathbf{x}'| \otimes$$


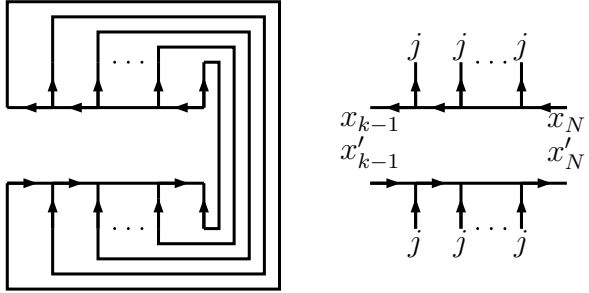
$$(5.86)$$

We now cut our system as above, giving

$$\rho_{cut} = \sum_{\substack{\mathbf{l}_A, \mathbf{l}_B, \mathbf{x}, \\ \mathbf{l}'_A, \mathbf{l}'_B, \mathbf{x}'}} \frac{\psi_{\mathbf{l}_A, \mathbf{l}_B, \mathbf{x}} \psi_{\mathbf{l}'_A, \mathbf{l}'_B, \mathbf{x}'}^*}{\sqrt{d_{x_{k-1}} d_{x'_{k-1}} d_{x_N} d_{x'_N}}} |\mathbf{l}_A, \mathbf{l}_B\rangle\langle\mathbf{l}'_A, \mathbf{l}'_B| \otimes$$


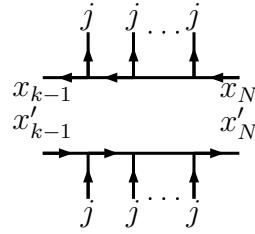
$$(5.87)$$

We now trace over A to get the reduced density matrix, ρ_B .

$$\rho_B = \sum_{\substack{\mathbf{l}_A, \mathbf{l}_B, \mathbf{x}, \\ \mathbf{l}'_A, \mathbf{l}'_B, \mathbf{x}'}} \frac{\psi_{\mathbf{l}_A, \mathbf{l}_B, \mathbf{x}} \psi_{\mathbf{l}'_A, \mathbf{l}'_B, \mathbf{x}'}^*}{\sqrt{d_{x_{k-1}} d_{x'_{k-1}} d_{x_N} d_{x'_N}}} \langle\mathbf{l}_A || \mathbf{l}'_A\rangle |\mathbf{l}_B\rangle\langle\mathbf{l}'_B| \otimes$$


$$(5.88)$$

which can be simplified to

$$\rho_B = \sum_{\substack{\mathbf{l}_A, \mathbf{l}_B, \mathbf{x}, \\ \mathbf{l}'_B, \mathbf{x}'}} \frac{\psi_{\mathbf{l}_A, \mathbf{l}_B, \mathbf{x}} \psi_{\mathbf{l}'_A, \mathbf{l}'_B, \mathbf{x}'}^* d_j^{\frac{k}{2}}}{\sqrt{d_{x_{k-1}} d_{x_N}}} |\mathbf{l}_B\rangle\langle\mathbf{l}'_B| \delta_{x_1, x'_1} \delta_{x_2, x'_2} \dots \delta_{x_{k-1}, x'_{k-1}} \delta_{x_N, x'_N} \otimes$$


$$(5.89)$$

Having calculated ρ_B , we can now calculate the entanglement spectrum, which is just the set of eigenvalues, λ_i , of ρ_B . This spectrum is related to the

energy levels, ϵ_i , of an 'entanglement Hamiltonian' [98], H_E , at the edge of B where

$$\rho_B = e^{-H_E}, \quad \lambda_i = e^{-\epsilon_i} \quad (5.90)$$

We calculated the entanglement spectrum of the ground state of a 5×4 lattice with 4 Fibonacci anyons, two of which are traced out, for various interaction strengths as in Figure 5.10. In these calculations, we apply energy -1 to a fusion of two anyons to the identity and energy 0 to fusion to a τ anyon. With this convention, $J > 0$ energetically favours fusion to the identity and we say the

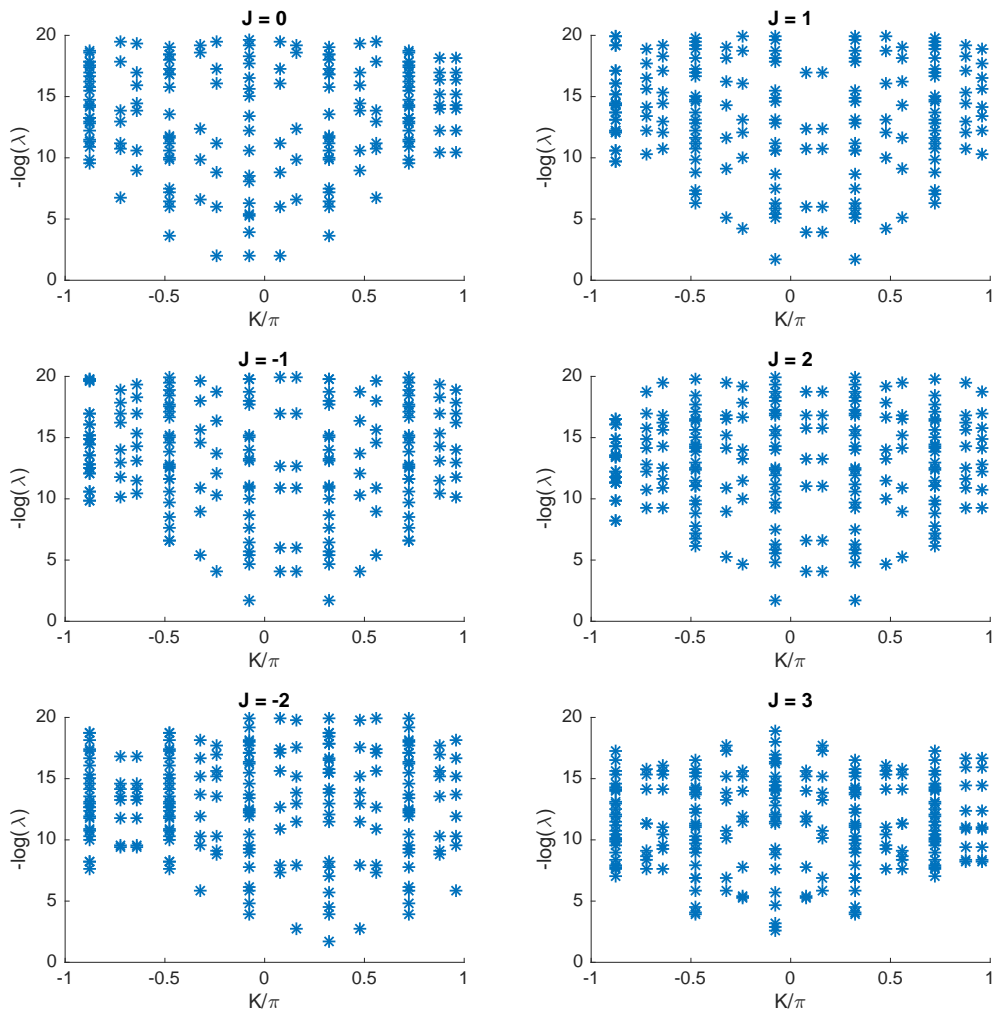


Figure 5.10: Spectra of entanglement Hamiltonians with various interaction strengths. We get linear dispersion relations, particularly for $J = -2$ and $J = 3$. We believe that for larger systems we may be able to identify these spectra as the $c = 7/10$ or $c = 4/5$ CFT spectra. In each case we got the entanglement spectrum of a ground state of a system consisting of a 5×4 lattice with 4 anyons and $t = 1$. Half of the lattice sites and 2 anyons traced out.

sorted by momentum as the remaining cylinder states still have translational symmetry around the non-trivial loop of the cylinder. The eagle-eyed reader will notice that we have 15 towers in Figure 5.10 when we might expect 5, one for each row in the lattice. This is due to different quantisation of momentum depending on the labels, x_{k-1} and x_N . If $x_{k-1} = x_N$ then the remaining cylinder state would also make a good torus state and the quantisation of momentum is the same as for the same state on the torus. If $x_{k-1} \neq x_N$ then we can have a different quantisation for each pair, $\{x_{k-1}, x_N\}$. For the systems plotted we have

$$\begin{aligned} T_y^{L_y} &= [R_\tau^{\tau\tau}]^{-2} \times \mathbf{1} & (x_{k-1}, x_N) &= (1, \tau) \\ T_y^{L_y} &= ([R_\tau^{\tau\tau}][R_1^{\tau\tau}])^{-2} \times \mathbf{1} & (x_{k-1}, x_N) &= (\tau, 1) \end{aligned} \tag{5.91}$$

We see that with interactions turned on, the low-lying states of the entanglement Hamiltonian have a linear dispersion relation, suggesting they may be described by a CFT spectrum and that the system is in a gapped phase for each value of J in Figure 5.10. In Figure 5.11 we calculate the energy gap of several systems, along with the entanglement spectrum of a system with 4 Fibonacci anyons on a 5×4 lattice with $t = 1$, $J = 10$ and 2 anyons traced out. This figure suggests that a phase transition may occur around $J = 7$ for the system size considered in Figure 5.10 when t is fixed at 1 for this system but system sizes much closer to the thermodynamic limit will be needed to say anything definitive about the phases of the system. The next step in this experiment will be to perform this calculation for larger systems and attempt to verify whether this spectrum can be identified with either of the CFT spectra described in [59] or with some other CFT spectrum. In that paper, the authors show that the spectrum of a ring of interacting Fibonacci anyons is given by the $c = \frac{7}{10}$ CFT spectrum for AFM interactions and the $c = \frac{4}{5}$ CFT for FM interactions.

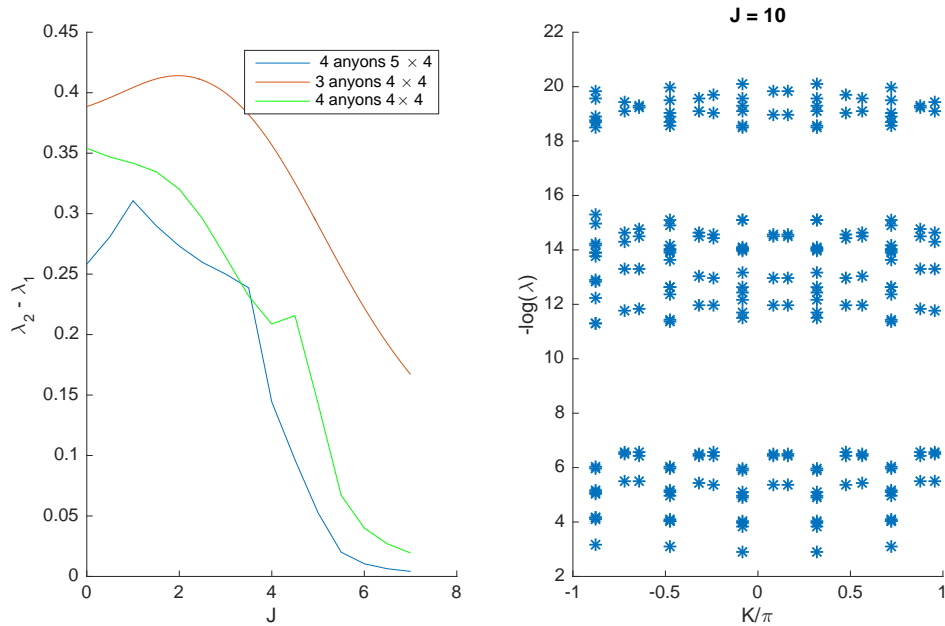


Figure 5.11: Energy gap for 3 systems with J ranging from 0 to 7 and $t = 1$. Energy gap appears to close around $J = 7$ for the 4 anyon systems and later for the 3 anyon system, indicating a possible phase transition. Obviously much larger system sizes are needed to draw any solid conclusions. Entanglement spectrum of a system with 4 anyons on a 5×4 lattice with 2 traced out and $J = 10$ is shown on the right. The previous structure of the spectrum has been lost, also indicating a phase transition has occurred.

5.7 Conclusion

In this chapter we constructed a hopping model of non-abelian anyons on a torus. We showed that this model has a translational symmetry around each non-trivial torus loop. We calculated the level spacing statistics of this model with Fibonacci anyons, Ising anyons and $\theta = \frac{\pi}{3}$ abelian anyons. These statistics show that each of these systems is non-integrable. We then added interactions to the Hamiltonian and calculated the entanglement spectrum of a ground state after cutting the torus into two cylinders. With interactions turned on, the low lying states of this spectrum display a linear dispersion relation, suggesting it is possible that the entanglement spectrum is described by a conformal field theory spectrum.

Chapter 6

Conclusions and Outlook

We gave a brief introduction to abelian and non-abelian anyons. We mentioned the relationship between anyons and topological order before introducing symmetry protected topological phases and strong zero modes. From there, we shifted to a description of the tight-binding model for hardcore particles.

In Chapter 2 we gave a more detailed introduction to anyon models. In particular, we discussed the fusion vector space of multiple anyons and the operations we may perform on this space, such as F-moves, inner products and braiding. We introduced the diagrammatic formalism of anyon models as described in [20]. The chapter ended with an example of how to resolve the diagram associated with the 'spectacles diagram', $(S_c)_{ab}$.

Chapter 3 was focused on the definition and construction of strong zero modes. After presenting the definition of a strong zero mode, we described the quantum Ising chain and performed the iterative construction of its strong zero modes. This construction is described in full in [28]. We then gave a description of the \mathbb{Z}_n chiral clock model. This model is a generalisation of the quantum Ising chain and its zero modes have been studied in detail, for example in [28, 31–33].

We made the jump from strong zero modes in spin chains to strong zero modes in anyon chains in Chapter 4. We constructed Hamiltonians which model local anyon interactions as in [59]. We went on to impose a staggering on these Hamiltonians, modelling our system on the quantum Ising chain. This

approach bore fruit when we constructed such a Hamiltonian for a Tambara-Yamagami chain. This model is partially defined by the choice of an abelian group, G . For $G = \mathbb{Z}_n$, the Hamiltonian we constructed for this model was exactly the one defined for the \mathbb{Z}_n chiral clock model in [28]. This provided evidence that the staggered Hamiltonian could indeed describe anyon models with strong zero modes as we had hoped. Emboldened by this, we applied the construction to more anyon models, namely Fibonacci anyons and $SU(2)_4$ anyons. We showed that a Fibonacci chain constructed this way allowed for no strong zero modes. Degeneracy along the spine of the fusion tree caused the degeneracy between states which could be related by a potential strong zero mode to split at first order. This issue is analogous to the issue of quantum resonance described in [32, 33]. To circumvent this issue, we turned our attention to the $SU(2)_4$ model. Here, the existence of a non-trivial anyon with quantum dimension 1 minimised the degeneracy along the spine of the fusion tree which would, theoretically, protect the degeneracy of states which were exactly degenerate with $f = 0$. This proved to be the case as we showed numerically that the splitting of degenerate states was proportional to $f^{\frac{1}{2}}$.

Having produced numerical evidence for the existence of a strong zero mode, we attempted to construct it. We were able to write the chain Hamiltonian as the Hamiltonian of a D_3 -symmetric XXZ spin chain as in [71]. This allowed us to use the methods developed in [33] to construct the zero mode in terms of spin operators. To write this zero mode in the diagrammatic formalism, there remained an issue writing operators that did not possess a D_3 symmetry in both the spin chain formalism and the anyon chain formalism. This was a problem as each term in the zero mode contained an operator, σ_i^z , for some integer, i , which does not possess a D_3 symmetry. The solution to this issue came in the form of an operator constructed identically to the topological symmetry operator in anyon rings [47, 76]. This operator takes an extra anyon line, running parallel to the spine of the fusion tree, and fuses it with each label along the spine. This operator, with the 2 anyon in $SU(2)_4$ being used as the

extra label, is the starting point in the iterative construction of the zero mode. This operator has the same action in the anyon chain as σ_1^z in the spin chain. A similar operator was constructed for each σ_i^z where $i > 1$. We would expect a similar construction to be possible for any anyon model with a non-trivial anyon, say a , with $d_a = 1$ and another anyon, j , such that $j \times j = j + a + \dots$. This construction could be identical to the one for the zero mode in the $SU(2)_4$ chain if $a^n = a$ for some n where $a^n = a \times a \times \dots \times a$. Another interesting avenue to explore would be to investigate if this construction only works with an anyon of quantum dimension 1 or if there exists a model where this construction with an anyon of quantum dimension greater than 1 describes a strong zero mode.

In Chapter 5, we switched our focus to tight-binding. We presented a solution for a tight-binding model of spinless fermions. We went on to describe systems of anyons on a torus using the material in [50, 78, 80]. We then presented the description of a tight-binding model of abelian anyons on a torus given in [80]. This laid the foundation for a similar construction for non-abelian anyons, which we showed in Appendix A is identical to the abelian construction if we use \mathbb{Z}_n anyons in our construction. This model possesses a translational symmetry around each non-trivial torus loop. We defined the operators which generate this symmetry and verified that they commute with the Hamiltonian and each other. Using this symmetry, we wrote the solution of the single anyon system and calculated the level spacing statistics of multi-anyon systems containing abelian anyons, Fibonacci anyons and Ising anyons. These statistics showed that a hopping model of 'free' anyons on a torus is not solvable in general, in contrast to the same model for bosons and fermions. The anyons are not totally free as their braiding acts similarly to the inclusion of an interaction term in a tight-binding model of fermions. On the topic of interactions, we were able to add a term to the Hamiltonian which models local interactions between the anyons, similar to the Hubbard model, although not to be confused with the anyon Hubbard model described in [42]. We performed a basic entanglement experiment on this interacting Hamilto-

nian. This involved cutting the torus into two cylinders and tracing one of them out. Calculating the entanglement spectrum of a ground state of the system with these cuts, one might expect to see that it is described by the conformal field theory spectrum of a state living on the edge of the cuts, an anyon ring in this case [98, 101, 102]. The spectrum of the interaction Hamiltonian of a Fibonacci anyon ring was shown to match the spectrum of the $c = \frac{7}{10}$ CFT for anti-ferromagnetic (AFM) interactions or the $c = \frac{4}{5}$ CFT for ferromagnetic (FM) interactions in [59]. We would naively expect our entanglement spectrum to be described by one of these spectra, depending on the phase of the model [91]. Our preliminary results look promising in this regard. Sorting the entanglement spectra of systems with various interaction strengths by momentum in the direction which was not cut, we find that the low lying states have a linear dispersion relation. Unfortunately, the system sizes studied are too small to identify primary fields of the CFT, we can only speculate which states are descendants of others. Current results were obtained from systems of just 4 anyons. This leaves the obvious future direction of research of either obtaining time on a supercomputer or optimising our code to the extent that we may identify the CFT which describes the entanglement spectrum. As well as this, the development of anyonic tensor network tools [103, 104] in the future may allow for more possibilities such as producing phase diagrams for this model with a chemical potential term also included in the Hamiltonian, giving more insight into the behaviour of non-abelian anyons on a 2D surface.

Appendix A

\mathbb{Z}_N Anyon Torus Construction

We demonstrate that our construction of a non-abelian anyon hopping model on a torus is equivalent to the construction in [79] when the lattice is populated with \mathbb{Z}_N anyons. The full list of properties of \mathbb{Z}_N anyons is listed in [20] but we list the important properties for our construction here.

Anyon types in this theory are labeled by $[a]_N$ where $a \in \mathbb{Z}$ and $[a]_N$ is the least residue of $a \bmod N$. In this appendix, we will just say an anyon has type a when we refer to the anyon of type $[a]_N$. The fusion rules for this model are

$$[a]_N \times [b]_N = [a + b]_N \quad (\text{A.1})$$

and so these are abelian anyons. The exchange statistics of this model are

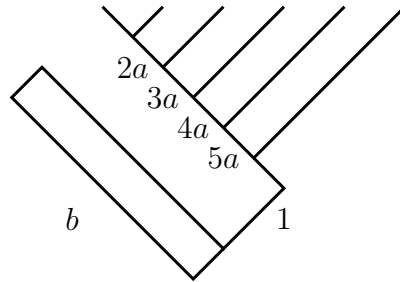
$$R_{a+b}^{ab} = \exp\left(\frac{2\pi n}{N}iab\right) \quad n \in \{0, 1, \dots, N-1\} \quad (\text{A.2})$$

Each of the constructions in this thesis featured lattices with anyons of only one type. Here we say that all anyons on the lattice are of type a and

$$R_{2a}^{aa} = \exp\left(\frac{2\pi n}{N}ia^2\right) = e^{i\theta} \quad (\text{A.3})$$

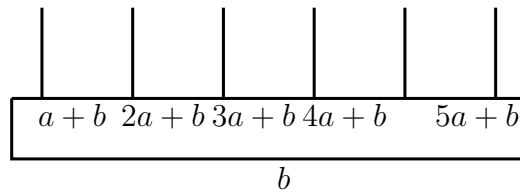
making this a lattice of abelian anyons with exchange angle θ . For this model, $(S_c)_{ab}$ is only defined when c is the identity. This condition enforces that the anyons on the lattice must fuse to the vacuum. This is equivalent to

the condition 5.20 and gives an N component wave-function where the N components are labeled by the N anyon types of the model. A value of b for this component is represented by a loop with charge b in basis B_2 .



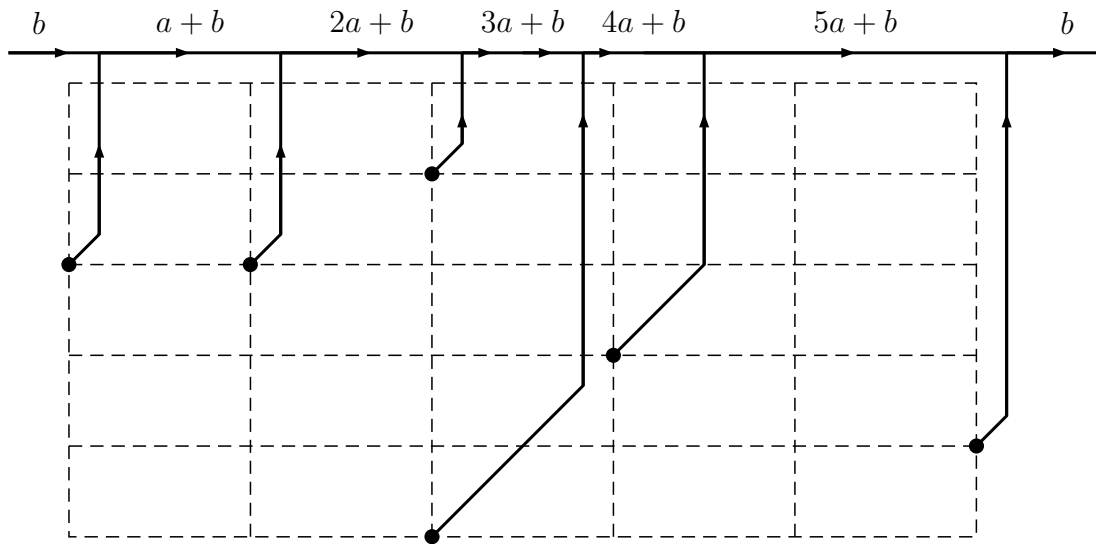
(A.4)

This state in basis B_1 is given by



(A.5)

and we can perform the lattice construction as



(A.6)

Clearly, exchanging two anyons in the bulk is equivalent to the exchange in the abelian construction. In the construction of Hatsugai and colleagues, a phase correction of $e^{i2l\theta}$ was applied when the $l + 1^{\text{th}}$ anyon in the ordering crossed the lattice boundary downward. Using the non-abelian anyon construction,

this correction is

$$[R_{(l+1)a+b}^{a(la+b)}]^{-2} = e^{-i2l\theta} e^{-i2\theta \frac{b}{a}} \quad (\text{A.7})$$

which is the opposite of the phase applied in the abelian construction. The direction of this phase is just a choice of convention and the models are equivalent if the phase correction due to a loop in the x direction in our construction is also the opposite of the phase correction in the abelian construction. The label b just indicates the sheet index of the wavefunction. Let us now consider a particle traversing the other non-trivial loop. In the abelian construction this lowers the sheet index by 1 and applies a phase correction $e^{-i\theta(N_a-1)}$ where N_a is the number of anyons on the lattice. In our non-abelian construction, we cyclically permute the labels by one space and apply a phase correction

$$R_1^{a\bar{a}} = e^{-i\theta} \quad (\text{A.8})$$

Using 5.20, this phase correction can be written as $e^{i\theta(N_a-1)}$, which is the opposite of the phase given in the abelian construction. Therefore the two constructions are equivalent.

Appendix B

Gauge Choice for Hopping

Model of Non-Abelian Anyons

Here, we present a brief argument to show our choice of branch cuts in the anyon hopping model on a torus is merely a gauge choice and so any hopping model which satisfies the torus braid group relations, 5.11, 5.12 and 5.13, will give an equivalent model.

Let us consider a lattice with two anyons, a and b . We say a is at the lattice point, $|i + y, j - x\rangle$ and b is at $|i, j\rangle$ where $x, y \in \mathbb{Z}$. This is illustrated in Figure B.1. We consider the scenario where a is earlier than b in our linear ordering. This gives $x > 0$ or $x = 0, y < 0$. For a generic nearest-neighbour

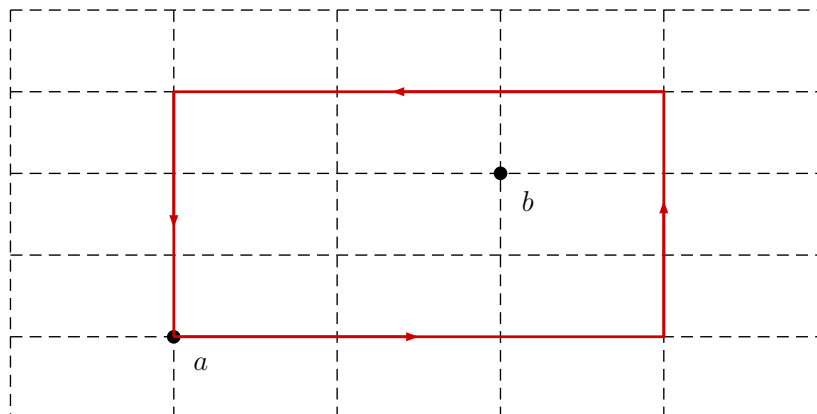


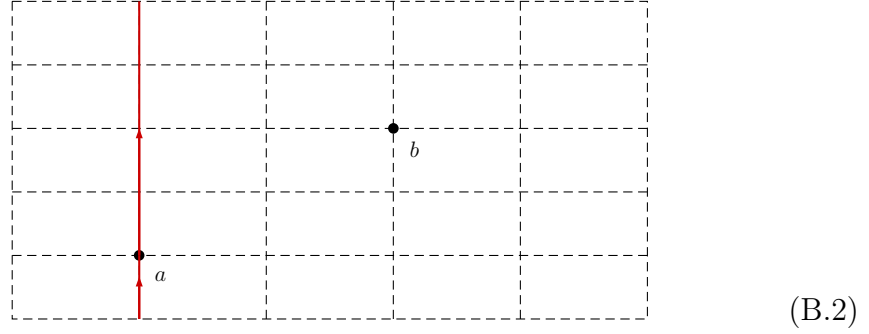
Figure B.1: Lattice with anyon b at $|i, j\rangle$ and a at $|i + 2, j - 2\rangle$. The red line indicates a possible counter-clockwise loop of a encircling b .

hopping model, the Hamiltonian terms acting which hop a to the right and

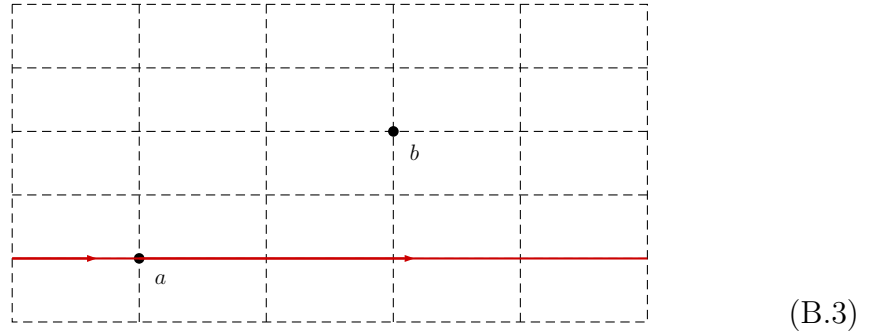
downward along with their Hermitian conjugates are

$$\begin{aligned}
 H_a = & U_{v,y,x}^\dagger |i+y+1, j-x\rangle \langle i+y, j-x| + U_{h,y,x}^\dagger |i+y, j-(x-1)\rangle \langle i+y, j-x| \\
 & + U_{v,y,x} |i+y, j-x\rangle \langle i+y+1, j-x| + U_{h,y,x} |i+y, j-x\rangle \langle i+y, j-(x-1)|
 \end{aligned}
 \tag{B.1}$$

where $U_{v,y,x}$ and $U_{h,y,x}$ are unitary transformations applied to the fusion space which depend on the relative position of a and b . To satisfy the torus braid group relations, a combination of hopping terms which have a traverse a loop which encircles b must act on the fusion space with σ^2 or σ^{-2} depending on the direction of the loop. As in 5.11, σ is the braid group generator which braids a and b counter-clockwise. We also require that a combination of hopping terms which have a traverse the loop



or any topologically equivalent loop, acts on the fusion space as ρ_1 . Similarly, if a traverses a loop topologically equivalent to



the fusion space is acted on by τ_1 . The braid group generators, ρ_i and τ_i , are the same as those given in Figure 5.1. The construction given in Chapter 5 satisfies the torus braid group relations. To arrive at that construction, we

perform a gauge transformation on H_a and get

$$\begin{aligned} \tilde{H}_a = & V_{y+1,x} V_{y,x}^\dagger U_{v,y,x}^\dagger |i+y+1, j-x\rangle \langle i+y, j-x| \\ & + V_{y,x-1} V_{y,x}^\dagger U_{h,y,x}^\dagger |i+y, j-(x-1)\rangle \langle i+y, j-x| + \text{h.c} \end{aligned} \quad (\text{B.4})$$

In Chapter 5, we chose this gauge transformation such that

$$\begin{aligned} V_{y+1,x} V_{y,x}^\dagger U_{v,y,x}^\dagger &= \mathbb{1} & i+y \neq L_y \\ V_{y+1,x} V_{y,x}^\dagger U_{v,y,x}^\dagger &= \rho_1^{-1} & i+y = L_y \\ V_{y,x-1} V_{y,x}^\dagger U_{h,y,x}^\dagger &= \sigma & y > 0, x = 1 \\ V_{y,x-1} V_{y,x}^\dagger U_{h,y,x}^\dagger &= \sigma^{-1} & y < 0, x = 0, j \neq L_x \\ V_{y,x-1} V_{y,x}^\dagger U_{h,y,x}^\dagger &= \tau \sigma^{-1} & y < 0, x = 0, j = L_x \\ V_{y,x-1} V_{y,x}^\dagger U_{h,y,x}^\dagger &= \mathbb{1} & \text{otherwise} \end{aligned} \quad (\text{B.5})$$

where τ acts similarly to \tilde{T} from 5.32. We can write similar equations so that the non-trivial loops traversed by b also satisfy the torus braid group relations and this construction can be extended to give the construction in Chapter 5. Changing the sites where $V_{y+1,x} V_{y,x}^\dagger U_{v,y,x}^\dagger$ and $V_{y,x-1} V_{y,x}^\dagger U_{h,y,x}^\dagger$ act non-trivially will give different branch cuts where non-trivial braids are applied.

Bibliography

- [1] J. M. Leinaas and J. Myrheim. On the theory of identical particles. *Nuovo Cimento B*, 37B:1, 1977.
- [2] F. Wilczek. Magnetic flux, angular momentum, and statistics. *Phys. Rev. Lett.*, 48:1144–1146, 1982.
- [3] Emil Artin. Theorie der zöpfe. *Abh. math. Sem. Hamburg*, 4:47–72, 1926.
- [4] F. A. Bais. FLUX METAMORPHOSIS. *Nucl. Phys. B*, 170:32–43, 1980.
- [5] G. A. Goldin, R. Menikoff, and D. H. Sharp. Comments on “general theory for quantum statistics in two dimensions”. *Phys. Rev. Lett.*, 54:603, 1985.
- [6] V. G. Turaev. *Quantum Invariants of Knots and 3-Manifolds*. Walter de Gruyter, Berlin, New York, 1994.
- [7] Christian Kassel. *Quantum Groups*. Springer-Verlag, New York, Berlin, Heidelberg, 1995.
- [8] Bojko Bakalov and Alexander Kirillov. *Lectures on Tensor Categories and Modular Functors*, volume 21 of *University Lecture Series*. American Mathematical Society, 2001.
- [9] P. Etingof, S. Gelaki, D. Nikshych, and V. Ostrik. *Tensor Categories*. Mathematical Surveys and Monographs. American Mathematical Society, 2016.
- [10] Kerstin Beer, Dmytro Bondarenko, Alexander Hahn, Maria Kalabakov, Nicole Knust, Laura Niermann, Tobias J. Osborne, Christin Schridde,

- Stefan Seckmeyer, Deniz E. Stiegemann, and Ramona Wolf. From categories to anyons: a travelogue. *arXiv e-prints*, page arXiv:1811.06670, Nov 2018.
- [11] R. B. Laughlin. Anomalous quantum Hall effect: an incompressible quantum fluid with fractionally charged excitations. *Phys. Rev. Lett.*, 50(18):1395–8, 1983.
- [12] J. P. Eisenstein and H. L. Stormer. The fractional quantum hall effect. *Science*, 248(4962):1510–1516, 1990.
- [13] G. Moore and N. Read. Nonabelions in the fractional quantum Hall effect. *Nucl. Phys. B*, 360(2-3):362–396, 1991.
- [14] Horst L. Stormer, Daniel C. Tsui, and Arthur C. Gossard. The fractional quantum hall effect. *Rev. Mod. Phys.*, 71:S298–S305, Mar 1999.
- [15] C. Nayak, S. H. Simon, A. Stern, M. Freedman, and S. Das Sarma. Non-Abelian anyons and topological quantum computation. *Reviews of Modern Physics*, 80:1083–1159, July 2008.
- [16] A. Yu. Kitaev. Fault-tolerant quantum computation by anyons. *Ann. Phys.*, 303:2, 2003.
- [17] Michael H. Freedman, Alexei Kitaev, Michael J. Larsen, and Zhenghan Wang. Topological Quantum Computation. *arXiv e-prints*, pages quant-ph/0101025, January 2001.
- [18] J. Nakamura, S. Liang, G. C. Gardner, and M. J. Manfra. Direct observation of anyonic braiding statistics. *Nature Physics*, 16(9):931–936, 2020.
- [19] H. Bartolomei, M. Kumar, R. Bisognin, A. Marguerite, J. M. Berroir, E. Bocquillon, B. Plaças, A. Cavanna, Q. Dong, U. Gennser, Y. Jin, and G. Fève. Fractional statistics in anyon collisions. *Science*, 368(6487):173–177, April 2020.

- [20] Parsa Bonderson, Kirill Shtengel, and J. K. Slingerland. Interferometry of non-Abelian anyons. *Annals of Physics*, 323(11):2709–2755, Nov 2008.
- [21] X. G. Wen. Topological orders in rigid states. *Int. J. Mod. Phys. B*, 4(2):239–71, 1990.
- [22] X. G. Wen and Q. Niu. Ground-state degeneracy of the fractional quantum Hall states in the presence of a random potential and on high-genus riemann surfaces. *Phys. Rev. B*, 41(13):9377–96, 1990.
- [23] X.G. Wen. *Quantum Field Theory of Many-Body Systems: From the Origin of Sound to an Origin of Light and Electrons: From the Origin of Sound to an Origin of Light and Electrons*. Oxford Graduate Texts. OUP Oxford, 2004.
- [24] B.A. Bernevig and T.L. Hughes. *Topological Insulators and Topological Superconductors*. Princeton University Press, 2013.
- [25] Xiao-Gang Wen. Colloquium: Zoo of quantum-topological phases of matter. *Reviews of Modern Physics*, 89(4):041004, October 2017.
- [26] Andrew Resnick. Topological aspects of condensed matter physics: lecture notes of the les houches summer school: Volume 103, august 2014. *Contemporary Physics*, 59(3):320–321, 2018.
- [27] A. Y. Kitaev. 6. QUANTUM COMPUTING: Unpaired Majorana fermions in quantum wires. *Phys. Usp.*, 44:131, October 2001.
- [28] P. Fendley. Parafermionic edge zero modes in Z_n -invariant spin chains. *J. Stat. Mech.*, 11:11020, November 2012.
- [29] A. S. Jermyn, R. S. K. Mong, J. Alicea, and P. Fendley. Stability of zero modes in parafermion chains. *Phys. Rev. B*, 90(16):165106, October 2014.

- [30] Jason Alicea and Paul Fendley. Topological Phases with Parafermions: Theory and Blueprints. *Annual Review of Condensed Matter Physics*, 7:119–139, March 2016.
- [31] P. Fendley. Free parafermions. *J. Phys. A Math. Theor.*, 47(7):075001, February 2014.
- [32] N. Moran, D. Pellegrino, J. K. Slingerland, and G. Kells. Parafermionic clock models and quantum resonance. *Phys. Rev. B*, 95(23):235127, June 2017.
- [33] Domenico Pellegrino, Graham Kells, Niall Moran, and Joost K. Slingerland. Constructing edge zero modes through domain wall angle conservation. *arXiv e-prints*, page arXiv:1908.03459, Aug 2019.
- [34] M. F. Maghrebi, S. Ganeshan, D. J. Clarke, A. V. Gorshkov, and J. D. Sau. Parafermionic zero modes in ultracold bosonic systems. *Phys. Rev. Lett.*, 115:065301, Aug 2015.
- [35] J. Alicea and A. Stern. Designer non-Abelian anyon platforms: from Majorana to Fibonacci. *Phys. Scripta*, 164(1):014006, December 2015.
- [36] W.A. Harrison. *Electronic Structure and the Properties of Solids: The Physics of the Chemical Bond*. Dover Books on Physics. Dover Publications, 1989.
- [37] A.P. Sutton. *Electronic Structure of Materials*. Clarendon Press, 1993.
- [38] D.G. Pettifor and I.W.P.M.D.M.D.G. Pettifor. *Bonding and Structure of Molecules and Solids*. Bonding and Structure of Molecules and Solids. Clarendon Press, 1995.
- [39] M. Finnis and Oxford University Press. *Interatomic Forces in Condensed Matter*. EBSCO ebook academic collection. Oxford University Press, 2003.

- [40] J. C. Slater and G. F. Koster. Simplified LCAO Method for the Periodic Potential Problem. *Physical Review*, 94(6):1498–1524, June 1954.
- [41] J. Hubbard. Electron correlations in narrow energy bands. *Proceedings of the Royal Society of London. Series A, Mathematical and Physical Sciences*, 276(1365):238–257, 1963.
- [42] Tassilo Keilmann, Simon Lanzmich, Ian McCulloch, and Marco Roncaglia. Statistically induced phase transitions and anyons in 1d optical lattices. *Nature Communications*, 2(1):361, 2011.
- [43] J. Arcila-Forero, R. Franco, and J. Silva-Valencia. Critical points of the anyon-Hubbard model. , 94(1):013611, July 2016.
- [44] Davide Rossini, Matteo Carrega, Marcello Calvanese Strinati, and Leonardo Mazza. Anyonic tight-binding models of parafermions and of fractionalized fermions. *Phys. Rev. B*, 99(8):085113, 2019.
- [45] Sebastian Greschner and Luis Santos. Anyon Hubbard Model in One-Dimensional Optical Lattices. , 115(5):053002, July 2015.
- [46] John Preskill. Topological quantum computation. Lecture notes, 2004.
- [47] Alexei Kitaev. Anyons in an exactly solved model and beyond. *Ann. Phys.*, 321(1):2–111, 2006.
- [48] Damien Calaque and Pavel Etingof. Lectures on tensor categories, 2004.
- [49] Parsa Bonderson. Measuring Topological Order. *arXiv e-prints*, page arXiv:2102.05677, February 2021.
- [50] Robert N. C. Pfeifer, Oliver Buerschaper, Simon Trebst, Andreas W. W. Ludwig, Matthias Troyer, and Guifre Vidal. Translation invariance, topology, and protection of criticality in chains of interacting anyons. , 86(15):155111, Oct 2012.
- [51] Elliott Lieb, Theodore Schultz, and Daniel Mattis. Two soluble models of an antiferromagnetic chain. *Ann. Phys.*, 16:407–466, 1961.

- [52] Steven Howes, Leo P Kadanoff, and Marcel Den Nijs. Quantum model for commensurate-incommensurate transitions. *Nucl. Phys. B*, 215(2):169–208, 1983.
- [53] H. Au-Yang and J. H. H. Perk. The Many Faces of the Chiral Potts Model. *Int. J. Mod. Phys. B*, 11:11–26, 1997.
- [54] Günter von Gehlen and Vladimir Rittenberg. \mathbb{Z}_n -symmetric quantum chains with an infinite set of conserved charges and \mathbb{Z}_n zero modes. *Nucl. Phys. B*, 257:351–370, 1985.
- [55] S. Ostlund. Incommensurate and commensurate phases in asymmetric clock models. *Phys. Rev. B*, 24:398–405, Jul 1981.
- [56] David A. Huse. Simple three-state model with infinitely many phases. *Physical Review B*, 24(9):5180–5194, January 1981.
- [57] David A. Huse, Anthony M. Szipilka, and Michael E. Fisher. Melting and wetting transitions in the three-state chiral clock model. *Physica A: Statistical Mechanics and its Applications*, 121(3):363 – 398, 1983.
- [58] E. Fradkin and L. P. Kadanoff. Disorder variables and para-fermions in two-dimensional statistical mechanics. *Nucl. Phys. B*, (1):1–15, 1980.
- [59] A. Feiguin, S. Trebst, A. W. W. Ludwig, M. Troyer, A. Kitaev, Z. Wang, and M. H. Freedman. Interacting Anyons in Topological Quantum Liquids: The Golden Chain. *Physical Review Letters*, 98(16):160409, April 2007.
- [60] S. Trebst, M. Troyer, Z. Wang, and A. W. W. Ludwig. A short introduction to Fibonacci anyon models. *ArXiv e-prints*, February 2009.
- [61] Daisuke Tambara and Shigeru Yamagami. Tensor categories with fusion rules of self-duality for finite abelian groups. *Journal of Algebra - J ALGEBRA*, 209:692–707, 11 1998.

- [62] Jacob Siehler. Near-group categories. *ALGEBR.GEOM.TOPOL.*, 3:719, 2003.
- [63] Michael H. Freedman, Michael J. Larsen, and Zhenghan Wang. A modular functor which is universal for quantum computation. *Commun. Math. Phys.*, 227:605–622, 2002.
- [64] N. E. Bonesteel, L. Hormozi, G. Zikos, and S. H. Simon. Braid topologies for quantum computation. *Phys. Rev. Lett.*, 95:140503, 2005.
- [65] A. Yu. Kitaev. Fault-tolerant quantum computation by anyons. *Ann. Phys.*, 303:2, 2003.
- [66] R. S. K. Mong, D. J. Clarke, J. Alicea, N. H. Lindner, P. Fendley, C. Nayak, Y. Oreg, A. Stern, E. Berg, K. Shtengel, and M. P. A. Fisher. Universal Topological Quantum Computation from a Superconductor-Abelian Quantum Hall Heterostructure. *Phys. Rev. X*, 4(1):011036, January 2014.
- [67] Abolhassan Vaezi and Maissam Barkeshli. Fibonacci anyons from abelian bilayer quantum hall states. *Phys. Rev. Lett.*, 113:236804, Dec 2014.
- [68] E. M. Stoudenmire, David J. Clarke, Roger S. K. Mong, and Jason Alicea. Assembling Fibonacci anyons from a Z_3 parafermion lattice model. , 91(23):235112, June 2015.
- [69] J. Alicea and P. Fendley. Topological Phases with Parafermions: Theory and Blueprints. *Annu. Rev. Condens. Matter Phys.*, 7:119–139, March 2016.
- [70] G. J. Sreejith, Achilleas Lazarides, and Roderich Moessner. Parafermion chain with $2\pi/k$ floquet edge modes. *Phys. Rev. B*, 94:045127, Jul 2016.
- [71] Peter E. Finch. From spin to anyon notation: the XXZ Heisenberg model as a D_3 (or $su(2)_4$) anyon chain. *Journal of Physics A Mathematical General*, 46(5):055305, Feb 2013.

- [72] Natalia Braylovskaya, Peter E. Finch, and Holger Frahm. Exact solution of the D_3 non-Abelian anyon chain. *Phys. Rev. B*, 94(8):085138, Aug 2016.
- [73] Paul Fendley. Strong zero modes and eigenstate phase transitions in the xyz/interacting majorana chain. *Journal of Physics A: Mathematical and Theoretical*, 49(30):30LT01, 2016.
- [74] Romain Vasseur, Aaron J. Friedman, S. A. Parameswaran, and Andrew C. Potter. Particle-hole symmetry, many-body localization, and topological edge modes. *Phys. Rev. B*, 93(13):134207, April 2016.
- [75] G. Schaller. *Open Quantum Systems Far from Equilibrium*. Lecture Notes in Physics. Springer International Publishing, 2014.
- [76] C. Gils, E. Ardonne, S. Trebst, D. A. Huse, A. W. W. Ludwig, M. Troyer, and Z. Wang. Anyonic quantum spin chains: Spin-1 generalizations and topological stability. *Phys. Rev. B*, 87(23):235120, Jun 2013.
- [77] Yasuhiro Hatsugai, Mahito Kohmoto, and Yong-Shi Wu. Braid group and anyons on a cylinder. *Phys. Rev. B*, 43:2661–2677, Feb 1991.
- [78] Torbjörn Einarsson. Fractional statistics on a torus. *Phys. Rev. Lett.*, 64:1995–1998, Apr 1990.
- [79] Yasuhiro Hatsugai, Mahito Kohmoto, and Yong-Shi Wu. Anyons on a torus: Braid group, aharonov-bohm period, and numerical study. *Phys. Rev. B*, 43:10761–10768, May 1991.
- [80] Y. Hatsugai, M. Kohmoto, and Yong-Shi Wu. Braid group and anyons on an annulus and a torus. In Yasuhiro Iye and Hiroshi Yasuoka, editors, *The Physics and Chemistry of Oxide Superconductors*, pages 485–488, Berlin, Heidelberg, 1992. Springer Berlin Heidelberg.
- [81] Joan S. Birman. On braid groups. *Communications on Pure and Applied Mathematics*, 22(1):41–72, 1969.

- [82] X. G. Wen, E. Dagotto, and E. Fradkin. Anyons on a torus. *Phys. Rev. B*, 42:6110–6123, Oct 1990.
- [83] Courtney G. Brell, Simon Burton, Guillaume Dauphinais, Steven T. Flammia, and David Poulin. Thermalization, error correction, and memory lifetime for ising anyon systems. *Phys. Rev. X*, 4:031058, Sep 2014.
- [84] Didier Poilblanc, Andreas W. W. Ludwig, Simon Trebst, and Matthias Troyer. Quantum spin ladders of non-abelian anyons. *Phys. Rev. B*, 83:134439, Apr 2011.
- [85] M. Berry and M. Tabor. Level clustering in the regular spectrum. *Proceedings of the Royal Society of London. A. Mathematical and Physical Sciences*, 356:375 – 394, 1977.
- [86] O. Bohigas, M.J. Giannoni, and C. Schmit. Characterization of chaotic quantum spectra and universality of level fluctuation laws. *Phys. Rev. Lett.*, 52:1–4, 1984.
- [87] F. Haake. *Quantum Signatures of Chaos*. Physics and astronomy online library. Springer, 2001.
- [88] S. Wimberger. *Nonlinear Dynamics and Quantum Chaos: An Introduction*. Graduate Texts in Physics. Springer International Publishing, 2014.
- [89] M. Fremling, Cécile Repellin, Jean-Marie Stéphan, N. Moran, J. K. Slingerland, and Masudul Haque. Dynamics and level statistics of interacting fermions in the lowest Landau level. *New Journal of Physics*, 20(10):103036, October 2018.
- [90] Simon Trebst, Eddy Ardonne, Adrian Feiguin, David A. Huse, Andreas W. W. Ludwig, and Matthias Troyer. Collective states of interacting fibonacci anyons. *Phys. Rev. Lett.*, 101:050401, Jul 2008.

- [91] Charlotte Gils, Eddy Ardonne, Simon Trebst, Andreas W. W. Ludwig, Matthias Troyer, and Zhenghan Wang. Collective states of interacting anyons, edge states, and the nucleation of topological liquids. *Phys. Rev. Lett.*, 103:070401, Aug 2009.
- [92] Luigi Amico, Andreas Osterloh, and Ulrich Eckern. One-dimensional XXZ model for particles obeying fractional statistics. *Phys. Rev. B*, 58:R1703–R1706, Jul 1998.
- [93] Andreas Osterloh, Luigi Amico, and Ulrich Eckern. LETTER TO THE EDITOR: Fermionic long-range correlations realized by particles obeying deformed statistics. *Journal of Physics A Mathematical General*, 33(48):L487–L492, December 2000.
- [94] Pasquale Calabrese and Mihail Mintchev. Correlation functions of one-dimensional anyonic fluids. *Phys. Rev. B*, 75:233104, Jun 2007.
- [95] Raoul Santachiara, Franck Stauffer, and Daniel C. Cabra. LETTER: Entanglement properties and momentum distributions of hard-core anyons on a ring. *Journal of Statistical Mechanics: Theory and Experiment*, 2007(5):L05003, May 2007.
- [96] Vadim Oganesyan and David A. Huse. Localization of interacting fermions at high temperature. *Phys. Rev. B*, 75:155111, Apr 2007.
- [97] Y. Y. Atas, E. Bogomolny, O. Giraud, and G. Roux. Distribution of the ratio of consecutive level spacings in random matrix ensembles. *Phys. Rev. Lett.*, 110:084101, Feb 2013.
- [98] H. Li and F. D. M. Haldane. Entanglement Spectrum as a Generalization of Entanglement Entropy: Identification of Topological Order in Non-Abelian Fractional Quantum Hall Effect States. *Phys. Rev. Lett.*, 101(1):010504, July 2008.

- [99] Michael A. Nielsen and Isaac L. Chuang. *Quantum Computation and Quantum Information: 10th Anniversary Edition*. Cambridge University Press, 2010.
- [100] Parsa Bonderson, Christina Knapp, and Kaushal Patel. Anyonic entanglement and topological entanglement entropy. *Annals of Physics*, 385:399–468, October 2017.
- [101] A. Sterdyniak, A. Chandran, N. Regnault, B. A. Bernevig, and Parsa Bonderson. Real-space entanglement spectrum of quantum hall states. *Phys. Rev. B*, 85:125308, Mar 2012.
- [102] J. Dubail, N. Read, and E. H. Rezayi. Real-Space Entanglement Spectrum of Quantum Hall Systems, November 2011.
- [103] Babatunde M. Ayeni, Sukhwinder Singh, Robert N. C. Pfeifer, and Gavin K. Brennen. Simulation of braiding anyons using matrix product states. *Phys. Rev. B*, 93:165128, Apr 2016.
- [104] Babatunde M. Ayeni, Robert N. C. Pfeifer, and Gavin K. Brennen. Phase transitions on a ladder of braided non-abelian anyons. *Phys. Rev. B*, 98:045432, Jul 2018.